Electric-Field Enhanced Fluidized Beds

-

A Low-Energy Bubble Control Method

Flip Kleijn van Willigen

Electric-Field Enhanced Fluidized Beds

-

A Low-Energy Bubble Control Method

Proefschrift

ter verkrijging van de graad van doctor
aan de Technische Universiteit Delft,
op gezag van de Rector Magnificus prof. dr. ir. J.T. Fokkema,
voorzitter van het College voor Promoties,
in het openbaar te verdedigen op
woensdag 18 januari 2006 om 13:00 uur

door

Flip KLEIJN VAN WILLIGEN

scheikundig ingenieur
geboren te Marum

Dit proefschrift is goedgekeurd door de promotoren:
Prof. ir. C.M. van den Bleek
Prof. dr. ir. J. van Turnhout

Samenstelling promotiecommissie:

Rector Magnificus, voorzitter	
Prof. ir. C.M. van den Bleek	Technische Universiteit Delft, promotor
Prof. dr. ir. J. van Turnhout	Technische Universiteit Delft, promotor
Prof. dr. ir. M.-O. Coppens	Technische Universiteit Delft
Prof. dr. ir. J.A.M. Kuipers	Universiteit Twente
Prof. dr. J.R. Grace	University of British Columbia, Canada
Dr. ir. J.C.M. Marijnissen	Technische Universiteit Delft
Dr. ir. J.R. van Ommen	Technische Universiteit Delft

Ruud van Ommen heeft als begeleider in belangrijke mate aan de totstandkoming van dit proefschrift bijgedragen.

Printed by PrintPartners Ipskamp

ISBN: 90-9020298-6

Summary

Summary of 'Electric-Field Enhanced Fluidized Beds - A Low-Energy Bubble Control Method', Ph.D. thesis, F. Kleijn van Willigen, 2005.

The work described in this thesis is an investigation into the applicability of low-energy electric fields in gas-solid fluidized beds, with the aim of decreasing the size of gas bubbles in the fluidized bed and thus increasing the effectiveness of processes in which fluidized beds are typically applied.

Gas-solid fluidized beds are one of the most commonly applied types of reactor in the chemical and process industries. A fluidized bed is no more than a vessel containing a bed of solid particles, e.g. sand or catalytically active particles, and a method of introducing gas from below. When the drag force of the gas is large enough to overcome the force of gravity, the particles will start to float in the gas. In this state, the system is *fluidized*, which means that the solid particles, due to the gas flowing past them, behave like a liquid: lighter materials will float on the surface, heavy objects will sink, the surface remains horizontal when the system is tilted, and when a port is opened in the side of the column, the particles will pour out. With these properties, the fluidized bed is a good method of gas-solid contacting, leading to efficient heat and mass transfer on the particle scale.

When the gas flow rate is increased, the most prominent feature of fluidized beds appears: pockets of gas with few particles within rising through the bed, known as voids or bubbles. These bubbles can decrease the conversion in a fluidized bed reactor by a factor of three because the gas they contain has little interaction with the particles, and thus form a significant limitation on the effectiveness of fluidized beds. In this work, we demonstrate a method to *control* and *decrease* the bubble size using *electric fields*.

The electric fields were introduced in the fluidized beds described in this work by stringing thin wire electrodes through the bed. The influence of these wires on the bubble behavior was so small as to not be measurable. Oscillating (AC) electric fields with a frequency of 1 – 200 Hz and a strength up to 8 kV/cm were applied. Due to the electrode design, the electric field in the column is strongly inhomogenic, with regions with strong vertical and horizontal components separated by regions with a

low field density. The field intensity is not high enough to cause any electrical breakdown of the fluidizing air. The relative humidity is an important parameter to control the electrical response of the system.

Although the conductivity of the particles (various glass and alumina particles were used) was influenced via the relative humidity of the system, the particles are only slightly conductive. The response of particles with a low but non-zero conductivity to a low frequency electric field can be described by the Maxwell-Wagner theory of polarization. This theory describes how the particles are polarized because of the migration of charge to the poles of the particles. This migration is a relatively slow process, and thus requires the typical field frequencies mentioned above. The degree of polarization achieved, *i.e.* the dielectric response, can be several orders of magnitude larger than typically found at higher frequencies. In addition, the diffusion of charge around the poles of the particles introduce a dependence of the dielectric response on the particle size.

The particle response to an applied electric field is thus to be polarized; the net electric charge on each particle remains zero. The electric dipoles lead to an electric field induced interparticle force. This is a force which depends strongly on the particle separation distance and the relative orientation of the particles in the electric field, both in magnitude and direction. Particles with the center to center axis aligned to the electric field will attract each other, while particles adjacent to each other in the field will repel one another. Particles at an angle to each other will experience a torque that attempts to align them to the field. Due to the electric field induced interparticle force, the particles in the bed will tend to form strings in the direction of the field.

The net effect of these interparticle forces is a decrease of the diameter of bubbles in a fluidized bed by as much as 80% in experiments with Geldart B particles. The fields were always such that the *fluidity* of the bed, that is, the free movement of particles, was always preserved. Discrete particle simulations suggest that the electric fields cause a better distribution of gas bubbles in the bottom part of the bed, and reduce the rate of coalescence of these bubbles higher in the bed. In the simulations of relatively shallow fluidized beds with homogeneous alternating fields, the maximum bubble size was reduced by as much as 55% before defluidization occurred.

When the field strength is very high, particles were confined to relatively nonmoving strings of particles stretching through the whole column, either horizontally or vertically, depending on the field orientation.

To demonstrate that the decrease in bubble size is indeed beneficial to the degree of conversion attained in a chemical reactor, ozone was decomposed in an electric field enhanced fluidized bed. Both untreated and Fe-impregnated alumina particles were tested. Although the system was neither optimized, nor the work intended to be an exhaustive investigation of ozone decomposition reactors, the bubble size reduction due to the applied electric field increased conversion by as much as 15%. As predicted by the Kunii and Levenspiel fluidization model, the system with more active catalysts stands to gain more from bubble size reduction than the less active catalyst.

Clearly, the chemical conversion can benefit significantly from the reduced bubble size, depending on the application. It is even more interesting when the energy cost of the application of electric fields is considered. Although it varies slightly with the relative humidity of the system (which, as described above, directly influences the conductivity of the bed), the typical power consumption of an electric field enhanced fluidized bed is approximately 40 Watt per cubic meter of reactor – about as little an incandescent light bulb.

Besides the *application* of electric fields in fluidized bed systems, the work was extended to *measuring* electric fields to gain an understanding of how triboelectrically charged particles are distributed around bubbles in *non-electric field enhanced* fluidized beds. It was found that there is a decrease of charge density when moving inwards from the negatively charged emulsion phase towards the bubble interface, with essentially zero charge density inside the bubble. However, the charge distribution was shown to be non-trivial in that the wake of a bubble typically contains particles with a much stronger charge, of the same sign, as the particles in the emulsion phase. The triboelectric, or frictional, charging of particles in a fluidized bed is rather weak and not relevant in the electric field enhanced fluidized beds.

Although the research presented in this thesis was fundamental in nature, both experimentally and in modeling, the future viability of industrial application was always a guiding element. The most important consequence this had on the work was the electrode design; through the modular use of wire electrodes strung through

the bed, the electrode design is inherently scalable. The electric field enhanced fluidized bed phenomena, parameters, insights, and understanding that are presented in this thesis provide a basis both to extend the work to new applications as well as to developing new technologies in which the electrical phenomena in fluidized beds can be exploited or controlled.

Samenvatting

Samenvatting van 'Electric-Field Enhanced Fluidized Beds - A Low-Energy Bubble Control Method', proefschrift, F. Kleijn van Willigen, 2005.

Het onderzoek dat wordt beschreven in dit proefschrift is gericht op de toepassing van elektrische velden in gas-vast gefluïdiseerde bedden. Het doel is om de grootte van de gasbellen in het gefluïdiseerde bed te verminderen en daardoor de efficiëntie van de chemische en fysische processen waarin fluïde bedden worden toegepast te verhogen.

Gas-vast gefluïdiseerde bedden zijn één van de meest veelvuldig toegepaste reactortypes in zowel de chemische- als de procesindustrie. Een fluïde bed bestaat uit een vat gevuld met deeltjes, bijvoorbeeld zand of katalytisch actieve deeltjes, en een manier om daar van onder gas in te blazen. Als de wrijving die het gas op de deeltjes uitoefent groter is dan de zwaartekracht zullen de deeltjes als het ware gaan drijven in het gas. In deze staat noemt men het systeem *gefluidiseerd*. Dit wil zeggen dat de deeltjes, onder invloed van het gas, zich gaan gedragen als een vloeistof: lichtere materialen drijven op het oppervlak, zware voorwerpen zinken, het oppervlak blijft horizontaal als het vat gekanteld wordt, en als er een opening in de zijkant van het vat is, dan stromen de deeltjes eruit. Vanwege zijn eigenschappen is het gefluïdiseerde bed een goede methode om gassen en vaste stoffen met elkaar in contact te brengen, waarbij op deeltjesschaal de warmte- en stofoverdracht zo efficiënt mogelijk zijn.

Als de gasstroom vergroot wordt, doet zich één van de meest opvallende verschijnselen van het fluïde bed voor: bellen gevuld met gas en weinig deeltjes beginnen door het bed te stijgen. Deze bellen beperken de maximaal haalbare conversie in fluïde bed reactoren, omdat het gas in de bellen weinig wisselwerking heeft met de deeltjes. De effectiviteit van fluïde bedden kan wel een factor drie lager zijn dan ideaal haalbaar. In dit werk wordt daarom een methode gepresenteerd om de grootte van bellen te *beheersen* en te *verkleinen* door middel van *elektrische velden*.

De elektrische velden worden in het gefluïdiseerde bed opgewekt door dunne draadelektroden die door de kolom zijn gespannen. De fysieke invloed van deze draden zelf op het gedrag van bellen is zo klein dat zij niet meetbaar was. Wisselspanningsvelden (AC) met een frequentie tussen 1 en 200 Hz en een maximale sterkte van 8 kV/mm werden gebruikt. Het ontwerp van de draadelektroden was zodanig dat het veld sterk niet-homogeen was, waardoor gebieden met sterke

horizontale of verticale veldcomponenten werden afgewisseld met gebieden met lagere veldsterkte. De veldsterkte was altijd zodanig dat elektrische ontlading door vonkoverslag niet kon optreden in de kolom. Een belangrijke parameter om de elektrische respons van het systeem te beïnvloeden was de relatieve vochtigheid.

Alhoewel de relatieve vochtigheid de geleidbaarheid van de toegepaste deeltjes (verschillende soorten glazen en alumina deeltjes zijn gebruikt) sterk beïnvloedt, werd altijd gezorgd dat de deeltjes hun zeer hoge weerstand behielden. De elektrische respons van deeltjes met hoge, maar niet oneindige, weerstand op een laagfrequent elektrisch veld kan worden beschreven met de Maxwell-Wagner theorie voor polarisatie. Deze theorie omschrijft hoe de deeltjes polariseren door de migratie van tegenovergestelde ladingen naar de polen van de deeltjes. Dit is een relatief traag proces, en vindt alleen plaats bij lage veldfrequenties zoals hierboven beschreven. De polarisatiegraad, d.w.z. de diëlektrische respons, kan in dit geval enkele ordes van grootte sterker zijn dan de respons die men bij hogere frequenties waarneemt. Bovendien treedt er diffusie van lading rond de polen van de deeltjes op, waardoor de polarisatiegraad afhankelijkheid is van de deeltjesgrootte.

Het effect van elektrische velden op de deeltjes is dus een elektrische polarisatie; hierbij blijft de totale lading op een deeltje nul. De elektrische dipolen veroorzaken op hun beurt een kracht tussen deeltjes als gevolg van het elektrische veld, de *electric field induced interparticle force*. Deze kracht is zowel in richting als in sterkte sterk afhankelijk van de afstand tussen de deeltjes en de relatieve oriëntatie van de deeltjes in het veld. Twee deeltjes waarvan de middenpunten beide op dezelfde lijn liggen als de richting van het elektrische veld zullen tot elkaar aangetrokken worden, terwijl deeltjes die in het veld naast elkaar zitten elkaar afstoten. Als de as tussen de middelpunten van de deeltjes op een hoek met het veld staat, zullen de deeltjes een torsiekracht ondervinden die ze in de richting van het veld draait. Het gevolg van deze richtingsafhankelijkheid van de elektrisch-geinduceerde kracht is dat deeltjes in het bed de neiging hebben ketens of strengen te vormen in de richting van het veld.

Het effect van deze krachten is dat de grootte van bellen in een gefluïdiseerd bed tot 80% verminderd kan worden. Dit werd experimenteel aangetoond met Geldart B deeltjes. De kracht van het veld was altijd zodanig dat de *fluidity* van het bed, dus het vloeistofachtige gedrag, altijd bewaard bleef. Discrete deeltjes simulaties wijzen erop dat door de elektrische velden de verdeling van gas onder in het bed

verbeterd wordt, en dat de snelheid waarmee de bellen hoger in de kolom samenkomen verminderd wordt. In deze computersimulaties van, relatief kleine, gefluïdiseerde bedden met een homogeen wisselspanningsveld werd de maximale belgrootte tot wel 55% beperkt voordat de veldsterkte zodanig hoog werd dat defluïdisatie optrad. Als de gesimuleerde veldsterkte erg hoog werd, hoger dan in de experimenten, werden lange strengen van vrijwel niet-bewegende deeltjes gevormd in de richting van het veld.

Om aan te tonen dat kleinere bellen ook daadwerkelijk leiden tot een hogere conversie in een chemische reactor, werd ozon ontleedt tot zuurstof in een gefluïdiseerd bed met elektrische velden. Hiervoor zijn zowel onbehandelde als ijzergeïmpregneerde alumina deeltjes getest. Alhoewel het systeem niet geoptimaliseerd werd, noch het werk bedoeld was als uitgebreid onderzoek naar ozon ontleding, is aangetoond dat de kleinere bellen als gevolg van elektrische velden de conversie kan verhogen met 15%. Het fluïdisatie model van Kunii en Levenspiel voorspelt dat systemen met meer actieve katalysatordeeltjes meer profijt hebben van een vermindering van de belgrootte dan minder actieve katalysatoren.

Het is duidelijk dat de chemische conversie in een reactor veel kan winnen van de verminderde belgrootte door elektrische velden; hoeveel is natuurlijk afhankelijk van de specifieke applicatie. Minstens zo interessant is de energetische prijs van de toepassing van elektrische velden in de reactor. Hoewel de relatieve vochtigheid (wat de geleidbaarheid van het systeem beïnvloedt) enige variatie veroorzaakt, is de typische energieconsumptie van een fluïde bed met elektrische velden ongeveer 40 Watt per kubieke meter reactor – ongeveer evenveel als één gloeilamp!

Naast de toepassing van elektrische velden in gefluïdiseerde bedden, is er onderzoek gedaan naar het meten van de natuurlijk optredende electrostatische verschijnselen in gefluïdiseerde bedden, met als doel inzicht te krijgen in het gedrag van triboelektrisch (wrijvings-) geladen deeltjes rond bellen. Hieruit bleek dat, beschouwd vanaf de buitenkant van de bel naar binnen, er buiten de bel een afname is van de ladingsdichtheid als men naar de bel toe beweegt en er vrijwel geen lading in de bel zelf aanwezig is. Opmerkelijk hierbij is dat bleek dat de ladingsverdeling onder de bel, in de zogenaamde *wake*, niet triviaal is. In deze *wake* hebben de deeltjes een zeer sterke lading, met hetzelfde teken als de rest van de deeltjes. Sterk geladen deeltjes bouwen zich blijkbaar op aan de onderkant van bellen. Deze triboelektrische

verschijnselen zijn betrekkelijk zwak en niet relevant wanneer de elektrische velden aangelegd werden zoals eerder beschreven.

Het onderzoek dat in dit proefschrift is beschreven was fundamenteel van aard. Echter, zowel in het ontwerp van de experimenten als in de simulaties is de eventuele toekomstige toepassing in industriële applicaties altijd een leidraad geweest. Dit is duidelijk te zien in het modulaire ontwerp van de elektrodes die door de kolom werden gespannen, welke zodanig was dat deze inherent schaalbaar was. De verschijnselen, de parameters, de inzichten en het begrip van fluïde bed reactoren die zijn uitgerust met elektrische velden, zoals gepresenteerd in dit proefschrift, vormen een gedegen basis voor zowel industriële toepassingen alsmede nieuw onderzoek naar andere toepassingen van elektrische velden voor het beïnvloeden of verbeteren van systemen.

Table of Contents

1. Introduction

Video still image of bubbles rising through a two-dimensional fluidized bed. The gas in these bubbles has little interaction with the catalytic emulsion phase – therefore, we use electric fields to control and decrease their size.

Gas/solid fluidized beds are one of the most commonly applied types of reactor in the chemical and process industries. The first commercial application of gas-solids fluidized beds was accomplished in Germany in 1926, the so-called Winkler process for coal gasification. In the early 1940's, the demand for high-octane aviation fuel boosted the use of the fluidized bed reactor to the center stage of chemical industry, from where it has spread to one of the most common reactors for chemical processes.

Interestingly, it was at this point that the term "fluidization" was coined to describe the hydrodynamics of this technique of gas-solids contacting (Epstein, 2004). At about the same time, Dorr-Oliver applied fluidized beds to the roasting of sulfide ores and the drying of powders, extending the domain of applications to non-catalytic reactions and to physical processes (Kunii and Levenspiel, 1991). Since then, the fluidized bed has found a wide range of applications.

One of the most prominent features of a fluidized bed is the appearance of rising pockets of gas through the system, known as bubbles. These bubbles strongly influence the hydrodynamic behavior of the system, thereby dictating the performance and applicability of any fluidized bed.

In the work described in this thesis, we demonstrate a method to *control* and *decrease* the bubble size using *electric fields*. It will be shown how the particle-particle behavior can be influenced with electric fields to reduce the size of bubbles and, ultimately, increase the degree of conversion and selectivity in a bubbling fluidized bed. The amount of energy required to control the bubbles in an electric field enhanced fluidized bed is approximately 40 Watt per cubic meter of reactor – no more than a common incandescent light bulb!

1.1 Outline of this thesis

The effect of electric fields on fluidized bed behavior is considered on three scales: the microscopic, the mesoscopic, and the macroscopic scale. The microscopic scale, or particle scale, describes the response of one or two particles to an electric field. Central questions on this scale are to what degree interparticle forces result from the electric fields, and how to describe both the temporal and spatial effects of oscillating fields.

The mesoscopic scale describes the bubble behavior in a fluidized bed, with and without applied electric fields. Here, we no longer consider the behavior of

individual particles, but rather focus on how the electric field induced inter-particle forces lead to changes in the bubble behavior. The most important item here is how the average size of bubbles decreases, and also in what ways the hydrodynamics of the system changes when the bubble size decreases. We investigate, for example, how the bubble hold-up, i.e. the inventory of gas in bubbles, changes with changing bubble size.

The scale of reactors is viewed as the macroscopic scale. On a reactor scale, the central issue is: what is the benefit and what are the costs? In other words, whether we can enhance the performance of the fluidized bed with electric fields, and what the advantages and disadvantages are.

Before delving into the combination of fluidized beds and electric fields, a brief review will be presented of both, in light of the application presented here. A basic description of the bubbling behavior is given, followed by an introduction to electric phenomena in electric field enhanced fluidized beds.

In Chapter 2, we experimentally demonstrate the use of electric fields in fluidized beds, focusing on the mesoscopic (bubble) scale. Chapter 2 also gives an overview of earlier work as it has been presented in the scientific literature over the past 50 years. In addition, a method is demonstrated for quantitatively determining the size of bubbles (analysis of pressure fluctuations) that has been used throughout this work.

In Chapter 3, the features of the electric field enhanced bed are compared to a different approach with the same goal, the fractal injection of secondary gas. While both systems lead to a smaller mean bubble size, their differences make that they have different potential applications. The experimental work described in that chapter focuses on the mesoscopic bubble scale, i.e. the size, distribution, and hold-up of bubbles in the bed.

The microscopic scale is treated in Chapter 4. The mechanism of Maxwell-Wagner polarization is shown to describe the response of particles to electric fields rather well, and we demonstrate that at the low frequencies of the oscillating fields that we employ in the experimental work presented in the previous and later chapters, the particle response can be considerably larger than expected at first sight.

The electric field enhanced fluidization can be described as electro-dynamics. That is, the periodic movement of small charges on the microscopic scale is what influences the mesoscopic bubble response. The net charge on a particle is in

principle neutral. In Chapter 5 we investigate the influence of electrostatics. The particle interaction is now no longer due to polarization effects following from the applied field, but due to the electrostatic charges on particles caused by triboelectric charging. We examine how a static charge is built-up in a fluidized bed without applied electric fields, through the interaction of particles with the wall, and, more importantly, how this charge distributes spatially through the system. Instead of applying electric fields, the much weaker electric fields originating from the charged particles are measured.

Chapter 6 returns to the mesoscopic scale of electric field enhanced fluidization: the bubbles. Using discrete-particle computational fluid dynamics (CFD) simulations, the effect of the inter-particle forces on bubble behavior is shown in computer simulations of small beds. The effect of various field strengths and frequencies on the bubble behavior was investigated.

Chapter 7 makes the step to the macroscopic scale: a proof of principle of the beneficial effect of electric field enhanced fluidization on the conversion in a chemical reactor is given. A three-phase reactor model and an experimental investigation are used to demonstrate that reducing the mass transfer resistance from bubble to emulsion phase yields a higher conversion in electric field enhanced fluidized beds. The ozone decomposition reaction is used as a model system to experimentally demonstrate that smaller bubbles do indeed lead to a higher efficiency.

1.2 Introduction to fluidization

A short introduction is given to the homogeneous and bubbling fluidization behavior of Geldart A and B particles[*]. An extensive treatise is beyond the scope of this thesis; the reader is referred to the excellent book 'Fluidization Engineering' (Kunii and Levenspiel, 1991) for a detailed description of all aspects of fluidization technology, or, alternatively, to the web (Rhodes, ERPT website, 2001).

A fluidized bed is in principle no more than a vessel containing solid particles,

[*] Particles classified as Geldart A are particles with a size range of 20 to 80 μm, particles with a size range of 80 – 500 μm are classified as Geldart B particles, for a density of ~2500 kg/m^3 (Geldart, 1973).

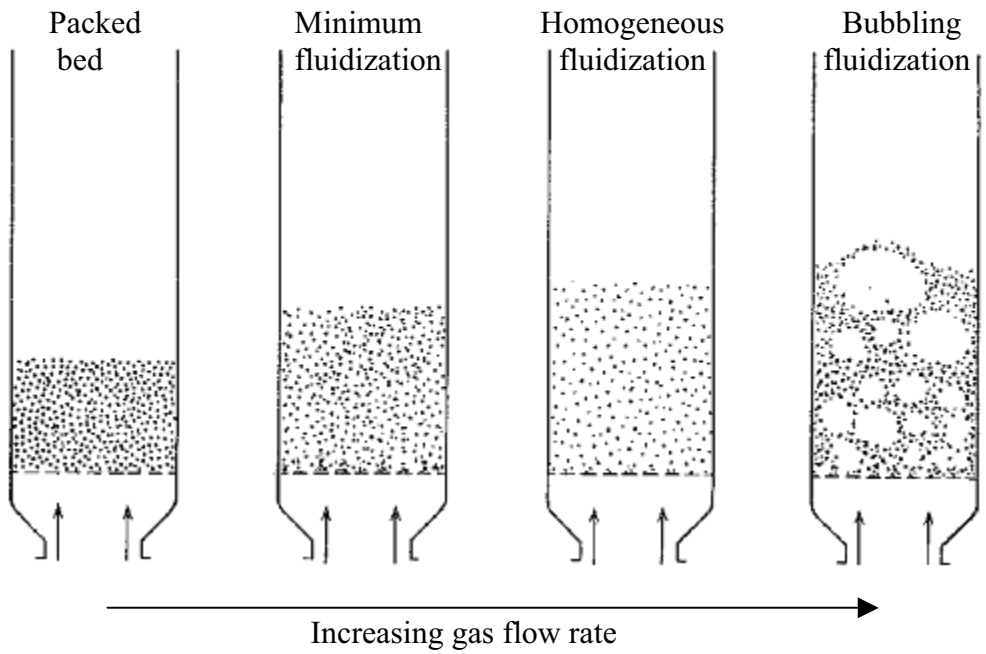

Figure 1-1. The various states of a bed of solid particles under increasing flow conditions. In a fixed bed the particles are grid-locked and not able to move. As the gas flow is increased to minimum fluidization flow, the particles start to float in the gas and start to behave as a fluid. When the gas flow is increased further, the excess gas flow is present in the form of bubbles. For Geldart A particles, an intermediate regime of homogeneous fluidization exists (adapted from Kunii and Levenspiel, 1991).

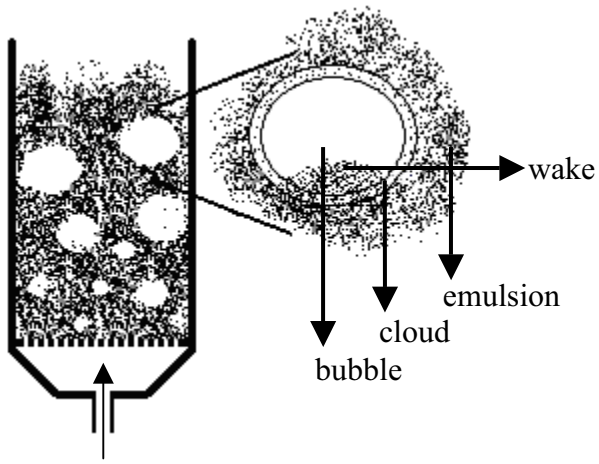

Figure 1-2. Schematic representation of a bubbling fluidized bed, with the inset showing the emulsion phase containing most of the particles, the cloud phase, and the virtually particle-free bubble phase. Bubbles are not spherical: the bottom part of the bubble is the wake region, a region of turbulent mixing of gas and particles which are typically carried for some distance with the rising bubble. A cloud, with a lower concentration of particles than the emulsion phase, surrounds the bubble.

e.g. sand, and a means of introducing a gas flow from below (Figure 1-1). When the force that the flowing gas exerts on the particles (the drag force) is large enough to overcome the force of gravity, the particles will start to lift and the bed expands. This is the transition from the packed state to the fluidized state. The particles are now relatively free to move, resulting in these solids behaving as if they were a liquid, with properties normally associated with liquids. For example, light things will float and heavy things will sink, and the surface will stay horizontal if the bed is tipped. The required gas velocity at this point is called the minimum fluidization velocity.

If the drag force increases, e.g. by increasing the flow rate or the pressure in the system, the fluidized bed expands further. By doing this, the interstitial space increases slightly, resulting in a drop of the drag force until it is once again balanced by the force of gravity. However, at this point an interesting phenomenon occurs for 'small', or Geldart A, particles: homogeneous fluidization. For particles smaller than approximately 70 μm and a density of approximately 2500 kg/m^3, the bed expansion is uniform – all particles are separated by approximately the same distance. In other words, the emulsion or particle phase can contain more gas than that required for minimum fluidization. This behavior is attributed to the fact that at this scale, interparticle forces such as van der Waals forces can play a significant role (Figure 1-3).

Particles larger than approximately 70 μm, i.e. Geldart B classification, do not display this behavior. Any gas introduced into the system beyond that required for minimum fluidization is present in the form of voids, better known as bubbles (cf. Figure 1-2). These bubbles, much like gas bubbles in a liquid, rise through the bed, with the particles in the particle phase, or emulsion phase, moving out of the way. These bubbles typically have a kidney-like shape. Larger bubbles travel faster than smaller bubbles, and the diameter of these bubbles may vary from millimeters in the bottom of a bed of small particles (70 μm) to many decimeters higher in the bed when larger particles (700 μm) are fluidized at higher flow rates.

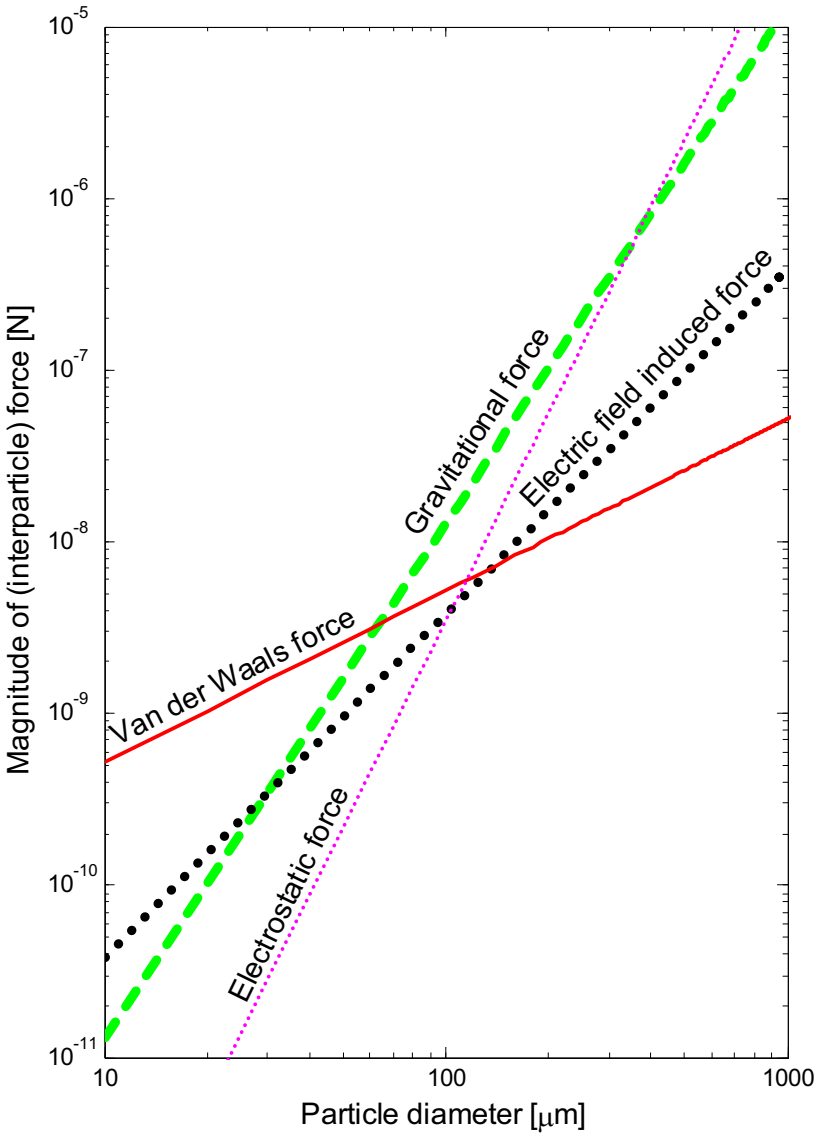

Figure 1-3. Magnitude of the gravitational force, the electric field induced force, the electrostatic force, and the van der Waals force. The applied field strength is 1 kV/cm leading to an attractive electric field induced force. Note that for particles smaller than 50 μm the van der Waals forces play a large role in the interaction, whereas for larger particles the electric field induced force is a significant interparticle force. The electrostatic force is a repulsive force between particles with a net charge of 50 μC/kg. Experiments (Chapter Five) show that such a charge is easily attained in a very dry fluidized bed with particles susceptible to triboelectric charging, without such problems as sheeting or agglomeration of particles occurring. Other parameters: d_p / a_{ij} = 2 × 10^5, ε_p = 7, ρ_s = 2500 kg/m^3, A = 5 × 10^{-21} J.

A fluidized bed derives many of its good properties (summarized in Table 1-1) from the good contact between gas and particles in the emulsion phase, such as efficient use of the catalytic properties of the particle. However, as stated above, most, if not all, of the gas in excess of the minimum fluidization velocity (aptly named the excess gas velocity) rises through the bed in the form of bubbles – and this excess velocity can be as much as 20 times the minimum fluidization velocity for a bubbling fluidized bed of Geldart B particles. While they enhance the mixing behavior of the bed, the gas the bubbles contain typically must transfer from the bubble phase to the emulsion phase for the desired 'work' to be done on it. This is frequently a limiting step in the efficiency of a fluidized bed reactor, and therefore the control and reduction of bubbles is the focus of this work.

Table 1-1. Advantages and disadvantages of bubbling fluidized beds as gas-solid reactor (adapted from Howard, 1989).

Advantages	Disadvantages
Good gas-solid contact	Lower conversion than packed bed
Good particle mixing	Excessive gas by-pass
Low pressure drop compared to packed beds	Erosion of vessel and pipes, and production of fines by attrition
Uniform temperature and control of process giving uniform quality of products	Segregation of particles of different size or density
Can use wider particle size range than packed beds	Elutriation of fines can limit performance
High bed-to-surface heat transfer coefficients	
Ease of transport of solids in and out of reactor	

1.3 Introduction to electric fields and particles

It has already been described above how, for Geldart A particles, a regime of homogeneous fluidization exists. Usually, this phenomenon of homogeneous fluidization is limited to a narrow range up to about 25% above the minimum fluidization velocity. When the superficial velocity is higher, or the particles larger, the magnitude of the interparticle forces becomes so much smaller than the drag and gravitational force that they no longer play such a significant role. The work

described in this thesis introduces an additional interparticle force to the system, the *electric field induced interparticle force*. This force can be tuned by the designer of the system to reduce the volume of bubbles in the system significantly, much in the way that van der Waals forces induce homogeneous fluidization.

To create this interparticle force, we make use of electric fields. Using electrodes placed inside the fluidized bed, alternating electric fields induce dipoles in the particles, which in turn results in periodic short-range attractive or repulsive forces between the particles. The electrodes used to achieve this are small enough that they do not measurably influence the fluidization behavior unless a potential is applied to them. Without an electric field, the wires in the bed do not influence the bubble size or bed hydrodynamics (cf. Chapter 3). Just as van der Waals forces lead to homogeneous fluidization for Geldart A particles, the electric field induced forces lead to a reduction of the bubble size in a fluidized bed of Geldart A or B particles.

The following sections describe how the electric fields result in this interparticle force, and what the parameters and limitations are. Conceptually, the response of particles to an electric field in a fluidized bed may be compared to the response of magnetically susceptible particles in a bed with an applied magnetic field. Clearly, when the particles in a bed are magnetized, they will experience interparticle forces, causing them to attract or repel one another. In electric fields, particles must be not magnetically susceptible, but electrically susceptible, i.e. they must have a dielectric response to the electric field. A dielectric response occurs in many more materials than a magnetic response. The dielectric response manifests itself as a polarization of the particle to a dipole. Just as for the magnetic fields, this leads to an interparticle force. While the energy cost of applying magnetic fields to a fluidized bed is very significant, the power consumption of electric field enhanced fluidized beds is as little as 40 Watt per cubic meter of reactor (Kleijn van Willigen, 2001). This is, in fact, three orders of magnitude less than the power consumption of magnetically stabilized fluidized beds (Geuzens, 1985).

Besides the electric field induced interparticle force, electrostatic forces, corona (dis)charging, and a description of the electric field as we apply it will now be given.

Dielectrics and interfacial polarization

The first step in determining the response of particles to an applied electric field is determining their dielectric response. When a non-conductive particle is placed in an electric field, a charge separation occurs and the particle becomes *polarized*, cf. Figure 1-5a. This charge separation can be on the scale of electrons or molecules to the scale of particles, depending on the frequency of the electric field applied (cf. Figure 1-4) and the properties of the system. Any unit in which this charge separation has occurred, be it on the atomic or the particles scale, now has a positive and negative 'pole', and it is termed a *dipole*. The *relative permittivity* (ε_r) is a measure for the degree of charge separation under an electric field, and can be measured with a technique known as dielectric spectroscopy. The permittivity is an intrinsic physical property of the material, and a material with a relative permittivity larger than unity is called a *dielectric* material. Dielectric materials are commonly used for their dielectric properties in manufactured capacitors, which are electronic devices for holding a charge. However, many materials that are perhaps not used because of their specific electric insulation properties are, in fact, dielectrics.

The particles considered in this thesis are insulating particles (i.e. glass beads) with a *very* slightly conductive surface layer (since the fluidized air is slightly humidified), and the electric field alternates at frequencies ranging from 1 to 200 Hz. The dielectric response of such a system can be described by the Maxwell-Wagner theory of interfacial polarization (Kleijn van Willigen et al., 2005). This means that the degree of polarization, and the ensuing particle interaction, is not dictated by the particle and gas permittivities, but by the particle and gas conductivities. The polarization is now not mainly due to dipoles on the atomic or molecular scale, but rather due to the migration of charges to the surface of the particle, as shown in Figure 1-5b. For charges to migrate over such large distances, relatively slow electric fields are required, i.e. the 1-200 Hz alternating fields previously mentioned. At higher frequencies, only the (smaller) effect of the molecular dielectric permittivities on the polarization of the material is seen.

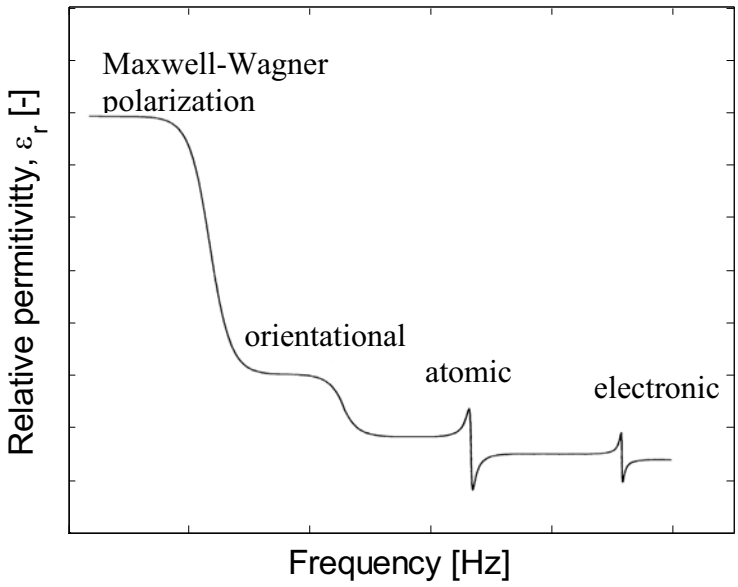

Figure 1-4. The frequency dependence of the dielectric response of a material in which various polarization mechanisms are present (adapted from Sihvola, 1999).

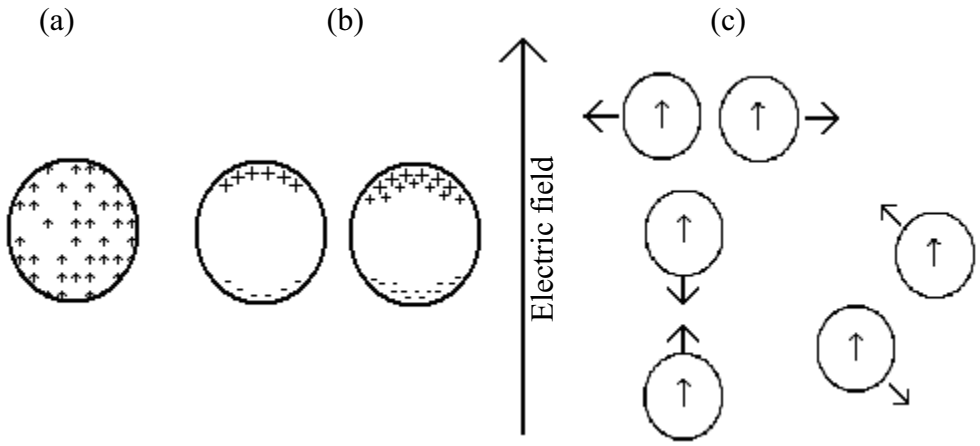

Figure 1-5. (a) Orientational polarization. (b) Maxwell-Wagner polarization of spherical particles, showing the influence of drift (left, particle radius much larger than charge diffusion length) and diffusion of charge (right, particle radius of the same order of magnitude as the charge diffusion length). (c) The direction of the electric field induced interparticle forces for various particle orientations.

The effect of the larger degree of polarization manifests itself as an increase of the effective dielectric constant, ε_r, by several orders of magnitude. This is shown in Figure 1-6, where the relative dielectric constant for glass beads has been measured versus frequency of the AC field, while varying the conductivity of the surface of the

particles. This was done by regulating the relative humidity of the surrounding air. The dielectric response at frequencies lower than 100 Hz is 2-4 orders of magnitude larger for the more conductive system, due to Maxwell-Wagner polarization, than that of the 'dry' system, in which the response of the glass molecules (orientational polarization) is seen. Also, the effect quickly drops off as the frequency is increased, showing that a certain time is required for the charges to migrate to the poles of the particles. This is explained in more detail in Chapter 4; it depends on the ratio of the migration distance, the Debye length, and the particle diameter.

Note that in the current application, electric field enhanced fluidization, the conductivity remains low even in humidified conditions, typically 10^{-7} – 10^{-9} S/m.

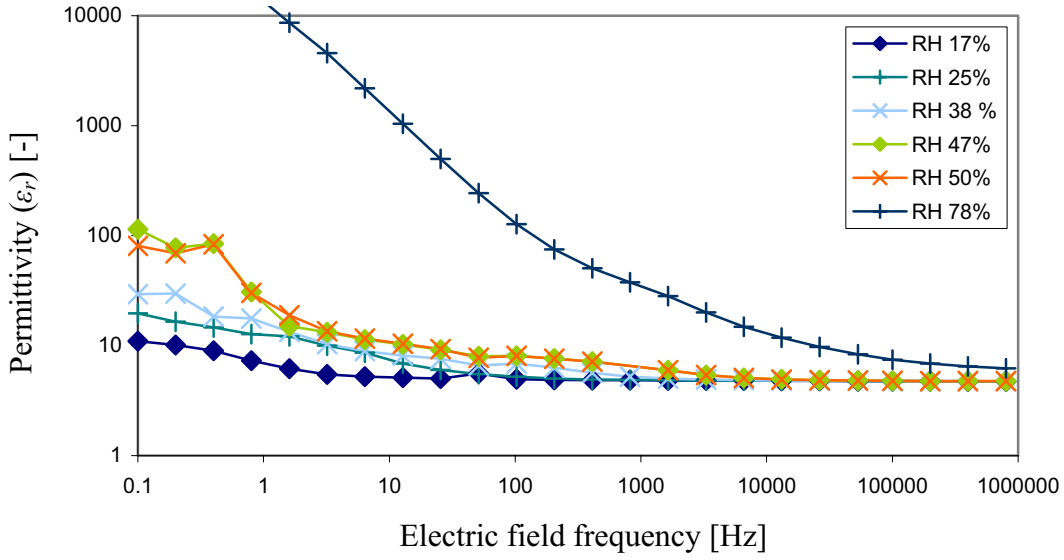

Figure 1-6. Experimental measurement of the dielectric spectrum of the permittivity of glass beads (d_p=77 µm) while varying the relative humidity (RH) of the surrounding air. The frequency sweeps were performed at 1 V, 26 ºC in a parallel plate cell with randomly packed particles.

Dipole moment

When the electric field has induced a small movement of positive and negative charges in opposite directions, the particle becomes an electric dipole, quantized in the electric dipole moment p situated at the center of the particle, and this is related to the electric field E by:

$$p = \tfrac{1}{2}\,\pi\,\varepsilon_0\,K\,d_p^{\,3}\,E \qquad [1 - 1]$$

where ε_0 is the permittivity of free space, d_p the particle diameter, and K the Clausius-Mossotti function, which provides a measure of the strength of the effective polarization of a spherical particle:

$$K= (\varepsilon_p - \varepsilon_{air}) / (\varepsilon_p + 2\,\varepsilon_{air}) \qquad [1 - 2]$$

The relative permittivity of the particle is ε_p, the relative permittivity of air is approximately $\varepsilon_{air} = 1$.

The above description of the dipole moment applies to a homogeneous dielectric sphere in a dielectric medium. Extensions and approximations for conductive spheres, conductive media, and lossy (time dependent) media and particles can be made (Boersma and van Turnhout, 1998). With a value for the *effective* dipole moment, the mechanism of polarization and any geometric issues have been incorporated, approximated, or neglected. The dipole moment allows us to capture the electrical polarization state of a particle in a single variable.

Electric field induced interparticle force

Having established the electrical properties of the particles and the dipole moment formed due to the electric field, the induced interparticle force between two particles in air can be calculated:

$$\vec{F}_{ij} = \frac{6 \cdot \vec{p}_i \cdot \vec{p}_j}{4 \cdot \pi \cdot \varepsilon_0 \cdot a_{ij}^{\,4}} \qquad [1 - 3]$$

It is useful to rewrite this as follows (Parthasarathy, 1996):

$$\vec{F}_{ij} = \frac{3}{16} \cdot \pi \cdot \varepsilon_0 \cdot \varepsilon_{air} \cdot d_p^{\,2} \cdot K^2 \cdot E^2 \cdot \left(\frac{d_p}{a_{ij}} \right)^4 \cdot \left[\left(3\cos^2 \theta_{ij} - 1 \right) \vec{e}_r + \left(\sin 2\theta_{ij} \right) \vec{e}_\theta \right] \qquad [1 - 4]$$

In this derivation, particles are assumed not to alter each other's charge distribution, and the interaction is solely between two dipoles at the centers of the particles (the point-dipole approximation).

A more rigorous derivation including the dependence on field frequency and the conductivities through the Maxwell-Wagner effect has been given by Parthasarathy (1996). Multibody effects were reviewed by Jones (1995). The important conclusion of these multibody studies is that interparticle forces may be up to an order of magnitude higher for particles in chains than approximated by the above point dipole model.

Eq. 1 - 4 shows that particle pairs oriented with their center-to-center axis aligned with the direction of the electric field will attract, while particles with their centers perpendicular to the field will repel one another (cf. Figure 1-5c). Particles in any other orientation will attempt to align to the field, suggesting that particles will have the *tendency to form chains* or *strings* in an electric field. Also note that in an infinite matrix of regularly spaced particles, the net force on each individual particle will be zero. A comparison of the maximum electric field induced force, i.e. when center-to-center axis of the particles is aligned with the field, is made to the other forces in a fluidized bed in Figure 1-3. For this comparison, a pair of particles is considered to be separated by 5% of their diameter. As particle diameter increases, the electric field induced force plays a larger and larger role than the van der Waals forces, thereby decreasing the mean bubble size for a bed of larger, Geldart B, particles much in the way that van der Waals forces do for small, Geldart A, particles.

At this point it is also interesting to point out that it has been reported that electrorheological fluids containing particles with a high dielectric constant, such as barium titanate, $\varepsilon_p \approx 1000$, do not show a significant electrorheological effect, while other materials with lower dielectric constants show strong changes in viscosity that decrease with increasing field frequency (Block and Kelly, 1988). This substantiates the theory that Maxwell-Wagner polarization is responsible for the polarization of particles in fluids with non-zero conductivity.

Dielectric breakdown and corona

In the previous section, the polarization of particles in low frequency electric fields was explained not due to their dielectric permittivity per se, but due to the slight conductivity of the particles. A side effect of this is the constriction of electric fields in the polar regions of particles when they are both aligned to the direction of the electric field and relatively close together. As a result, the strength of the electric field may locally increase to values at which the medium in between the poles breaks down (cf. Figure 1-7). In a gas, this means an ionization of the gas molecules, which is an avalanche-like process leading to the formation of channels of conduction plasma between the caps and the production of large numbers of ions (corona discharge). When this occurs, the electrical resistance of the gas, normally very high, decreases virtually to zero. The critical magnitude at which the breakdown takes place is called the dielectric strength of the material. Many variables such as the composition of the

gas, the electrode shape, the shape and frequency of the voltage curve, temperature, and the moisture content influence this value.

Besides breakdown at the poles of the particles, breakdown is possible between the electrodes placed in the bed. However, measurements (i.e. measuring current as a function of voltage) in columns with electrodes, but without particles, have not shown this to occur inside the bed. On the outside of the column, electrodes occasionally come into closer proximity than inside the bed, and there breakdown or sparking may occur. Careful design and insulation prevented this as much as possible.

The dielectric breakdown field of air is typically in the order of magnitude of 3 kV/mm, which means its dielectric strength is approximately 1 (the dielectric strength is always given relative to that of nitrogen). It is mentioned here because the dielectric strengths of many gases often used in chemical reactions (cf. Table 1-2) are significantly higher, thereby not precluding their use in electric field enhanced fluidized beds. However, many diatomic gases, notably hydrogen, have lower breakdown strengths, and application of these in an electric field enhanced bed should be considered with caution. Dilution of these gases with an inert gas, such as N_2, may provide a possible method of safe operation.

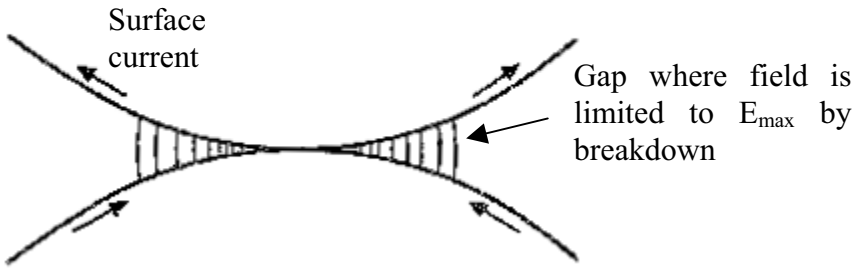

Figure 1-7. Constriction of the electric field close to the poles of the particles (adapted from Jones, 1995). The field intensity of two particles close to each other may increase to the level of breakdown.

Table 1-2. Dielectric strength of gases, relative to nitrogen. A relative dielectric strength of 1 means breakdown occurs between two flat electrodes at approximately 3 kV/mm (adapted from Handbook of Chemistry and Physics, 2000). The applied field strength in the experiments described in this thesis is always less than 1 kV/mm.

Material	Dielectric breakdown strength [-]*	Approximate field strength, E_{max} [kV/mm]
Nitrogen, N_2	1	3.0
Air	0.97	2.9
Hydrogen, H_2	0.5	1.5
Neon, Ne	0.16-0.25	0.48 - 0.75
Carbon monoxide, CO	1.02	3.1
Carbon dioxide, CO_2	0.85	2.6
Methane, CH_4	1.00	3.0
Ethyne, C_2H_2	1.1	3.3
Acetonitrile, ACN, CH_3CN	2.11	6.3

* Normalized to N_2

The breakdown of gas, or rather the production of ions, may have very beneficial effects on electric field enhanced fluidized beds. The ions produced by corona discharge are very mobile, and can strongly enhance the polarization of the particles. Attempts have been made (van Burgh, 2004) to use a controlled corona discharge in the feed of a fluidized bed in order to influence the electrical behavior of the system, but it was found to be difficult to create a consistent stream of both positive and negative ions, and to quantitatively measure them. Still, this seems a promising method of enhancing the effects of electric fields more, as well as a possible means of controlling electrostatic build-up in a system susceptible to static charging. Further treatment of corona discharge is, however, beyond the scope of this thesis.

Triboelectric charging

A completely different electrical phenomenon in fluidized beds than the polarization described above is *triboelectric charging*. Triboelectric charging occurs when two dissimilar materials are brought into contact, resulting in a redistribution of charge on the interface between them, and then are separated quickly enough that the charges

cannot return to their original locations. The result is a separation of charge, with one material acquiring a positive charge and the other an equal and opposite negative charge (see Figure 1-3 for a comparison of the strength of electrostatic forces to other forces).

In fluidized beds, the frequent contact and separation of particles with the wall will lead to the build-up of a significant level of charge if the rate of dissipation is lower than the rate of charging. When all particles are similar (i.e. a monodisperse size distribution and all of the same material), particle-particle tribocharging is in principle negligible, assuming that the material surfaces are not dissimilar. On the other hand, when particles with different dimensions are used, their surface morphology is usually dissimilar enough that a significant charging can occur. Still, it is usually the interaction of particles with the wall that is responsible for a net build-up of charge in the bed. The direction of charge separation is often difficult to predict, both between various particles and with walls. It has been reported (Moerman, 2005) that glass particles produced by the same manufacturing process but of different sizes in a Plexiglas column can charge positively for one size and negatively for another. In short, triboelectric charging in fluidized beds is a difficult phenomenon to predict.

The result of triboelectric charging of monodisperse particles in fluidized beds is the introduction of a particle-to-wall force. As the wall and particles charge with opposite signs, the force will be attractive. For this force to lead to an agglomeration of particles on the wall, a grounded conductive wall is not required. As long as the conductivity from particle to wall is low enough that charge does not dissipate, the particles will stick to the wall even if it is grounded (image force). Naturally, raising the gas velocity may tear the particles away from the wall, but higher flow rates also mean more agitation and movement of the particles, in turn leading to greater triboelectric charging.

In Chapter 5 of this thesis it is shown how the charge build-up is greatest on particles in the wake of the bubble. Although much work remains to be done in this field, it should be pointed out that particles in the wakes of bubbles are often ejected from the bed on bubble eruption, thus carrying large amounts of either positive or negative charge out of the bed. At low flow velocities, these particles will typically fall back, but at high velocities they are often carried out of the system.

The effect of the build-up of charge on particles in relation to electric field enhanced fluidization has not been shown experimentally. However, triboelectric charging is of particular importance for very dry, i.e. more insulating, systems, while electric field enhanced fluidization is most efficient at slightly elevated conductivity. Therefore, it would seem likely that under optimized electric field enhanced fluidization, triboelectric charges will quickly dissipate.

Conclusions

A short introduction to the description of electric field induced interparticle forces, as well as triboelectric charging, has been given in view of the application of electric fields to control and decrease the bubble size in fluidized beds. Some of these aspects, notably the Maxwell-Wagner effect on dielectric response and the electric charge distribution around bubbles due to triboelectric charging, are treated more rigorously later in this thesis. Other items, such as the corona charging and the effect of particle size on triboelectric charging, have been reported in other theses and in the scientific literature. However, the introduction that has been presented should give the reader enough background information for a proper understanding of electric field enhanced fluidization as presented in this thesis.

1.4 Notation

a_{ij}	center to center particle separation distance, m
A	Hamaker constant, J
d_p	particle diameter, m
e_r, e_θ	unit vectors in the r and θ directions, -
E	electric field strength, V / m
E_{max}	field strength at which dielectric breakdown occurs, V / m
F_{ij}	electric field induced interparticle force, N
K	Clausius-Mossotti function, -
p	dipole moment, C m

ε_0 permittivity of free space, 8.854 10^{-12} F / m

ε_{air} relative dielectric constant of air, -

ε_p relative dielectric constant of a particle, -

ρ_s density, kg / m^3

1.5 References

Block, H., and Kelly, J.P., 'Electro-rheology', *J. Phys. D Appl. Phys.*, **21** (1988), 1661-1677.

Boersma, A., and van Turnhout, J., 'Dielectric Study on Size Effects in Polymer Laminates and Blends', *J. Polym. Sci., Part B: Polym. Phys.*, **36** (1998), 2835-2848.

Epstein, N., 'Teetering', *Powder Technol.*, **151** (2005), 2-14.

Geldart, D., 'Types of gas fluidization', *Powder Technol.*, **7** (1973), 285-292.

Geuzens, P.L., 'Some Aspects of Magnetically Stabilized Fluidization', Ph. D. dissertation, Technische Hogeschool Eindhoven (1985).

Howard, J.R., 'Fluidized bed technology: principles and applications', Adam Hilger, Bristol and New York (1989).

Jones, T.B., 'Electromechanics of Particles', Cambridge University Press, Cambridge (1995).

Kleijn van Willigen, F., 'Electric Field Stabilized Fluidized Beds', internal report, Delft University of Technology (2001).

Kleijn van Willigen, F., van Ommen, J.R.,van Turnhout, J., and van den Bleek, C.M., 'Bubble Size Reduction in Electric-Field-Enhanced Fluidized Beds', *J. Electrostat.* **63** (2005), 943-948.

Kunii, D., and Levenspiel, O., 'Fluidization Engineering' (2nd ed.), Butterworth-Heinemann, Boston (1991).

Lide, D.R. (ed), *Handbook of Chemistry and Physics* (81st ed.), CRC Press, Boca Raton, FL (2000).

Moerman, M.J., 'Understanding the Electrostatic Charge Distribution in Gas-solid Fluidized Beds', M.Sc. thesis, Delft (2005).

Parthasarathy, M., and Klingenberg, D.J., 'Electrorheology: mechanisms and models', *Mater. Sci.Eng.: R: Reports*, **17** (1996), 57-103.

Rhodes, M., 'Fluidization of Particles by Fluids', *Educational Resources for Particle Technology*, **2**(1), http://www.erpt.org/012Q/rhod-00.htm (2001).

Sihvola, A., 'Electromagnetic mixing formulas and applications', Institution of Electrical Engineers, London (1999).

Van Burgh, M., 'Elimination of Electrostatic Charges in Fluidized Beds', B.Sc. thesis, Technische Hogeschool Rijswijk (2004).

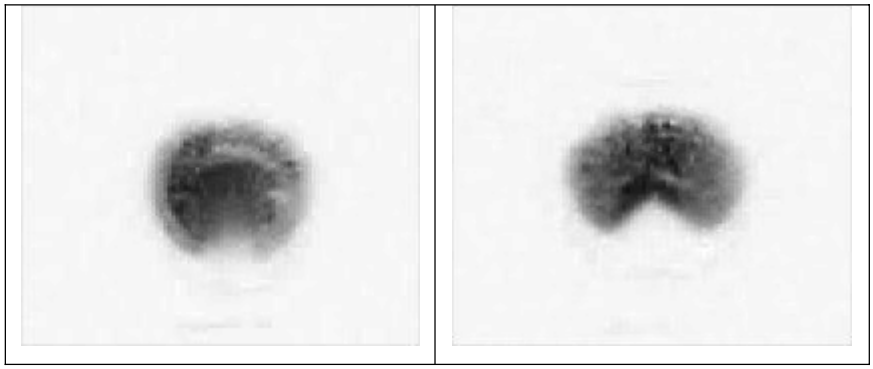

The change in bubble shape due to an electric field. Left: no field. Right: electric field, 10 Hz, 5 kV/cm.

(Kleijn van Willigen, F., van Ommen, J.R., van Turnhout, J., and van den Bleek, C.M., 'The influence of AC electric fields on bubbles in gas-solid fluidized beds', in: Proceedings of the 11th International Conference on Fluidization, Arena, U., Chirone, R., Miccio, M., and Salatino, P. (eds) (2004), 643-649.)

2. Bubble Size in Electric Field Enhanced Fluidized Beds

The first step taken in determing the viability of using electric fields as a means of controlling and reducing the size of bubbles in fluidized beds is experimental: is it possible to induce and to measure a change in bubble size in a fluidized bed with internal electrodes? The results of these experiments, the mesoscopic effects, are reported in this section. A pseudo-two-dimensional as well as a circular cross-section column were fitted with thin wire electrodes, pressure fluctuation measurements were verified and applied as a means of determining bubble size, and electric fields of various strenghts and frequencies were applied. The results reported show a marked decrease in bubble size – up to 85% for Geldart B glass beads, up to 25% for Geldart A glass beads.

The chapter is based on two published articles. Both provide the experimental results. Part A gives an overview of published literature, a verification of the use of pressure fluctuation analysis for determining bubble size, and experimental results for a two-dimensional and a circular cross-section electric field enhanced fluidized bed. Part B reviews the experimental results, and provides the initial link to the microscopic scale – the mechanism of particle polarization – and the macroscopic scale – the application of electric fields to large scale chemical reactors.

Part A

This part was published as:

Kleijn van Willigen, F., van Ommen, J.R., van Turnhout, J., and van den Bleek, C.M., 'Bubble Size Reduction in a Fluidized Bed by Electric Fields', *Int. J. Chem. Reactor Eng.*, **1**: A21 (2003). http://www.bepress.com/ijcre/vol1/A21.

2.A.1 Abstract

The reduction of the size of bubbles can improve both selectivity and conversion in gas-solid fluidized beds. Results are reported of the reduction of bubble size by the application of electric fields to uncharged, polarizable particles in fluidized beds. It is shown how average bubble diameters can be drastically reduced, with little change of the bed expansion. A literature review shows that to maintain smooth fluidization, electric fields in the direction of the gas flow, with a relatively low alternating frequency, are optimal. To measure average bubble diameters, a spectral decomposition technique of pressure fluctuation time series is used. Using this method, based on non-intrusive measurements, a characteristic length scale for bubble diameters can be found. It is shown experimentally, using video analysis, that this length scale is of constant proportionality for a given bed material and bed dimensions. The proportionality of the length scale to bubble diameter is independent of measuring height or gas velocity. With this, we have a tool for measuring bubble diameters in both 2-D and 3-D fluidized beds. Electric fields were applied to fluidized beds using thin wire electrodes placed inside the column. Both 2-D and 3-D columns were tested over a range of frequencies and field strengths. For Geldart A glass beads, an optimal range was determined at 5-20 Hz and 400-1600 V/cm fields. The reduction of bubble diameter was measured to be up to 25% for this system. Larger Geldart B glass particles show a larger reduction of bubble diameters - up to 85%. For these particles, the optimal frequency was at a higher range, 20-70 Hz. At higher frequencies (up to 100 Hz), bubble size reduction is less, but still substantial. Experiments in the 3-D column using Geldart A particles show a similar reduction in bubble diameters.

2.A.2 Introduction

Fluidized beds are quite common in the chemical and process industry, since they have several desirable properties. Their liquid-like behavior and continuous movement of particles allow for good heat transfer and temperature control. However, the appearance of gas bubbles lowers the mass transfer in bubbling fluidized beds. A reduction in bubble size by a factor of four can increase the conversion by as much as 84% (Levenspiel, 2002). Not only the conversion, but also

the selectivity will be affected positively (Kaart, 2002). Adaptations have therefore been proposed to reduce the bubble size and increase chemical conversion, selectivity and efficiency.

Baffles and staging are sometimes applied in industrial units, but the effect on the bubble size is often limited. More advanced methods of bubble size reduction have been reported as well: mechanical vibration of the bed (Kwauk, 1992), use of pulsed or fractal feeds (Coppens, 2001), and application of magnetic fields (Rosensweig, 1995, Hristov, 2002). However, the applicability of these methods is restricted by a high energy consumption or by problems associated with their implementation.

In this paper, results are reported of the application of electric fields to fluidized beds with the aim of reducing the bubble size in the bubbling fluidization regime. The fields applied require only a low power input (40-80 Watt per m^3 of fluidized bed. This is three orders less than for magnetic fields (Geuzens, 1985)). Moreover, only small electrodes need to be placed in the bed. The electric fields are applied in such a way that the free movement of particles – the basis for fluidization – is not impaired. Results will be given of the bubble size reduction achieved by applying electric fields of moderate strength (1-10 kV/cm), and low frequency (1-100 Hz).

A technique for determining the bubble size from pressure fluctuations measured in the bed is explored to assess changes in the bubble size both in flat, 2-D columns and in cylindrical, 3-D columns. By applying this technique, we are no longer limited to 2-D systems for visual observation, nor do we have to rely on measuring pressure drop or bed expansion in 3-D columns. A validation is presented of the pressure fluctuation method by using video image analysis.

2.A.3 Earlier Work

First, we will briefly review previous work on the effect of electric fields on fluidization. Much of this work lacked a sound, quantitative assessment of bubble behavior. Bed expansion and visual observation were often used, but these methods do not allow for a reliable measurement of the bubble size. The review also makes clear that the direction of the electric field, the fact whether an alternating (AC) or a constant (DC) field is used, and the relative humidity of the system are parameters

that have a strong impact, because they determine whether or not particle movement is preserved.

The electrical stabilization of fluidized beds is first mentioned in a patent granted to Katz (1967). He describes work on a circular fluidized bed of 10 cm in diameter. The electrodes consisted of a screen on which the fluidized material (glass, $d_p \approx 0.274$ mm) rests, and of a tapered brass rod located above the bed. A potential of 25 to 100 kV DC is placed between the electrodes. The field strength is so high that gas ionization occurs, which results in a non-fluidized bed. The dependence on surface conductivity is indicated. It is claimed that partial ionization of the fluidizing medium is required although this stabilizes the system so much that it collapses into a packed bed.

The first publication about the influence of electric fields on fluidization without gas ionization is by Johnson and Melcher (1975). They described the dynamics of stabilization of fluidized beds of semi-insulating particles. Cross-flow (field lines perpendicular to the gas flow), co-flow (field lines parallel to the flow), and bed suspension are discussed. Johnson et al. used sand particles with a mean diameter of 0.5 mm. The parameter examined most is the particle's conductivity, which is varied by changing the relative humidity of the gas from 8 to 99%. All experiments were done with DC. Examining a column with a square cross-section of 3.82×3.82 cm^2 equipped with electrodes on the column walls (cross-flow fields) and imposing a field of 2.62 to 9.18 kV/cm, they observed that the bubbles were distorted to fill the cross section of the bed, but that a state of fluidization was retained. At the higher field strengths, the bed became essentially frozen, with channeling of the gas flow. At lower field strengths, it is not clear whether the distorted bubbles passed through the fluidized bed, or whether agglomerates of particles above them suppress the gas voids – as if attempting to fluidize cohesive Geldart C material. At a low relative humidity, they observed a build-up of particles on the electrodes. After 2-10 minutes a thick layer of particles was formed. Frictional charging, which arises due to the long particle relaxation time at low humidities, is blamed for this phenomenon. Again, it is important to recall that the experiments were done with DC. They employed the same column in a co-flow configuration, but now with 0.635 cm square mesh screen electrodes, which allow particles to pass. From the photographs shown, it can be deduced that the setup had six alternating electrodes, spaced 4 cm apart. The

photographs also show that the screens have a strong influence on the fluidization: apparently some of the particles are suspended on the screens, resulting effectively in a stack of 5 small fluidized beds (multi-stage fluidized bed). Johnson et al. conclude that with DC fields in co-flow no 'state of fluidization seems to exist whereby particles and field form a rheologically unique continuum'. Between the electrodes strings of particles and little bubbles are seen at high relative humidities, whereas at lower humidities, large voids are created, which lead to frozen sub-beds. In a modified cross-flow set up, they also investigated an electromechanical bed support, using a slit orifice of 0.47 cm to support a 30 cm bed electrically. They conclude that the additional effect of the electric field is small, compared to the role the fluidization gas plays to support the bed.

In a later publication, Dietz and Melcher (1978) compared experimental results of a DC stabilized bed with theoretical calculations. Since a high DC voltage is used, the particles form strings, or are frozen in space. Both the minimum flow required to hold such a bed against a top screen and the minimum flow required to fluidize a stabilized bed were determined. Subsequently, measured shear stresses are compared with calculated ones. They use a simplification of the interparticle model proposed by Colver (2000) described below. The observations apparently corroborate the model, although it should be noted that frozen rather than fluidized beds are considered.

Zahn and Rhee (1984) and Moissis and Zahn (1986) describe experiments that build on Melcher's work. They focus on AC fields, and include the mechanisms of polarization and charge build-up around particle contacts, but they rule out electrostatic charging. Space charge effects were minimized by the use of dry air. These researchers have moved from electrostatic precipitator principles (static agglomeration of particles) to controlling fluidized beds. Stabilization (frozen beds) was no longer the issue – reduction of bubbles was. A stability analysis is included, but the experimental details and comparisons are rather sketchy. Zahn and Rhee state that 'under AC fields it is possible that attracting particles unlock twice each period when the fields go through zero so that the bed retains its fluidity. This small-scale jitter together with gas velocity perturbations may cause enough fluctuations for the particles not to clump together over a range of electric field strengths.' Their statement is in-line with what we will discuss later in this paper.

Wittmann et al. (1987) continued along the line started by Zahn and coworkers – the reduction of bubbles in fluidized systems. In a detailed set of experiments they

reported a change in bubble shape towards an ellipsoid under the influence of DC fields. The decrease in bubble velocity indicates that, like in the work of Melcher, DC fields provokes in a strong cohesion of particles in the bed, and a decrease in fluidity. Wittmann (1989) also provides a theoretical analysis of the effect of DC fields on semi-insulating particles with surface conductivity.

Elsdon and Shearer (1977) employed alternating electric fields to increase heat transfer. They use PMMA particles ($d_p \approx 240$ μm), which they allowed to acquire a static charge. They observed that in oscillating fields a maximum rise in heat transfer occurs at about 100 Hz. They also noticed that at lower gas velocities the optimum was not always reached at the highest potential.

Colver et al. (1977, 2000) presented an interparticle force model for a semi-insulating powder in alternating fields, and compared the model to several experimental data. Estimates for relevant characteristic times, as well as for the interparticle forces are given. Based on simple lumped circuit theory, field-frequency trends are predicted. They verify these trends experimentally on the basis of bed expansion. However, we will show that the measurement of bed expansion is insufficient to determine more subtle changes in bubble size; we therefore applied a pressure fluctuation analysis instead.

2.A.4 Interparticle Forces

The experiments described later, as well as those reviewed above, are based on the fluidization of semi-insulating particles in a non-conducting gas. In this section, the mechanisms of polarization are outlined. Sometimes reference will be made to the field of electrorheology. Electrorheological fluids are composed of small particles dispersed in non-conducting liquids, in which the flow properties (e.g. viscosity) are altered by applying electric fields. A review of the mechanisms and models has been given by e.g. Parthasarathy and Klingenberg (1996). Although the properties of the continuous phase in electrorheological fluids (liquid, often a non-conducting oil) differ from those of the gas used in fluidization, insight may be gained from the models proposed for particle-particle interaction.

Polarization

We will first consider the response of particles to an electric field. The particles do not carry a static charge which would result in Coulombic forces, but are polarized by a field-induced charge separation due to their relative dielectric constant $k_p > 1$ (cf. Figure 2A-1(A)). The molecular dipoles in the particles are oriented by the electric field. This alignment usually occurs much faster than the field oscillation frequencies used in our experiments (0.5-100 Hz). Because the particles are typically not uniformly dispersed, the calculation of the strength of the overall dipole moment becomes quite difficult, even after simplifying the particle dipoles to point dipoles. Approximations have been made and interparticle forces estimated. Such a model, however, cannot explain the frequency and conductivity dependence observed experimentally both in electrorheology and in electric field improved fluidization.

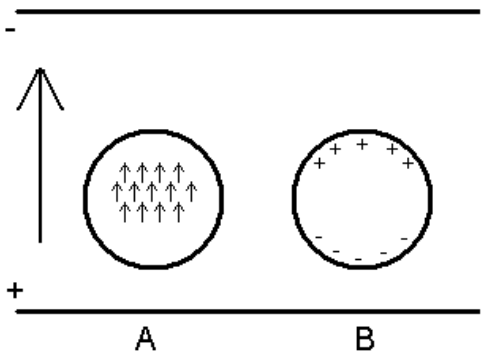

Figure 2A-1. Polarization of particles by an external field. (A) microscopic molecular dipole polarization. (B) macroscopic Maxwell-Wagner polarization by charge accumulation in the surface layer at the gas-solid interface.

The basic point that needs to be addressed is the polarization mechanism. As stated above, the polarization due to molecular dipole orientation reacts virtually instantaneously to field changes, and so this phenomenon cannot explain the observed frequency dependence. Therefore, the intrinsic particle bulk-conductivity and/or the particle surface conductivity (influenced by humidity) play a role in the experiments. The Maxwell-Wagner effect (see e.g. Parthasarathy, 1996) offers the simplest description of the data – it captures the polarization based on the movement of charges to the gas-solid interface owing to a finite conductivity (cf. Figure 2A-1(B)).

The conductivity may stem from both bulk and surface conductivity. The often strong influence of relative humidity on the hydrodynamics in electric fields and the less-than-expected influence of high dielectric constants in electrorheology, make it reasonable to assume that Maxwell-Wagner polarization by surface conduction is generally the dominant mechanism. The interfacial positive and negative charges then reside in the surface layer.

Magnitude of Interparticle Forces

After attributing the charge separation in the particle, either to molecular dipole orientation or interfacial Maxwell-Wagner polarization, or to a combination of both, the maximum interparticle force can be calculated. Figure 2A-2 illustrates the interactions between particles in an electric field in two positions. The particle-particle forces are an order of magnitude larger than for simple two dipole-dipole interactions. Chen et al. (1990) used an expansion of spherical harmonics to calculate interparticle forces in infinite chains of dielectric spheres in electrorheological suspensions. They report forces of 10^{-9} N / particle for 70 μm glass beads such as employed in our experiments. The forces calculated by Colver (2000) range from 10^{-10} to 10^{-8} N / particle. The electrical forces are of the order of the drag force and the force of gravity, but they decay quickly as the distance between the particles increases. In other words, the electric force is a relatively short-range attractive or repulsive force.

As the particle diameter increases, the drag and gravity forces grow faster in magnitude than the electric forces (see e.g. Jones, 1995). However, by virtue of the definition of fluidization, the drag and gravity forces balance each other. This allows even small forces to play a significant role in the fluidization. Such small forces are not only the polarization forces described here, but also van der Waals forces and electrostatic effects (Seville et al., 2000).

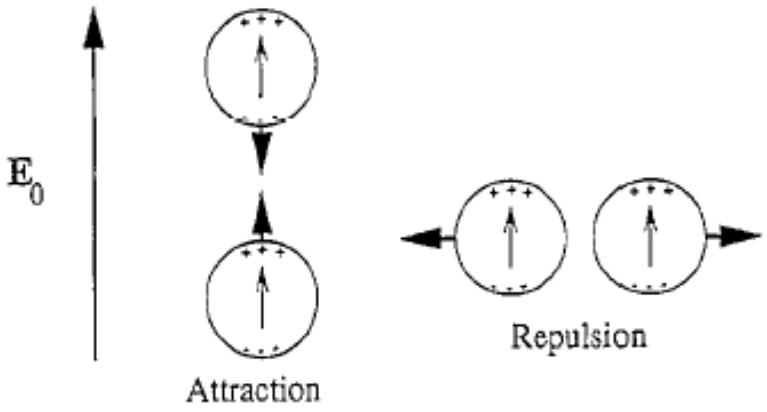

Figure 2A-2. Electric forces between particles polarized in an electric field by the Maxwell-Wagner effect due to the migration of opposite charges provided by the bulk conductivity. Drawing adapted from Parthasarathy et al. (1996).

What does this mean for fluidization in alternating electric fields? The particles will periodically experience a cohesive force in the direction of the field. This attraction force will depend on the frequency and is relatively stronger for smaller particles. The interparticle force, and its cyclic variation, will affect the hydrodynamic behavior of the fluidized bed. Under the right circumstances (force / frequency / direction) the tendency of the particles to form loose agglomerates will decrease the bubble size found in fluidized beds. The field strength must not be so high as to freeze the bed. We will show in section 5 that the range of frequencies that produce optimal bubble size reduction is bounded as well.

2.A.5 Experimental

Three types of fluidization experiments were conducted – in three different columns:

- Verification of the pressure fluctuation analysis to determine bubble sizes in a flat 2-D column.
- The influence of electric fields on fluidization in a flat, 2-D column.
- The influence of electric fields on fluidization in a cylindrical, 3-D column.

The 2-D column built to demonstrate that the bubble size can be deduced from pressure fluctuations measured along the side of the column will be described first. This first setup was operated without any electric field applied. A second column was fitted with electrodes and used for experiments on electric field improved fluidization.

The 2-D setups will be referred to by their cross-section, 400 × 15 mm^2 and 200 × 15 mm^2 respectively. The apparatus with the 3-D column, also equipped with electrodes, will be described last.

Validation of Pressure Fluctuation Analysis for Determining Bubble Sizes

The correlation between bubble size and the spectral power density analysis was verified in a transparent two-dimensional column with an internal cross-section of 400x15 mm^2. The bed support consists of a porous sintered bronze plate. The settled bed height was 800 mm.

At a height of 10, 200, 400, 600, and 800 mm above the support plate, as well as in the wind box, pressure fluctuations were measured using Kistler piezo-electric pressure transducers, type 7261. The charge from the piezo element was amplified and converted to a voltage using a Kistler amplifier type 5011. The signals were high-pass filtered with a cut-off frequency of 0.16 Hz. The transducers measured the pressure fluctuation relative to the average pressure with an accuracy of 2 Pa, and owing to the high-pass filter, the average of the measured pressure time series is zero. The sensors were connected to the column by 100 mm copper* tubes (i.d. 4 mm), which were covered with 40 μm mesh wire gauze at the tips to prevent particles from entering. The probe tips were fitted flush with the sidewalls. The total dead volume of sensor and probe was 2500 mm^3. In the range of frequencies typical for gas-solid fluidized systems (0-50 Hz), no significant distortion of the amplitude or phase of the pressure fluctuations was found (Van Ommen et al., 1999). The data were recorded with a SCADAS II data acquisition system from LMS-Difa. Time series typically consist of 184,320 points, sampled at 400 Hz (approximately 7.5 minutes).

A digital video camera (Sony DCR-TVR130E) was used to film the column. The area of the column under investigation was visible through a 'window' – the rest of the setup was covered to prevent stray light and reflections being recorded. The data were analyzed using Mathworks Matlab, Mathworks Image Analysis Toolbox, and the image analysis package DIPImage (Delft University of Technology). The recorded images were processed and filtered, after which the mean bubble diameter was determined for the first, second, third, and fourth quarter of the settled bed height.

* It was erroneously reported in the publication that the tubes were copper. In fact, Teflon tubes were used.

Bubble Size Reduction in a 2-D Column by Electric Fields

The 2-D electric field equipped column has an internal cross section of 200 × 15 mm^2. The support consists of a grounded porous sintered steel sieve plate, ΔP = 13 mbar at U = 1 cm/s, with a wind box of 300 ml. The walls, made from 6 mm thick transparent Plexiglas, are 700 mm high. The electrodes pass through the bed and consist of a regular wire pattern strung through the column front and rear. The electrodes are alternately, both horizontally and vertically, grounded or connected to a Trek 20/20C high-voltage power supply (Figure 2A-3). The electrodes thus create a quadrupole field with horizontal and vertical components (cf. inset). The nichrome wires have a diameter of 250 μm. The volume density of the wires is about 0.008%. The holes in the outer walls through which the wires pass were sealed. The column was placed in a temperature-controlled cabinet. The settled bed height is 300 mm.

At 10, 100, 190, and 300 mm above the support plate, pressure fluctuations were measured using Kistler piezo-electric pressure transducers. The sensors are connected by 500 mm Teflon tubes (tips flush with the sidewalls); this results in a total dead volume of sensor and probe of 7500 mm^3. Again, such probes will not distort the pressure fluctuations (Van Ommen et al., 1999).

An LMS SCADAS III system is used for data acquisition. This system samples the measuring probes and provides the source signal for the Trek high-voltage power source. The potential generated by the HV source is sinusoidal, with a mean of zero. The frequencies range from 0.5 to 100 Hz. The measured time series consist of 102,400 points sampled at 400 Hz (approximately 4.25 minutes).

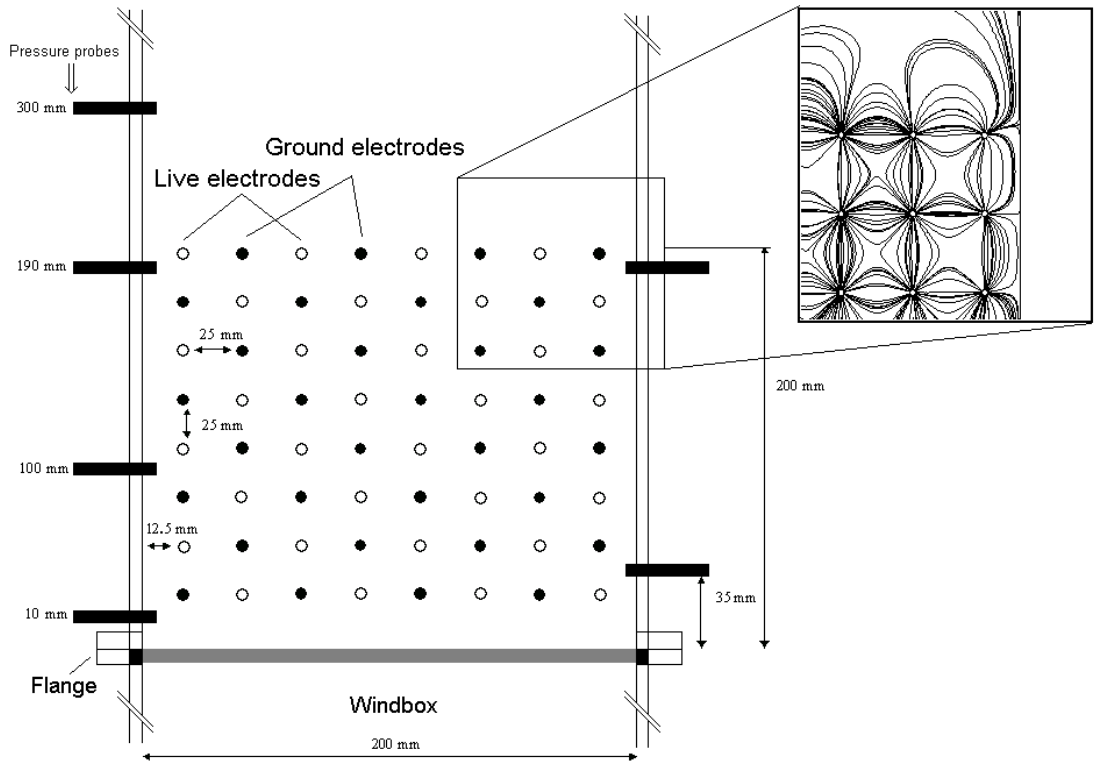

Figure 2A-3. 2-D column design, inset depicts the quadrupole-like electric fields between the electrodes. Open circles represent live electrodes, while closed dots represent grounded electrodes. The positions of the pressure probes are also indicated.

Bubble Size Reduction in a 3-D Column by Electric Fields

The design of the 3-D column (Figure 2A-4) is similar to the 2-D column with electrodes, albeit that for practical reasons the electrodes are now so situated that the field is purely co-flow (vertical field lines). This implies that although the electrode wires are again located inside the column, the horizontally alternating electrode pattern depicted in Figure 2A-3 is no longer present. The horizontal external field component is therefore absent. The cylindrical system consists of a Plexiglas inner column, i.d. 80 mm. At eight levels (i.e. 12.5 mm, 25 mm, etc. of the column height) a continuous wire is strung, creating a grating-like pattern of wire with a spacing of 10 mm. The electrode grating on the next level is rotated by 90˚ (cf. Figure 2A-4 top view). Each electrode grating thus runs crosswise to its nearest neighbors. The total height of the electrode section is 100 mm. The volume density of the electrodes is approximately 0.004%. For safety reasons, the wired inner column was placed in a Plexiglas outer column.

Pressure fluctuation sensors were installed in the wind box and at 20, 70, and 120 mm above the porous bed support. The measurement and data acquisition part of the setup is identical to the previously described 200 × 15 mm^2 2-D column, with the exception of the electrical power source. The frequencies that could be applied were limited to 1, 2, and 3.3 Hz square waves, and 50 Hz sine waves.

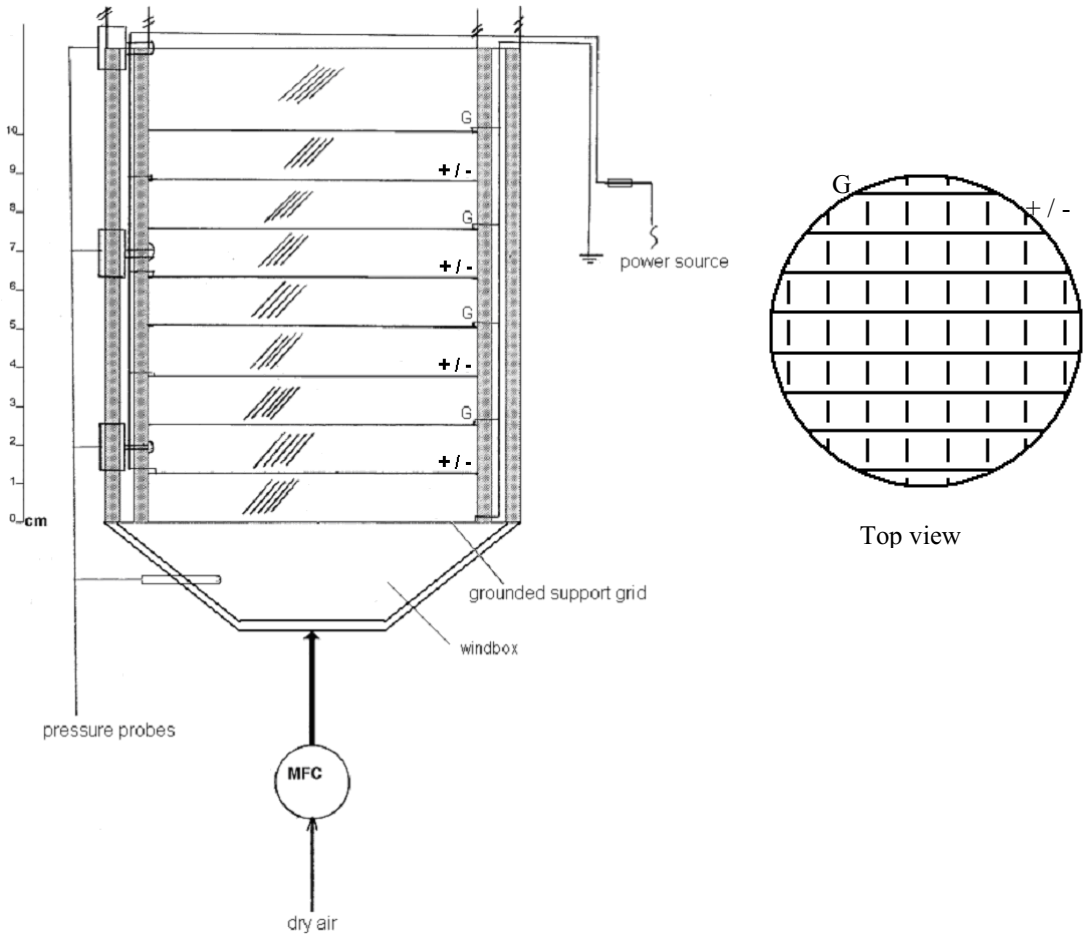

Figure 2A-4. Side view of the 3-D column showing electrodes and pressure probe connection points. The top view depicts the intercrossing of two of the eight electrode-gratings, one of which is connected to the HV-supply, while the other is grounded.

Particle Properties

We took two types of particles for the experiments conducted in the 400 × 15 mm^2 column, to validate the relation between bubble diameters and pressure fluctuations:

- Mono-disperse glass beads, diameter d_p = 77 μm, minimum fluidization velocity U_{mf} = 1.0 cm/s. This powder is classified as Geldart A material.

- Sand, diameter range d_p = 200 – 400 μm, U_{mf} = 11.0 cm/s. This is Geldart B material.

For the electric field experiments, two types of glass beads were chosen:

- Mono-disperse glass beads, diameter d_p = 77 μm, U_{mf} = 1.0 cm/s, same as for the experiments above. The relative dielectric constant of settled bulk material was determined in a dielectric cell to be k_b = 7 at low frequencies.
- Mono-disperse glass beads, diameter d_p = 700 μm, U_{mf} = 33 cm/s, this is Geldart B material. The bulk dielectric constant, k_b, for this material is 3. This material was not used in the 3-D experiments.

2.A.6 Results and Discussion

Measuring Pressure Fluctuations to Determine Bubble Size

The measurement of pressure fluctuations is an attractive method to characterize the hydrodynamic behavior of a fluidized bed because it is virtually non-intrusive and applicable in industrial situations. The pressure fluctuations can be measured using the probes described in the experimental section, in a manner that causes minimal disturbance of the hydrodynamic behavior. In our case, we are especially interested in the bubble characteristics, and the pressure fluctuations associated with the rising of bubbles through a fluidized bed provide an indirect measurement of their size and velocity. However, the pressure fluctuations are not only caused by the bubbles themselves – the phenomenon we are interested in – but also by other sources such as the formation, coalescence, and eruption of bubbles.

A technique proposed by van der Schaaf et al. (2002) was used to decompose the pressure fluctuation time series in its different components. They used the coherence between two time series measured at different heights in the fluidized bed to distinguish between the different components of the pressure signals. Bubble coalescence, gas flow fluctuations, bubble eruption, and bed mass oscillations generate a fluctuation in gas velocity, which produces pressure waves that are measured almost simultaneously throughout the entire bed. These signals are therefore *coherent*. However, the gas bubbles rising through the bed cause local fluctuations in pressure, and are not measured along the entire column. These fluctuations are *incoherent*. Using a spectral decomposition technique, the incoherent

power spectral density is calculated, and subsequently the corresponding incoherent standard deviation, σ_i, is determined.

As gas bubbles rise through a fluidized bed, they create pressure fluctuations with an amplitude directly proportional to their diameter (Davidson and Harrison, 1963); this can be expressed in an incoherent standard deviation, σ_i. This standard deviation is proportional to the amplitude of the fluctuation, and is a characteristic length scale (L_I) of the bubble diameter:

$$\frac{\sigma_i}{\rho_s g(1-\varepsilon_{mf})} = L_I \approx F \cdot D_b \qquad [2A - 1]$$

By measuring the pressure fluctuations at two bed heights, decomposing these in a coherent and an incoherent part, representing fast waves and bubble phenomena respectively, and examining the incoherent standard deviation, the characteristic length scales of bubbles can be ascertained. This length scale is proportional to the bubble diameter D_b. F is a constant, which is independent of bed height and superficial gas velocity. Typically, the measurements from the wind box are compared to the height under consideration. If the support plate distorts the signal too much, for example due to a high pressure drop, the measurements from within the bed just above the support plate can be used. In the results given in this paper, the incoherent power spectral density is always determined relative to the wind box signal.

Van der Schaaf et al. showed that the above method holds in a three-dimensional column (0.385m diameter, sand particles) by comparing the Darton bubble diameters (Darton, 1977) to the diameters derived from pressure fluctuations, but they did not present any direct experimental evidence. In the experiments in the 400x150 mm^2 2-D column, we used a digital video camera to verify the relation between pressure fluctuations and bubble size. The results are plotted over a range of fluidization velocities for two bed materials in Figure 2A-5, both at a height of 600 mm (settled bed height H_b = 800 mm). Figure 2A-5A presents the results for Geldart A glass beads. For these particles, the proportionality constant F between the bubble diameters determined from video analysis or the Darton relation and the characteristic length determined from the pressure fluctuations is ca. 8.1. For the Geldart B material (cf. Figure 2A-5B), the proportionality factor is ca. 1.3.

The video image analysis was sensitive enough to detect bubbles smaller than the column depth (15 mm) as well as larger bubbles – the cutoff size is 7.5 mm. However, in this method we overestimate the size of the smaller bubbles. In addition, it appears that the Darton relation for bubble diameters holds well for the Geldart A material, but the fact that we are analyzing bubbles in a flat 2-D column plays a much greater role for the bubbles in Geldart B material. The Darton bubble diameters for Geldart B particles are much larger, and not shown in the figure.

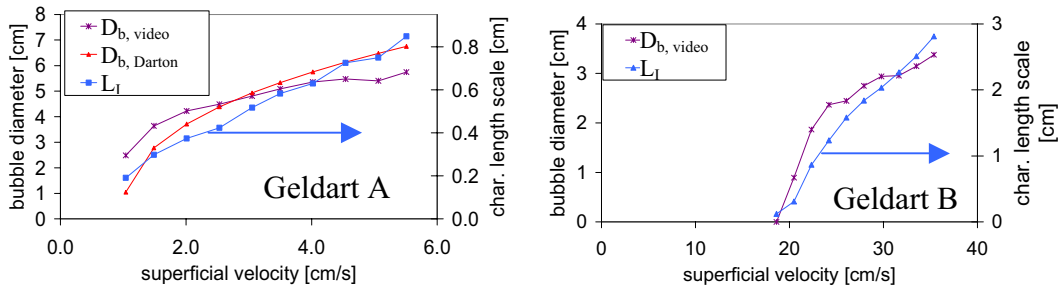

Figure 2A-5. Comparison between mean bubble diameter determined by pressure fluctuation analysis, at 75% of the bed height, and video and Darton diameters. Left vertical axes show the arithmetic mean bubble diameter obtained from the video analysis (video: $D_{b,video}$) and the calculated (Darton relation: $D_{b,Darton}$) bubble diameter. The vertical axes on the right show the characteristic length scale calculated from the pressure fluctuations (L_I). The data in Figure 5A were gathered from fluidization of Geldart A glass beads; the 5B data are from the fluidization of Geldart B sand.

From these and other results it can be concluded that the bubble diameter calculated from the incoherent standard deviation correspond well to that determined by video analysis. The proportionality constant F is a constant for a given bed material and a range of velocities and measuring heights, but cannot yet be predicted for various bed materials.

Bubble Size Reduction in a 2-D Column by Electric Fields

The effectiveness of electric fields on the bubbling behavior in the electrically wired columns can be evaluated using the quantitative correlation between pressure fluctuations and bubble size established in section 5.1. Because the exact values of the proportionality constant, F, are not known, all results are given as a decrease in

percent or fraction of the bubble diameter for the situation without electric field. The experiments were all performed in the 200 × 15mm^2 column using sinusoidal AC fields of varying frequency and strength.

The results of two different bed materials are shown in the color plots of Figs. 2A-6 and 2A-7. Figure 2A-6 shows the impact of the electric field on the Geldart A material, the 77 μm glass beads. The results represent data for a gas flow of three times the minimum fluidization velocity. Bed expansion during fluidization with and without electric field was visually observed to be very similar, and fluidity (particle movement) was conserved. However, the fact that the bed expansion is not changed does not mean that the bubble behavior remains unchanged. In fact it changes considerably, as we could prove by our pressure fluctuation analysis. The reduction in bubble diameter at the measuring height shown is about 25% compared to the blank experiments. This corresponds to a decrease in bubble volume (assuming spherical bubbles) of approximately 60%. In view of the drop in total bubble volume, we speculate that the interstitial gas flow is increased. Further experiments will be carried out to check this.

From Figure 2A-6 it is also clear that an optimal regime of electric fields exists: the applied fields should range from 400 to 2000 V/cm, although an effect is observed even at low field strengths. The frequencies are most optimal between 5 and 20 Hz. The limits seen on the frequency range can be understood in a qualitative manner: at low frequencies, the bed characteristics change to a DC-like behavior, eventually resulting in compaction and agglomeration. This leads to a (partially) frozen bed. At high frequencies, there is not enough time for the macroscopic charge separation to develop – confer the relaxation times listed by Colver (2000). At the lower voltage limit, the electric interparticle forces are too small to play a role in the bubble behavior. At too high field strengths, it is likely that the particles stick together too strongly, resulting in more cohesive fluidization with its associated gas voids.

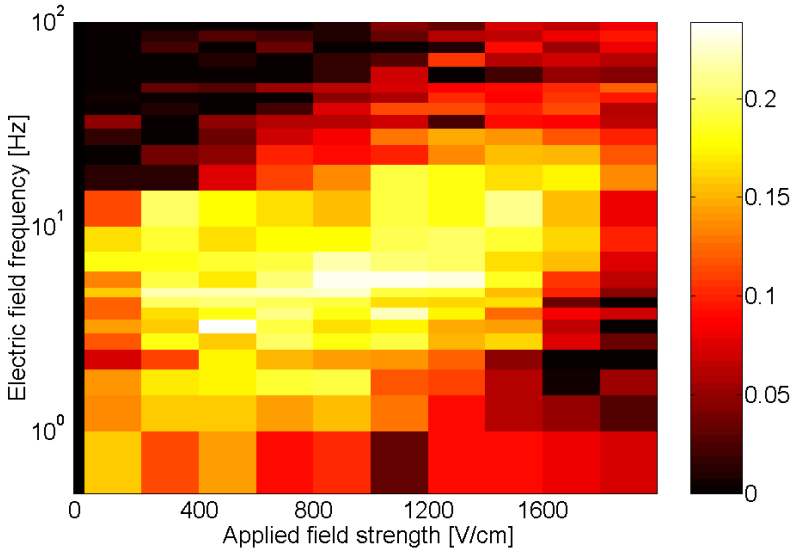

Figure 2A-6. Color plot of bubble size decrease at 190 mm (63% of bed height) as a function of frequency and applied field. The color scale displays the decrease as a fraction of the mean bubble diameter for the situation without field i.e. before and after application of the external field. Bed material: 77 µm glass beads. The optimal working region is the yellow one, in which the decrease amounts to about 25%.

Similar experiments were conducted for larger glass beads (d_p=700 µm). For these Geldart B particles bubbling behavior is much more pronounced, and homogeneous fluidization is not a standard feature. The flow rate was 1.5 × U_{mf}. It was confirmed visually that fluidization was maintained throughout the experiment. The results show a much larger decrease in incoherent standard deviations than for the smaller particles, up to 85% as compared to the zero-field situation. Again an optimal frequency range of 20 to 70 Hz emerges, although less pronounced than in the Geldart A experiments. Still a strong dependence on the frequency and voltage combination is evident. The stronger tendency of the Geldart B particles to bubble is responsible for the shift to higher fields. Contrary to the experiments with finer particles, no bubble size reduction is noticed at low field strengths in these experiments.

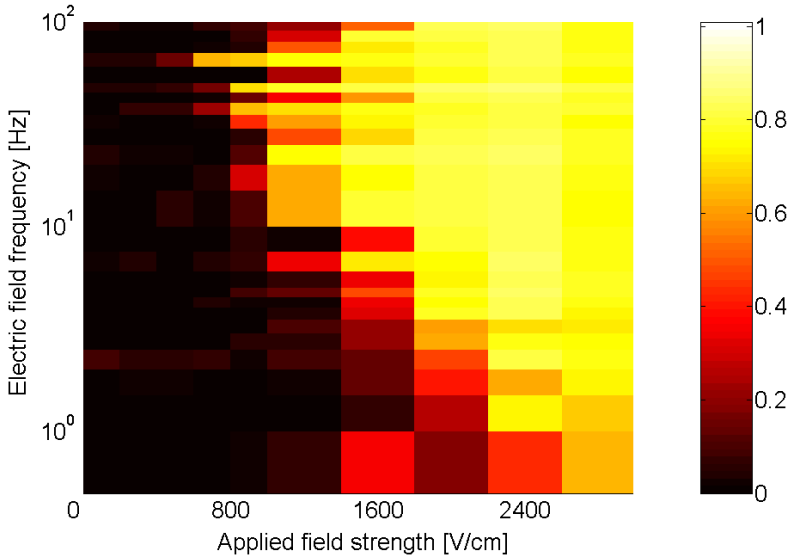

Figure 2A-7. Color plot of bubble size decrease at 190 mm (63% of bed height), as function of frequency and applied field. Bed material: 700 µm glass beads. Note that the color scale range now extends to a fraction of 1 of the bubble size at zero field. The optimal region, in which the decrease goes up to 0.8 or 80%, is again colored yellow.

Bubble Size Reduction in a 3-D Column by Electric Fields

In the 3-D column the direction of the electric field is different from the 2-D design due to practical limitations. The applied AC-field between all 90°-to- 90° stacked gratings or electrode layers is directed up- and downward, as can be seen from Figure 2A-4. In addition, the electric field frequencies were limited to square waves of 1, 2, and 3.3 Hz, and sine waves of 50 Hz. The top electrode is located at 71% of the settled bed height.

Results are shown at the same flow velocity as the 2-D experiments with Geldart A particles: 3 × U_{mf}. The preference for slowly oscillating frequencies is clearly demonstrated (Figure 2A-8A). In addition, an optimal voltage range is again observed, at various heights in the column (Figure 2A-8B). The decrease in bubble size is comparable to that measured in the 2-D experiments. It is interesting to note that the drop in bubble diameter as a function of frequency in the 3-D column does not show the maximum seen in the 2-D experiments. A likely explanation is that the low frequency (1, 2, and 3.3 Hz) fields in the 3-D experiments are square waves – therefore, a period of relaxation of the interparticle force basically does not exist,

allowing little time for the particles to separate. This in turn is not beneficial to the fluidity of the bed.

Experiments to compare the effect of square wave alternating fields with sinusoidal ones will be carried out in the near future. We also plan to investigate the frequency and field dependence in a 3-D column in more detail.

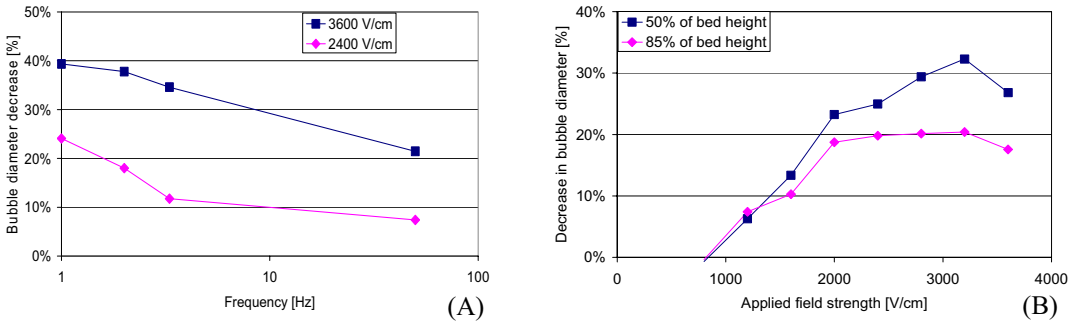

Figure 2A-8. A. Frequency dependence of bubble decrease in the 3-D column, measured at 50% of the bed height. B. Field strength dependence in the 3-D column, with 3.3 Hz block waves. The measurements were done at 50 and 85% of bed height.

2.A.7 Conclusions

We showed that the use of electric fields yields a significant bubble reduction. In order to maintain smooth fluidization, co-flow AC-fields with a relatively low frequency are optimal. The literature review showed that DC fields, on the other hand, tend to inhibit the free movement of particles and result in a build-up of particles on the electrodes.

The mechanism of polarization is related to that found in electrorheology. In this field, as well as in fluidization experiments, it was observed that the field frequency affects the strength of the dipole moment, suggesting that the surface conductivity is the dominant factor in the interfacial Maxwell-Wagner polarization of the particle. In addition, the strength of the interparticle force depends strongly on the interparticle distance, and is relatively stronger for smaller than for larger particles. For Geldart A particles, the electric force is comparable to the drag and gravity forces. For the larger Geldart B particles, drag and gravity forces quickly exceed the

electrical forces. However, because the drag and gravity forces balance each other, small forces can still play a significant role in the fluidization of larger particles.

Time series analysis of pressure fluctuations was explored to quantify the changes in bubble size. By comparing the time series measured simultaneously in the wind box and in the fluidized bed, a characteristic length scale for the bubble diameter could be derived. This technique, proposed by van der Schaaf et al. (2002), was tested in a 2-D column using video image analysis. It was found that the bubble diameter is proportional to the incoherent standard deviation at the range of fluidization velocities and measuring heights studied, but that the proportionality factor depends on the type of material being fluidized. The influence of the dimensions of the column was not investigated.

By invoking the pressure fluctuation analysis, a marked reduction in bubble size was found in both 2-D and 3-D columns with electrodes. For 77 μm particles, it turned out that bubble diameters could be decreased by 25-35%, both in 2-D and 3-D columns. The reduction in bubble diameter when larger particles are fluidized is even more dramatic, up to 85%. The use of sinusoidal, low frequency fields allows particle movement, and thus the state of fluidization, to be preserved – an improvement over much of the earlier work. The optimal frequency differs for the different particle sizes – approximately 5-20 Hz for small particles, to 20-70 Hz for particles with a diameter of 700 μm. The bed height was seen to change very little upon applying the electric fields, despite the fact that the average bubble volume becomes much smaller. Future work will be conducted to find out whether the total bubble volume is decreased likewise.

2.A.8 Notation

d_p particle diameter, m

D_b bubble diameter, m

F proportionality constant, -

g gravitational acceleration, m/s^2

H_b settled bed height, m

k_b dielectric constant of bulk material, -

k_p dielectric constant of particle, -

L_I characteristic length scale derived from pressure fluctuation analysis, m

U superficial velocity, m/s

U_{mf} minimum fluidization velocity, m/s

ΔP pressure drop, mbar

ε_{mf} bed porosity at minimum fluidization conditions, -

ρ_s solids density, kg/m^3

σ_i incoherent standard deviation, Pa

2.A.9 References

Chen, Y., Sprecher, A.F., and Conrad, H., 'Electrostatic particle-particle interactions in electrorheological fluids', *J. Appl. Phys.*, **70** (1991), 6796-6803.

Colver, G.M., 'Bubble control in gas-fluidized beds with applied electric fields', *Powder Technol.*, **17** (1977), 9-18.

Colver, G.M., 'An interparticle force model for ac-dc electric fields in powders', *Powder Technol.*, **112** (2000), 126-136.

Coppens, M.-O. 'Method for operating a chemical and/or physical process by means of a hierarchical fluid injection system', US Patent 6333019 (2001).

Darton, R.C., LaNauze, R.D., Davidson, J.F., and Harrison, D., 'Bubble growth due to coalescence in fluidised beds', *Trans. Inst. Chem. Eng.*, **55** (1977), 274-280.

Davidson, J.F., and Harrison, D., 'Fluidized Particles', Cambridge Univ. Press, Cambridge (1963).

Dietz, P.W., and Melcher, J.R. 'Interparticle electrical forces in packed and fluidized beds', *Ind. Eng. Chem. Fundam.*, **17** (1978). Pp. 28-32.

DIPImage image analysis software, Pattern Recognition Group, Department of Applied Physics, Delft University of Technology.

Elsdon, R., and Shearer, C.J., 'Heat transfer in a gas fluidized bed assisted by an alternating electric field', *Chem. Eng. Sci.*, **32** (1977), 1147-1153.

Geuzens, P.L., 'Some Aspects of Magnetically Stabilized Fluidization', PhD-thesis, Technical University of Eindhoven, The Netherlands (1985).

Hristov, J., 'Magnetic field assisted fluidization – a unified approach: a series of review papers', *Rev. Chem. Eng.*, **18**, Nos. 4-5 (2002).

Johnson, T.W., and Melcher, J.R., 'Electromechanics of electrofluidized beds', *Ind. Eng. Chem., Fundam.*, **14** (1975), 146-153.

Jones, T.B. 'Electromechanics of Particles' Cambridge University Press, Cambridge (1995).

Kaart, S., 'Controlling Chaotic Bubbles', PhD-thesis, Delft University of Technology (2002).

Katz, H., 'Method of stabilizing a fluidized bed using a glow discharge', U.S. Patent 3304249 (1967).

Kwauk, M., 'Fluidization: Idealized and Bubbleless, with Applications', Science Press, Beijing (1992).

Levenspiel, O., 'G/S reactor models – packed beds, bubbling fluidized beds, turbulent fluidized beds and circulating (fast) fluidized beds', *Powder Technol.*, **112** (2002), 1-9.

Moissis, A.A., and Zahn, M., Conf. Record 1986 IEEE Industry Applications Soc. Annual Meeting, Part II (1986), 1396-1403.

Parthasarathy, M., and Klingenberg, D.J., 'Electrorheology: mechanisms and models', *Mater. Sci.Eng.: R: Reports*, **17**, (1996), 57-103.

Rosensweig, R.E., 'Process concepts using field-stabilized two-phase flow', *J. Electrost.*, **34** (1995), 163-187.

Seville, J.P.K., Willett, C.D., and Knight, P.C., 'Interparticle forces in fluidisation: a review', *Powder Technol.*, **113** (2000), 261-268.

Van Ommen, J.R., Schouten, J.C., vander Stappen, M.L.M., van den Bleek, C.M., 'Response characteristics of probe-transducer systems for pressure measurements in gas-solid fluidized beds: how to prevent pitfalls in dynamic pressure measurements', *Powder Technol.*, **106** (1999), 199-218. Erratum: *Powder Technol.*, **113** (2000), 217.

Van der Schaaf, J., Schouten, C.C., Johnsson, F., van den Bleek, C.M., 'Non-intrusive determination of bubble and slug length scales in fluidized beds by decomposition of the power spectral density of pressure time series', *Int. J. Multiphase Flow*, **28** (2002), 865-880.

Wittmann, C.V., and Ademoyega, B.O., 'Hydrodynamic changes and chemical reaction in a transparent two-dimensional cross-flow electrofluidized bed. 1. Experimental results', *Ind. Eng. Chem. Res.*, **26** (1987), 1586-1593.

Wittmann, C.V., 'Hydrodynamic changes and chemical reaction in a transparent two-dimensional cross-flow electrofluidized bed. 2. Theoretical results', *Ind. Eng. Chem. Res.*, **28** (1989), 454-470.

Zahn, M., and Rhee, S-W, 'Electric field effects on the equilibrium and small signal stabilization of electrofluidized beds', *IEEE Trans. Ind. Appl.*, **IA-20** (1984), 137-147.

Part B

This part was published as:

Kleijn van Willigen, F., van Ommen, J.R., van Turnhout, J., and van den Bleek, C.M., 'Bubble Control in Fluidized Beds by Applied Electric Fields', proceedings of the 7th World Congress of Chemical Engineering, Glasgow, Scotland (2005).

2.B.1 Abstract

Reducing the size of gas bubbles can significantly improve the performance of gas-solid fluidized beds. However, such a control of bubbles is difficult to realize without measures that either use a lot of energy or deteriorate the fluidization behavior. In this paper, we present results on the application of low-energy electric fields capable of reducing the average bubble size by as much as 80%, while maintaining the free movement of particles so essential to fluidization. The power consumption in such a system, ideally consisting of non-conductive, dielectric particles in dry gas, is as low as 50 W/m^3.

2.B.2 Introduction

The applications of gas-solids fluidized bed reactors are widespread in chemical and physical processes. Their liquid-like behavior and continuous movement of particles allow for good heat transfer and temperature control. However, the appearance of gas bubbles lowers the mass transfer in bubbling fluidized beds. A reduction of the bubble size by a factor of four can almost double the conversion (Levenspiel, 2002). Moreover, for parallel and/or series reactions (which is the case in almost every realistic situation) smaller bubbles lead to a higher selectivity for the desired product (Kaart et al., 2002). A number of (more or less practical) methods are available to reduce bubble diameters and increase phase contact, such as internal baffles (Van Dijk et al., 1988), pulsed or fractal gas injection (Coppens and van Ommen, 2003), mechanical vibration (Kwauk, 1992), and magnetic fields (Hristov, 2002). Here, an alternative to these often energy-intensive methods is proposed: the application of electric fields as a means to control bubble size in bubbling fluidized beds.

The application of electric fields is a way to decrease the bubble size in fluidized beds at low energy costs. In this work, thin wire electrodes are placed in the fluidized bed, perpendicular to the flow. When fluidizing semi-insulating glass particles by air and applying an electric field of moderate strength (0-5 kV/cm) and low frequency (1-100 Hz), a significant decrease of gas bubble sizes can be observed. We will show that for both Geldart A and B materials, bubble size and number of bubbles decrease. This was determined using a Fourier analysis of pressure

fluctuation time-series and video analysis of 2-D columns. We stress that fluidization of the emulsion phase is maintained – particles are still free to move.

First, the underlying mechanism of polarization by the application of electric fields, and the resulting interparticle forces in fluidized beds, will be described. This is followed by the experimental results and discussion. In addition, some preliminary insights and views are offered on the extension of this work to full-scale fluidized-bed reactors at industrial conditions.

2.B.3 Theory

The influence of small variations in interparticle forces on fluidization behavior has been shown both experimentally (*e.g.* liquid bridges (Seville and Clift, 1984), magnetic forces (Saxena and Wu, 1999)) and in discrete element models (*e.g.* Rhodes et al., 2001). In this work, the interparticle forces are the result of the electric polarization of particles. The degree of polarization (or electric dipole moment), P, of the particles (diameter d_p) in a fluidized bed is a function of the electrical conductivity, σ, and dielectric constants of particle and continuous phase (ε_p and ε_c), as well as the electric field strength, E_0.

$$P = f(d_p^3, \varepsilon_p, \varepsilon_c, \sigma(\mathrm{RH}), E_0) \qquad [2B - 1]$$

The conductivity of the particles is strongly influenced by the relative humidity, RH, of the fluidizing gas.

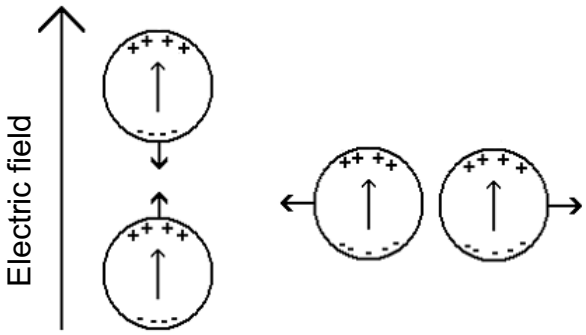

Figure 2B-9. Interparticle forces between polarized particles.

The interparticle force, F_{el}, between two particles *i* and *j*, with dipole moments P_i and P_j, separated by a distance *a* between their centers of mass, can then be calculated as follows:

$$F_{el} = \frac{6 \cdot P_i \cdot P_j}{4 \cdot \pi \cdot \varepsilon_0 \cdot a^4} \qquad [2B - 2]$$

ε_0 denotes the permittivity of free space. Clearly, these interparticle forces are strongly dependent on the separation distance and may be attractive or repulsive (*cf.* Figure 2B-9). The maximum strength of these forces, as they are created in the experiments described in this paper, ranges from 10^{-10} to 10^{-8} N per particle for Geldart A particles. This is comparable to the typical fluidization forces, such as drag and buoyant weight. For larger particles, *i.e.* Geldart B, the ratio between electrical interparticle forces and fluidization forces becomes much smaller. This is illustrated by the ratio between electrical forces and fluidization forces (drag, gravity) as a function of particle diameter. The electrical interparticle force, as seen from Eq. 2B - 1 and 2B - 2, scales roughly with the square of the particle diameter. Note that the center-to-center particle separation distance, *a*, is closely related to d_p (Eq. 2B - 3). The fluidization forces, on the other hand, scale with the particle diameter to the third power (Eq. 2B - 4).

$$F_{el} \propto \frac{P_i \cdot P_j}{a^4} \propto \frac{d_p^3 \cdot d_p^3}{a^4} \approx d_p^2 \qquad [2B - 3]$$

$$F_{fluidization} \propto d_p^3 \qquad [2B - 4]$$

In this interpretation of electrical interparticle forces we consider closely spaced particles under the constant influence of electric fields. While particle separation distances in bubbling fluidized beds are generally very small, the electric fields applied in the current design are oscillating – typically sine waves with a mean of 0 V/m and a frequency ranging from 0.5 to 200 Hz. The electrical interparticle forces thus vary periodically. Every sine period the interparticle forces relax twice, but their sign never changes: positive charges attract negative charges as strongly as vice versa.

The oscillation of the AC fields has the advantage over constant (DC) electric fields that agglomeration of particles is unlikely. Yet, the net effect of the electric fields is a decrease in the number and size of gas bubbles in the fluidized bed. The presence of the electric interparticle forces, acting in x-, y-, and z-directions, can prevent or reduce the instability that may lead to bubble formation (*cf.* Rietema and Piepers, 1990, Ye et al., 2004).

2.B.4 Experimental

In the description given above a reasonable case has been made for how interparticle forces resulting from non-homogeneous, oscillating electric fields can lead to a decrease in the bubble formation in a fluidized bed while maintaining the fluid-like behavior of the system. This has been demonstrated experimentally in both circular cross-section and so-called 2-dimensional columns. Measurements were conducted in two Plexiglas columns (2-D cross-section: 200 × 15 mm^2, 3-D inner diameter: 80mm) by pressure fluctuation analysis and/or video analysis. The electrodes consist of a regular wire pattern strung through the column, passing through the bed, as shown schematically in Figure 2B-10. The sintered porous distributor plate is grounded, and therefore serves as one of the electrodes. The wire electrodes are alternately, both horizontally and vertically, grounded or connected to a Trek 20/20c high-voltage power amplifier. The nichrome wires have a diameter of 250 μm. The holes on the outer walls through which the wires pass were sealed. An effect of the physical presence of the wires (with a volume density in the bed of 0.008%) on bubbles cannot be discerned using the employed measuring techniques. The experiments were conducted in a temperature-controlled cabinet, and the settled bed height was typically 300 mm. Glass beads of Geldart group A (d_p = 77 μm, u_{mf} = 1.0 cm/s, u_0 = 3 u_{mf}) and Geldart group B (d_p = 700 μm, u_{mf} = 33 cm/s, u_0 = 1.5 u_{mf}) were studied.

2.B.5 Results

Results are shown as a fractional decrease in the bubble diameter. This change in bubble diameter is based on analysis of pressure fluctuation time series before, during, and after the application of the electric field. The quantitative relation between the

visually observed bubble diameter and the bubble diameter derived from pressure fluctuations has been shown earlier by Kleijn van Willigen et al. (2003).

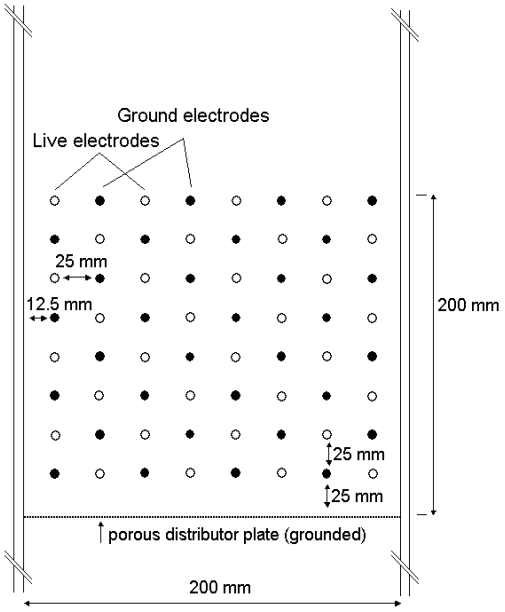

Figure 2B-10. Schematic of the 2-D column design.

Figure 2B-11 shows the results of applying electric fields to reduce bubble size for both Geldart A and B material. During fluidization with and without electric field, it was observed both visually and in pressure fluctuation data that the behavior of the emulsion phase is very similar and that fluidity (particle movement) is conserved. However, whereas the state of the emulsion phase does not change, the bubble behavior changes considerably. The fine powder (Figure 2B-11a) shows a decrease in bubble diameter of about 25%, while bubbles in the larger beads (Figure 2B-11b) decrease by as much as 85%! Experiments with Geldart A material carried out in the 3-D column show almost identical results, albeit that at a field strength greater than 3.5 kV/cm it was seen that the decrease in bubble size is somewhat less than at lower field strengths.

From Figure 2B-11 it is also clear that an optimal regime of electric fields exists: the applied fields should range from 400 to 2000 V/cm for Geldart A material, although a positive effect is observed even at lower field strengths. The frequencies are optimal between 5 and 20 Hz. For Geldart B material, the upper limit for the field strength is not found, and the frequency range is a bit higher, 20 - 70 Hz. The limits seen on the frequency range can be understood in a qualitative manner: at low

frequencies, the bed characteristics change to a DC-like behavior, eventually resulting in compaction and agglomeration. This leads to a (partially) frozen bed. At high frequencies, there is not enough time for the macroscopic charge separation to develop – confer the relaxation times calculated by Colver (2000). It is not yet fully clear why the experimental frequency range for the larger particles is higher than for the smaller particles, and this will be studied in more detail. At the lower voltage limit, the electric interparticle forces are too small to play a role in the bubble behavior. At too high field strengths, it is likely that the particles stick together too strongly, resulting in more cohesive fluidization with its associated gas voids.

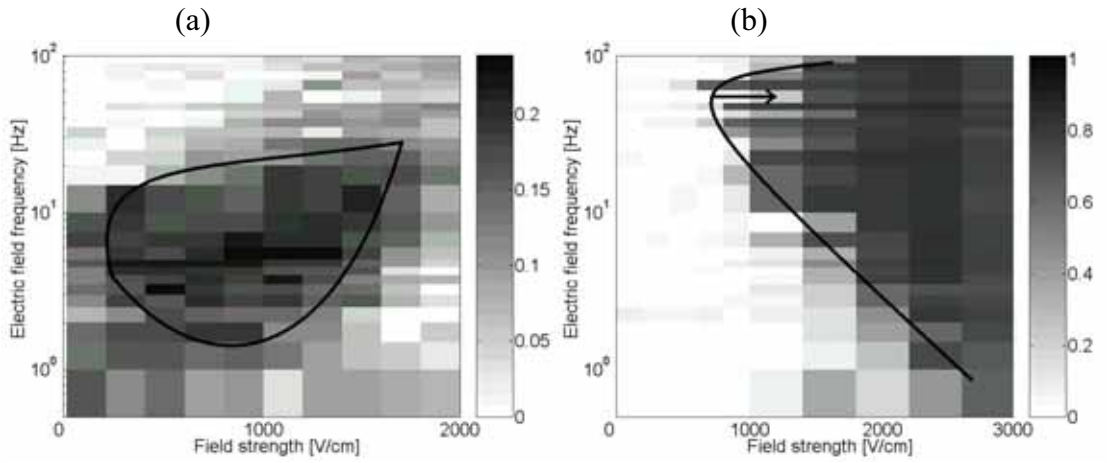

Figure 2B-11. Bubble size decrease at 190 mm (63% of bed height). The grayscale shows the fractional change in bubble diameter as a function of frequency and field strength. Bed material: (a) 77 µm glass beads, (b) 770 µm glass beads. Black lines denote the region of optimal electric field strength and frequency.

To determine the change in bubble size distribution and total bubble volume, bubbles were injected in a 2-D fluidized bed of Geldart B particles slightly above U_{mf}. Video analysis demonstrated that in the electrified region the bubbles are broken up, resulting in an increase in average number of bubbles, and that the bubble diameter and the total bubble volume decrease significantly. In the out-of-field top region, the number of bubbles is not changed when compared to the no-field situation, but the bubble diameter, and thus the total bubble volume, is still much lower with the electric field on. A small horizontal elongation of the bubbles is noticed. With this confirmation of a decrease in total volume, and the observation in the bubbling experiments described above that the bed volume does not change, we speculate that

the interstitial gas flow is increased. Further experiments will be carried out to confirm this.

2.B.6 Industrial application

The use of electric fields to reduce bubble size in industrial applications can clearly offer large benefits. Smaller bubbles lead to a better exchange of the gas in the bubbles with the gas in the dense phase. Mleczko (1996) clearly illustrated the effect of smaller bubbles (in his case achieved using gas redistributors) for the Sohio process for the production of acrylonitrile by the strongly exothermic catalytic oxidation of propylene and ammonia. By reducing the bubble diameter from 35 to 15 cm, it has been shown that conversion of propylene can be raised from 35 to 50%. In addition, the selectivity towards acrylonitrile is raised from 60 to 70%. Such improvements lead to a higher product yield, a higher energy efficiency, and a decrease in the amount of separation and recycling needed. The higher efficiency allows for a more compact reactor design (smaller volume) and/or lower flow rates while keeping production at similar levels.

For industrial applications, the energy consumption will be an important criterion. The electric energy consumption during typical experiments amounts to approximately 50 W/m^3 of fluidized bed – comparable to a single light bulb. This low energy consumption compares favorably with the parallel field of magnetically assisted fluidization, where the energy requirements are typically three orders of magnitude higher (Geuzens, 1985).

The current design of electric field enhanced fluidized bed reactors requires the implementation of thin wire electrodes inside the fluidized bed – typically not considered a durable design for the harsh conditions present inside fluidized bed reactors. Extending the functionality of – already present – heat exchanger tubes and other internals in existing reactors to electrodes may be a more interesting approach. Whereas this may not immediately lead to the most optimal electrode configuration, the combination of two functionalities lowers capital and maintenance costs while still gaining an enhancement of fluidized bed behavior, *i.e.* smaller bubbles, higher conversion, and better selectivity.

The last issue to be addressed here is the effect of temperature on the polarization behavior of the particles, *i.e.* does the stabilization process still work at

elevated temperatures? It is well known that electrostatic-charging problems become less of an issue at high temperatures due to the higher conductivity of insulators at higher temperatures. However, the increase in conductivity, in fact, works to the advantage of the polarization mechanism. The creation of a macroscopic dipole particle due to the electric field at low frequencies is dependent on the mobility of charges near the surface of the particle, and with higher conductivity the dipole moment will be higher. As long as the system does not become too conductive, the control of bubble size can still be achieved at elevated temperatures by selecting optimal field strengths (typically lower than at room temperature) and frequency (typically higher than at room temperature).

2.B.7 Conclusions

In this paper, results were reported on the use of electric fields as a low energy method to control bubble sizes in bubbling fluidized beds. In order to maintain smooth fluidization, co-flow AC-fields with a relatively low frequency are optimal. A proper balance between conductivity of the system (through RH control) and the electric dipole constant of the particle yields an optimal polarization of the particle. The periodic interparticle forces thus created between particles ensures this smooth optimization while yielding an optimal reduction in bubble size.

Analysis of pressure fluctuation time series demonstrated that the bubble diameter decreases by about 25% in the case of Geldart A material, and up to 85% for Geldart B particles. Video recordings demonstrated that the average number of bubbles increases, which means that, in combination with the unchanged expanded bed height, the smaller volume of gas in bubbles results in a larger amount of interstitial gas.

The large decreases in bubble sizes while fluidizing either Geldart A or B material are accomplished with electric fields with an energy consumption of approximately $50 W/m^3$. For Geldart A material, the method has been successfully applied to both 2-D and 3-D columns; for Geldart B material, results in 3-D columns will be reported on shortly.

2.B.8 Notation

a center to center particle separation distance, m

d_p particle diameter, m

E_0 electric field strength, V/m

F_{el} electric field induced interparticle force, N

P dipole moment, C m

u_0 superficial velocity, m/s

u_{mf} minimum fluidization velocity, m/s

ε_0 permittivity of free space, 8.854 10^{-12} F / m

ε_c relative dielectric constant of air, -

ε_p relative dielectric constant of a particle, -

σ electrical conductivity, S

2.B.9 References

Colver, G.M., 'An interparticle force model for ac-dc electric fields in powders', *Powder Technol.*, **112** (2000), 126-136.

Coppens, M.-O., van Ommen, J.R., 'Structuring chaotic fluidized beds', *Chem. Eng. J.*, **96** (2003), 117-124.

Geuzens, P.L., 'Some Aspects of Magnetically Stabilized Fluidization', PhD-thesis, Technical University of Eindhoven, The Netherlands (1985).

Hristov, J., 'Magnetic field assisted fluidization – a unified approach: a series of review papers', *Rev. Chem. Eng.*, **18**, Nos. 4-5 (2002).

Kaart, S., 'Controlling Chaotic Bubbles', PhD-thesis, Delft University of Technology (2002).

Kleijn van Willigen, F., van Ommen, J.R., van Turnhout, J., and van den Bleek, C.M., 'Bubble size reduction in a fluidized bed by electric fields', *Int. J. Chem. Reactor Eng.*, **1**: A21 (2003). http://www.bepress.com/ijcre/vol1/A21.

Kwauk, M., 'Fluidization: idealized and bubbleless, with applications', Beijing, China: Science Press (1992).

Levenspiel, O., 'G/S reactor models – packed beds, bubbling fluidized beds, turbulent fluidized beds and circulating (fast) fluidized beds', *Powder Technol.*, **112** (2002), 1-9.

Mleczko, L., 'Einfluß der Hydrodynamik in eimen Wirbelschichtreactor industriellen Maßstabs auf Selektivität und Ausbeute zu Acrilnitril bei der Ammoxidation van Propen', *Chem. Tech. – (Leipzig)*, **48** (1996), 130-138.

Rhodes, M.J., Wang, X.S., Nguyen, M., Stewart, P., and Liffman, K., 'Onset of cohesive behavior in gas fluidized beds: a numerical study using DEM simulation", *Chem. Eng. Sci.*, **56** (2001), 4433-4438.

Rietema, K., and Piepers, H. W., 'The effect of interparticle forces on the stability of gas-fluidized beds—I. Experimental evidence', *Chem. Eng. Sci.*, **45** (1990), 1627-1639.

Seville, J.P.K., and Clift, R., 'The effect of thin liquid layers on fluidisation characteristics', *Powder Technol.*, **37** (1984), 117-129.

Saxena, S.C., and Wu, W.Y., 'Hydrodynamic characteristics of magnetically stabilized fluidized admixture beds of iron and copper particles', *Can. J. Chem. Eng.*, **77** (1999), 312-318.

Van Dijk, J.-J., Hoffmann, A.C., Cheesman, D., and Yates, J.G., 'The influence of horizontal internal baffles on the flow pattern in dense fluidized beds by X-ray investigation', *Powder Technol.*, **98** (1998), 273-278.

Ye, M., van der Hoef, M.A., and Kuipers, J.A.M., 'A numerical study of fluidization behavior of Geldart A particles using a discrete particle model', *Powder Technol.*, **139** (2004), 129-139.

'Lightning Striking Tree', by Allan Davey (permission granted).

A somewhat different interaction between *high voltages* (in the shape of a discharge not normally present in electric field enhanced fluidized beds) and *fractal structures* than the work presented in this chapter.

3. Comparison of Electric Field Enhanced Fluidization and Fractal Injection

In Chapter 2, the decrease of bubble size under the effect of an electric field was quantitatively determined, and it was found that with Geldart B material, the bubble size decreases by as much as 85%. However, many details about the bubble behavior remain unanswered. The mesoscopic effects – i.e. the change in bubble behavior – are further discussed in this chapter.

The investigation of the hydrodynamic behavior of two methods of reducing bubble size is reported: the *electric field enhanced fluidized bed* and the secondary injection of gas using a *fractal injector*. Using pressure fluctuation analysis, a detailed study was done on the effect of the relative humidity and the flow rate of the fluidizing gas on the behavior of bubbles in three two-dimensional columns: a column without internals, a column fitted with electrode wires, and a column fitted with a fractal injector. Besides determining the change in bubble size for a range of flow parameters, video analysis at one set of conditions was used to gain insight into the number of bubbles and the bubble hold-up, providing a more complete insight into the changes in bubble dynamics.

Both the electric field enhanced fluidized bed and the fractal injector induce a marked decrease in bubble size. The electric field system is more effective at the lower flow rates; the fractal injector shows the largest effect at higher flow rates, as may be expected when using secondary injection. The influence of the relative humidity on the effectiveness of the electric fields is also shown to be significant. Also, the influence of the (unenergized) wires on the behavior of the bed is found to be so slight as to be not measurable.

This chapter was published as:

Kleijn van Willigen, F., Christensen, D., van Ommen, J.R., and Coppens, M.-O., 'Imposing Dynamic Structures on Fluidised Beds', *Catal. Today*, **105** (2005), 560-568.

3.1 Abstract

Structuring fluidised beds can increase the conversion and selectivity, and facilitate control and scale-up. Two methods for introducing a dynamic structure into gas-solid fluidised beds are compared based on their overall hydrodynamics: electric field enhanced fluidisation and distributed secondary gas injection by a fractal injector. It is shown that, under various conditions, these systems lead to significant decreases in bubble size and bubble hold-up and to an increase in the number of bubbles. It was found that the electric field enhancement can lead to homogeneous fluidisation at lower flow rates, and the distributed secondary flow leads to smaller bubbles at higher flow rates.

3.2 Introduction

Two common reactor types for heterogeneously catalysed gas phase reactions are the packed bed and the fluidised bed. Fluidised beds couple short intraparticle diffusion lengths to good heat transfer, but suffer from chaotic bubble behaviour [Van den Bleek et al. 2002), leading to back mixing, fluid bypassing, and particle-fluid separation problems (Kunii and Levenspiel, 1991). Packed beds show much less back-mixing and have virtually no catalyst attrition and separation problems, but have longer diffusion lengths that can only be overcome by an unacceptably large pressure drop. Moreover, they are sensitive to flow maldistribution that can lead to problems such as poor catalyst contact, hot-spot formation and runaway behaviour (Dudukovic et al. 1999). In the past few years, much effort has been devoted to the development of reactors in which the catalyst material is present in a static, structured way, e.g., monolith and Katapak® reactors (Cybulski and Moulijn, 1998). However, for reactions with large heat production and/or fast catalyst deactivation, it is often advantageous to use a mobile catalyst (Kunii and Levenspiel, 1991). In these cases, fluidised beds are preferred, despite the disadvantages of chaotic bubble behaviour and the difficulty of scaling fluidised beds from lab-scale to pilot- and industrial-scale. Just as for packed bed reactors, the structuring of fluidised beds is interesting from the point of view of process intensification, to facilitate scale-up and control, and to improve performance.

In this paper, we will show that it is possible to manipulate the hydrodynamic structure of fluidised-bed reactors, thereby increasing the number of degrees of freedom for the designer and helping to intensify the process. This is achieved by manipulating the interparticle forces and particle-fluid interactions to obtain the desired fluidisation behaviour for a given application. Two methods of structuring gas-solids fluidised beds are presented and compared: imposing an electric field and secondary injection of gas. By using these non-conventional 'active' internals, we introduce a dynamic structure into the fluidised bed, leading to better control over the hydrodynamics of the system (especially the bubbles). The contact of the gas in bubbles with the solid catalyst particles is often poor, and when the catalyst itself is sufficiently active, the mass-transfer from bubble to emulsion is the rate-limiting step. Therefore, our goal is to *control* the bubble behaviour and *decrease* the average bubble size in a structured manner. A decrease of the bubble diameter by a factor four can increase the conversion in a fluidized bed as much as 2.5 times, and is therefore well worth investigating (Levenspiel, 2002; Kaart et al., 1999).

Three cases are discussed and compared: the base case of a column with no active internals, a column using *electric field enhanced fluidisation* (EF), and a column with secondary gas injection by a *fractal injector* (FI). Using both pressure fluctuation analysis and video analysis of the quasi 2-D column, we attempt to discern the effect of these improvements on the hydrodynamics and bubble behaviour of bubbling fluidised beds.

Electric field enhanced fluidisation (EF)

One method to reduce bubble size is the application of an AC electric field to a fluidised bed of semi-insulating particles. In the presence of a relatively low intensity electric field, the particles (i.e., glass particles) become polarised, leading to attractive or repulsive forces.

The degree of polarisation, P, of particles with a diameter d_p in a fluidised bed dictates the magnitude of the interparticle forces, and is a function of the electrical conductivity, σ_e, and the dielectric constants of particle and continuous phase (ε_p and ε_c), as well as the electric field strength, E_0.

$$P = f(d_p^3, \varepsilon_p, \varepsilon_c, \sigma_e(\mathrm{RH}), E_0) \qquad [3 - 1]$$

The conductivity of the system is strongly influenced by the relative humidity, RH, of the fluidising gas.

The influence of small variations in interparticle forces on fluidisation behaviour has been shown both experimentally (e.g., liquid bridges (Seville and Clift, 1984), magnetic forces (Saxena and Wu, 1989), electric polarisation forces, e.g., (Colver, 2000; Kleijn van Willigen et al., 2003) and in discrete element models (e.g., Rhodes, 2001). The electrical forces thus induced by the electric field should be large enough to decrease the formation and growth of bubbles, but small enough to allow the free movement of particles, i.e., the fluidity of the system must be preserved. The oscillation of the AC fields has the advantage over constant (DC) electric fields that fixation of particles or defluidisation is unlikely.

In practice, the electric fields are introduced in the bed by stringing thin wires through the column (cf. Figure 3-1a), and alternately, both horizontally and vertically, driving these with an AC potential or grounding them. This creates a strongly inhomogeneous field in both the horizontal and vertical directions in the column.

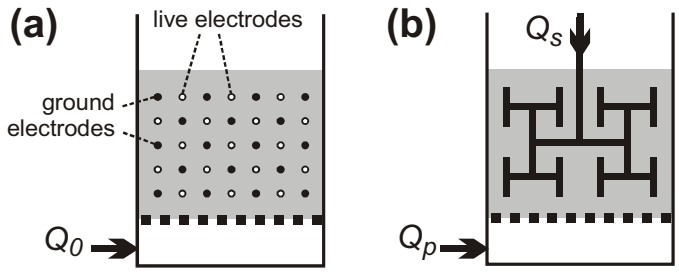

Figure 3-1. Two ways of structuring gas-solids fluidised beds with active internals: (a) imposing an AC electric field and (b) secondary (fractal) injection of gas (Cheng et al. 2001).

Secondary injection of gas using a fractal injector (FI)

The number of degrees of freedom available to optimise the fluidised bed hydrodynamics increases when part of the gas is injected at various other locations inside the bed rather than only feeding the gas via the bottom (Cheng et al., 2001). This is possible as long as enough "primary" gas (Q_p) is injected from the bottom in order to maintain fluidisation ($Q_p > Q_{mf}$), while an injector distributes the remaining "secondary" gas (Q_s) into the bed. This way, the amounts of gas distributed over the reactor space can be optimally dosed to control both hydrodynamics and reactor performance. Rising gas, depleted of reactants, is continuously replenished with fresh feed. Simultaneously, the bubble size can be controlled, as less primary gas (fraction

of primary gas to total gas flow, Q_p/Q_0) leads to smaller bubbles initially, while fresh feed blown into the reactor at various locations (fraction Q_s/Q_0) tends to break up existing bubbles or blow particles apart, leading to an emulsion phase of higher void fraction. Unstable emulsions take time to break up into equilibrated phases, and it is this delay that is exploited. The effects of using secondary gas injection are: increased gas-solid contact due to a higher-than-usual emulsion phase void fraction; smaller, more slowly rising bubbles; and the ability to increase yields and selectivities of chemical processes by a distributed feed. In principle, each injection point could be fed by a separate tube, but it is more useful and practical to connect all injection points by a hierarchical, tree-like fractal structure (cf. Figure 3-1b). This gives intrinsic scalability and ensures a uniform access to the smallest branch tips – the outlets. The optimal fractal injector design will depend on the application.

In this paper, we will compare the application of electric fields to the fractal injection of secondary feed, as well as to the baseline cases of a column with inactive internals and a column without internals altogether. The advantages and disadvantages of these two methods of structuring fluidised beds on the hydrodynamics and mass transfer of these systems will be discussed.

3.3 Experimental

Both columns (EF and FI) were built as similar as possible. By removing the fractal injector from its column, measurements could be conducted in a column without internals. The two quasi-2D Plexiglas columns, 20 cm × 1.5 cm × 80 cm, were fitted with 5 piezo-electric pressure transducers, Kistler type 7261, at 1, 10, 20, and 30 cm above the sintered metal porous distributor, and in the plenum (Van der Schaaf et al., 2002). The pressure drop was measured over the lowest 20 cm of the columns with a Validyne DP15-28. A data acquisition system (LMS-Difa) recorded all measurements at 200 Hz and provided outputs to control the mass flow controllers. The relative humidity (RH) at 1 atm of the fluidising air was controlled at either 2% or 40% at 30ºC. Baseline measurements were conducted in the column without internals and in the columns with internals but with those internals inactive. The higher RH allowed for enough static charge dissipation that particles did not stick to the walls. The mono-disperse glass beads, d_p=550 μm with a density of 2400 kg/m^3 (Geldart B), were dried in an oven before use, and fluidised at least overnight when the RH was set

to 40% before measurements were conducted. The settled bed height was 40 cm. The columns were operated within a cabinet controlled at 30ºC. A digital video camera (25 fps, 576 × 720 pixels) was set up with a viewing window on the column covering an area that spanned from 10 to 40 cm above the distributor. This viewing window was below the bed surface to prevent blinding of the camera by the backlight behind the column.

Electric field enhanced fluidised bed (EF) set-up

The lower 20 cm of the column were fitted with thin wire electrodes. The wires were threaded through the front and rear of the column at a vertical pitch of 1.25 cm and a horizontal pitch of 2.2 cm. In the horizontal plane, they were threaded diagonally relative to the column walls, so that the nodes of highest field strength are in the centre of the column. The wires were alternately grounded and driven at a potential. The porous metal distributor was also grounded. Frequencies ranging from 1 to 160 Hz (sine wave) and maximum field strengths from 2.4 to 7.2 kV/cm were applied using a Trek 20/20c high voltage amplifier. The LMS-Difa DAQ, besides recording all measurements, served as the signal generator. At least 51200 data points (4.26 min) were measured at every combination of flow rate, field strength, and field frequency. At all the measured field frequencies, a measurement series consisted of a baseline measurement (0 kV applied potential), the range of field strengths, followed by a second base measurement. The superficial velocities, as multiples of the minimum fluidization velocity, ranged from 1.5 to 3.5 × u_{mf}, in increments of 0.5 × u_{mf}.

Fractal injector fluidised bed (FI) set-up

A fractal injector, consisting of 16 uniformly spaced injection points, was constructed from 3 and 6 mm stainless steel tubing and brass connections. Excluding the main feed stem, the fractal injector had the dimensions: 15.6 cm wide by 7.4 cm high, and was centrally positioned in the column at a height of 10 cm above the distributor plate. The highest row of injection points is at approximately 14 cm, and the lowest row at approximately 6 cm. Therefore, the maximum bed height in contact with the fractal injector is somewhat less (~6 cm) than the EF column. The air fed through the fractal injector is heated but not humidified due to equipment limitations. It is not possible to add enough extra humidity to the primary airflow to make up for this

difference and, thus, the humidity of the primary flow was maintained at its normal level (*i.e.*, either the dry plant air or the 40% RH humidified air, depending on the experiment). As a result, the experiments with increasing secondary flow rate unavoidably had decreasing levels of humidity, but never to a level that particle adhesion to the walls or the injector was visible. Experiments were conducted with varying Q_s/Q_p ratios. The total superficial velocities (and therefore flow rates) ranged from 1.5 to 3.5 × u_{mf}, in increments of 0.5 × u_{mf}. At every total flow rate (Q_s+Q_p) corresponding to a superficial velocity higher than 1.5 × u_{mf}, Q_s was increased in steps corresponding to 0.5 × u_{mf}, but always with a minimum Q_p corresponding to 1.5 × u_{mf}. At least 204,000 data points (17 min) were measured at every combination of flow rates. Each set of flow conditions always contained a baseline experiment with no secondary flow.

Data analysis

The analysis of pressure fluctuations is an attractive method to characterize the hydrodynamic behaviour of fluidised beds because the fluctuations are closely associated with properties of the bubbles. Using the pressure probes described earlier, time-series of pressure fluctuations were measured at various heights in the column. A technique proposed by van der Schaaf et al. was used to decompose the time series into a variance of the pressure time series that is associated with the size of bubbles passing the probe (the incoherent variance, σ^2_{IOP}) and a variance associated with other processes such as the formation, eruption, and coalescence of bubbles (the coherent variance). For more details the reader is referred to van der Schaaf et al. (2002). This method requires measurement of pressure fluctuations in the plenum in addition to the height under consideration. The incoherent variance has been shown to be a good quantitative descriptor of the average bubble size at a certain height in a fluidised bed, although a calibration of this value (for example, using video analysis or optical probes) is required to determine absolute bubble sizes (Kleijn van Willigen et al. 2003). The measure of bubble size (defined as frontal area of the bubble – and, thus, volume for a fixed thickness of the column) derived from pressure fluctuations is theoretically determined by the vertical dimension of the bubble and averaged over long time spans. It does not give information about the total bubble hold-up, or about the number of bubbles. In this study, we are interested in the reduction of average bubble size due to the electric field or fractal injector, and therefore, only consider the

ratio of the σ^2_{IOP} in the EF or FI system to the σ^2_{IOP} at normal conditions (baseline with inactive internals).

The second analysis method employed for this comparative study is the use of digital video images. Although not applicable to long experiments (typically only measurements of a few minutes can be properly analysed because of the processing time), video analysis cannot only distinguish the changes in bubble size, like pressure fluctuation analysis, but can also distinguish the changes in the bubble frequency, which pressure fluctuation analysis cannot. The bubble hold-up can also be determined from video analysis. The video analysis was used as a complementary measurement method only for those settings considered most interesting (*i.e.*, the largest positive influence on the bubble size) based on the pressure fluctuation analysis.

Video analysis over the bed height stretching from 10 to 40 cm was performed for a series of experiments over all flow rates with the most optimal electric field frequency and strength for the EF set-up and the most optimal primary/secondary flow ratio for the FI set-up. For every experiment, 3000 frames (2 min) were recorded. The analysis was carried out in Matlab™, and consisted of filtering out the background image and the fractal injector stem, then filtering with a median filter and thresholding. The post-processing allows determination of the average bubble size, the bubble frequency, and the bubble hold-up as functions of height.

In this study, the bubble size is defined as the area of the face of the bubble in the pseudo-2D column, which implies that bubbles in these columns are essentially voids stretching directly from the front to the back.

3.4 Results

Minimum fluidisation

The minimum fluidisation velocity was determined for all set-ups (column without internals, column with wires, column with fractal injector) using pressure drop measurements at both low and elevated RH. The minimum fluidization velocity determined at low RH with the fractal injector present deviated significantly because of adhesion of particles to the walls and the injector due to static charges. For the other cases, the values for u_{mf} were reproducible and found to be $u_{mf} = 21 \pm 1$ cm/s.

The column without internals and the column with wires at low RH were less susceptible to particle clinging, perhaps because of small variations in (adsorbed) moisture or age of the particles (attrition), and, therefore, have a more stable minimum fluidization velocity.

Pressure fluctuation analysis

The pressure fluctuation analysis method was used to find the most optimal strength and frequency of the electric field and the optimal Q_s/Q_p ratio for the fractal injector for the conditions studied. For the EF system, the ratio of the average bubble size under the influence of various strengths to the base case was studied at superficial velocities of 1.5 to 3.5 × u_{mf}. The change in bubble size was determined at 20 and 30 cm above the distributor over the whole range of electric field strengths and frequencies, both for the low and elevated relative humidity. Fig. 2 shows the ratio of the bubble size as a function of field strength and frequency to the mean of the base measurements at 20 cm before and after the electric field was switched on. As expected, low field intensities (*i.e.*, less than 4 kV/cm) lead to virtually no change in average bubble size, but at higher field strengths the change in bubble size is very significant.

It has been predicted that the interparticle force increases significantly as the RH increases (Kleijn van Willigen et al. 2003). As stronger interparticle forces lead to a larger decrease in bubble size, we therefore expect that at a higher RH the bubble size ratio becomes smaller. This is confirmed in the right-hand column of Figure 3-2, where the bubble size at, for example, 3.5 × u_{mf}, is decreased by 39% at 20 cm, compared to 28% for the low RH experiment. As the field strength increases, the effect on bubble size also increases, but a dependence on the field frequency is also seen. Especially at the higher RH, lower frequencies lead to larger bubble size decrease, but one must be careful not to defluidise – DC or very low frequency AC fields may gridlock the particles. With increasing flow rate, the net effect of the electric fields becomes smaller, and the effect wanes above the electrified region. The optimal electric field frequency was chosen at 10 Hz on the basis of the data presented in Figure 3-2, although the results at 5 Hz were slightly better. This was done because low frequencies may lead to particle agglomeration, and the difference in EF efficiency between 5 and 10 Hz was small enough to warrant the choice for higher

frequency. The results at optimal frequency and field strength (7.2 kV/cm) are summarized in Table 3-1.

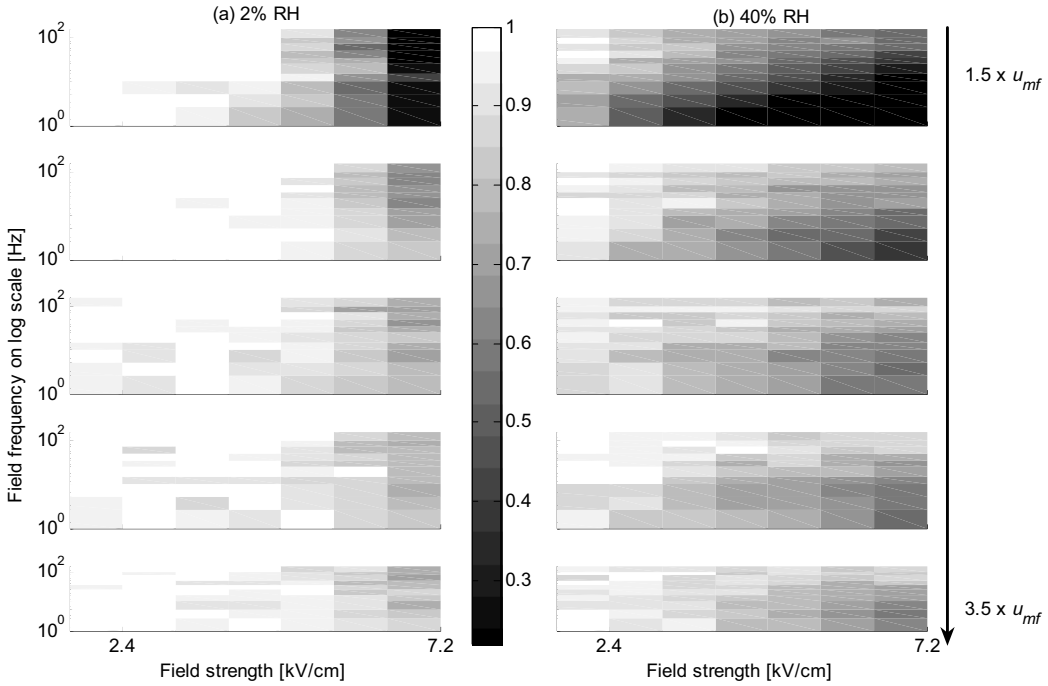

Figure 3-2. Ratio of bubble size with applied electric field and without field, as determined by pressure fluctuation analysis at 20 cm above the distributor. (a) 2% RH and (b) 40% RH. The flow rate increases from top (1.5 × u_{mf}) to bottom (3.5 × u_{mf}). Each subplot shows the bubble reduction ratio (*cf.* the colour scale) as a function of field strength (linear scale) and frequency (logarithmic scale).

The pressure fluctuation analysis was also used to estimate the changes in average bubble size in the FI system. This was done at bed heights of 20 and 30 cm over the full range of total flow rates and Q_S/Q_P ratios at both humidity levels. Figure 3-3 shows the effect of increasing the Q_S/Q_P ratio at the various total flow rates. It is apparent from the graph that at any total flow rate the bubble size based on incoherent variance decreases with increasing Q_S/Q_P ratio. This trend is consistent at both bed heights, but is slightly less pronounced at the higher height due to bubble coalescence, *i.e.* the effect of the secondary injection is beginning to wane as the bed tries to return to its equilibrium state. The largest change in bubble size (represented by lower numbers in Table 3-1 and Figure 3-3) always occurs at the highest secondary flow rates and also at the highest total flow rates.

Table 3-1. Ratios of bubble size with most optimal EF and FI to bubble size with passive internals, as determined by pressure fluctuation analysis (σ^2_{IOP}).

Superficial velocity [× u_{mf}]	EF optimal frequency	σ^2_{IOP} ratio (30 cm)	σ^2_{IOP} ratio (20 cm)	FI optimal Q_S/Q_P ratio	σ^2_{IOP} ratio (30 cm)	σ^2_{IOP} ratio (20 cm)
1.5	5Hz	.24	.08	N/A	N/A	N/A
2.0	5Hz	.63	.43	0.5/1.5	0.73	0.49
2.5	10Hz	.68	.57	1.0/1.5	0.71	0.42
3.0	5Hz	.69	.59	1.5/1.5	0.62	0.36
3.5	5Hz	.76	.61	2.0/1.5	0.51	0.30

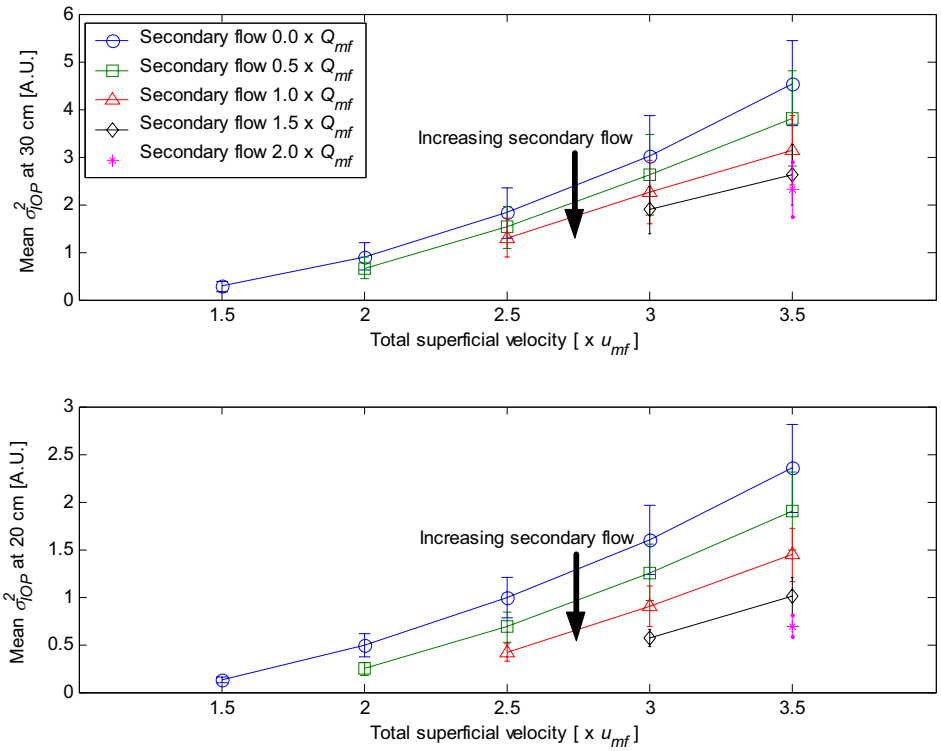

Figure 3-3. Effect of increasing the ratio of secondary to primary flow on the incoherent variance, when using the set-up with fractal injector, as a function of total flow rate. The σ^2_{IOP} is a measure for bubble size based on pressure fluctuation analysis. Measurements carried out at 40% RH.

Due to the inconsistent humidity levels, as was mentioned earlier, the effect of moisture could not be determined quantitatively. When the secondary flow stream was at its highest, the lowest RH of the combined stream (when humidified) was 17%,

compared to 2% for the dry case. However, it will be shown later on the basis of bubble hold-up that there is some influence on the results that is attributed to the relative humidity and how the RH is controlled.

Video analysis

Video analysis was used to determine average bubble size, frequency, and hold-up in the EF and FI systems at the most optimal settings, over the full range of flow rates. This was done at 40% RH. Figure 4-4 shows the ratios of average bubble size and the bubble frequency as a function of height for the EF system. As already shown by the pressure fluctuation analysis, the ratio of bubble size with and without electric field decreases, and this is most prominent in the electrified region. In the region above the electrodes, the bubble size at low flow rates stays low, but at higher flow rates, bubbles grow quickly. Nevertheless, within the electrified region, the bubble size is 10-60% smaller and up to 35% smaller above the wires.

The effect of the electric field on the bubble frequency is shown in Figure 4-4b, again as a ratio of bubble frequency with and without applied field. At low flow rates, the bubble frequency within the electrified region is decreased significantly. This is because bubbles are either non-existent or are too small to be detected by the video camera. There is also an oscillation in the bubble frequency due to the direct effect of the field on the bubbles. The number of bubbles in the region above the electrodes is increased by 10-70%, depending on flow rate. The emulsion phase can no longer contain as much gas as it is forced to in the electrified region, and thus many small bubbles are formed. As visually observed during experiments and confirmed by the lack of bubbles, at the lower flow rates almost homogeneous fluidisation is achieved in the electrified region.

The video analysis results for each total flow rate using the best Q_S/Q_P ratios in the FI system are shown in Figure 3-5. Above the internals, it is apparent that the bubble size is smaller and the bubble frequency higher, when compared to the baselines. Just as for the pressure signal analysis, the bubble size ratio decreases with increasing flow rate, while the number of bubbles increases with increasing flow rate. This means that the FI system is more efficient at higher flow rates. Bubble size reductions are all in the range of 15-55% when measured at the same heights as in the pressure signal analysis. The bubble size ratios increase slightly with increasing

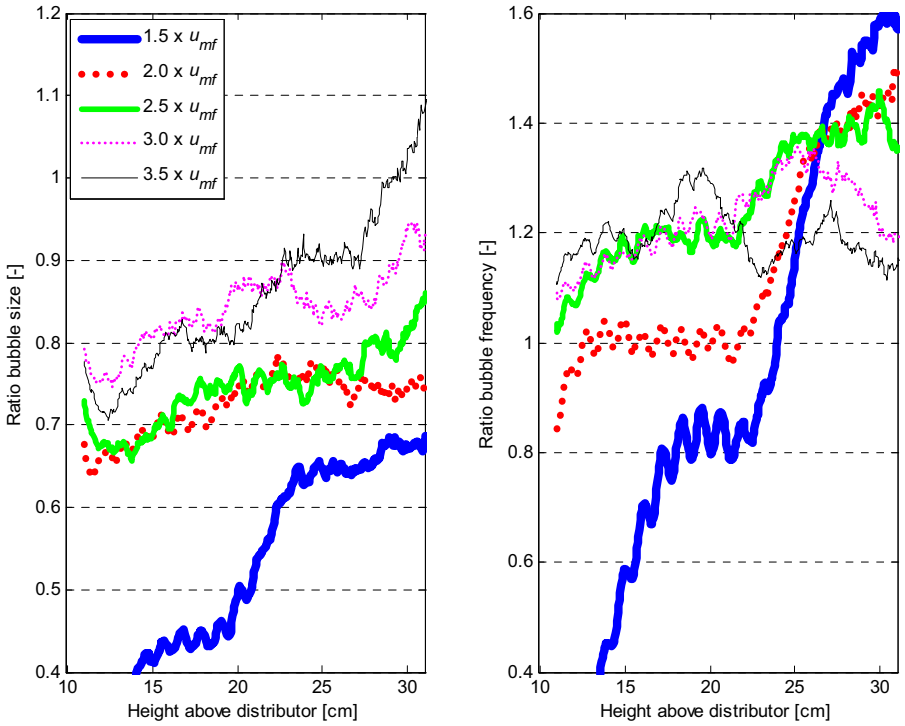

Figure 3-4. The relative bubble size (a) and frequency (b) under the effect of the electric fields, determined using video analysis. The electric fields reduce the bubble size and, at higher flow rates, increase the number of bubbles. Measurements carried out at 40% RH. The electrodes end 20 cm above the distributor.

height due to bubble coalescence while the system tries to return to its equilibrium state. This is corroborated by the slight decrease in bubble frequency over the same region. The fact that the bubble frequency ratio never returns to unity implies that bubble coalescence is delayed by the use of the fractal injector and that a maximum bubble size is not reached (as is expected with Geldart B particles). Results within the region containing the fractal injector are difficult to interpret, as the total gas throughput is changing in this region.

3.5 Discussion and comparison

Both of the systems presented here were designed to improve bubbling fluidised bed efficiency and both are inherently scalable. In the design of both internals, however, there is much room for optimisation: the spatial distribution of injection points for the fractal injector, and the electrodes in the EF system for highest average field density,

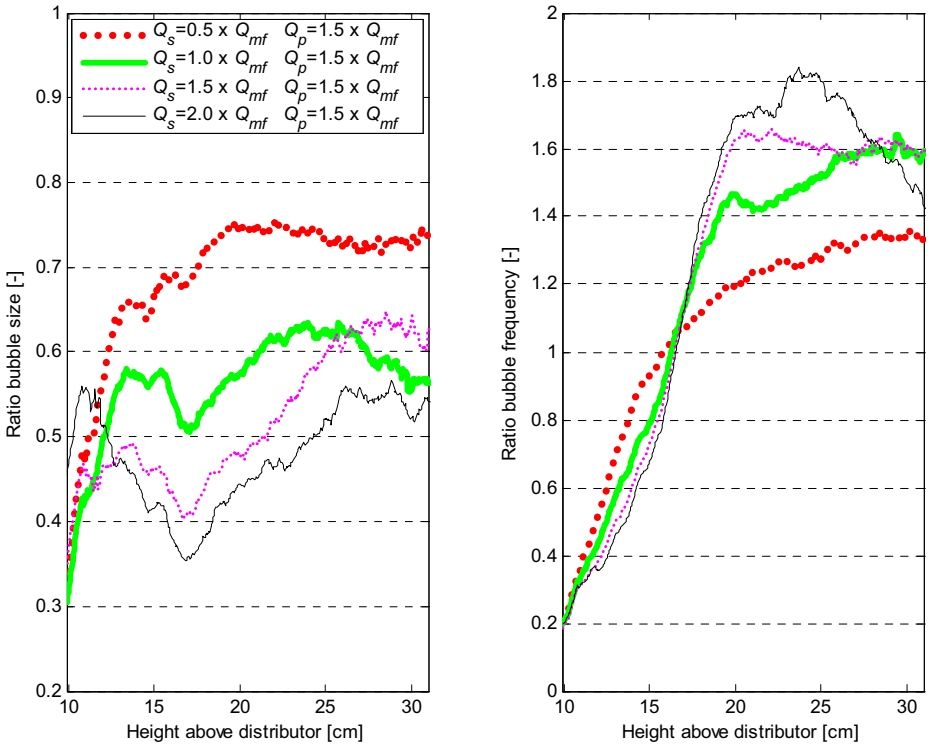

Figure 3-5. The effect of the fractal injector on bubble size (left) and bubble frequency (right). The primary flow rate is held constant, the secondary flow increases – this is the most optimal setting. Measurements carried out at 40% RH. The top injection point of the fractal injector is 14 cm above the distributor.

as well as an extension of the electrodes to the whole bed height. It should be noted, however, that the introduction of internals into a fluidised bed can be problematic due to attrition. The lifetime of the wires of the EF column is obviously lower than the sturdier fractal injector design, but, on the other hand, the volume density of the wires is much lower than the volume the fractal injector occupies (EF: 0.008%, FI: 1.67%). In addition, the electric field may be introduced using (adaptations of) existing internals or electrodes that are more robust.

Figure 3-6 compares the average bubble sizes determined by pressure fluctuation analysis for all different systems: a column without any internals, a column fitted with electrodes, and a column fitted with the fractal injector. Data are compared with both passive and active internals, at elevated RH. The base lines at 30 cm are not significantly different. At 20 cm, the influence of the (passive) fractal injector breaking up bubbles is seen to be significant, causing an estimated 12% bubble size reduction at the highest flow rate. The influence of the wires on bubble

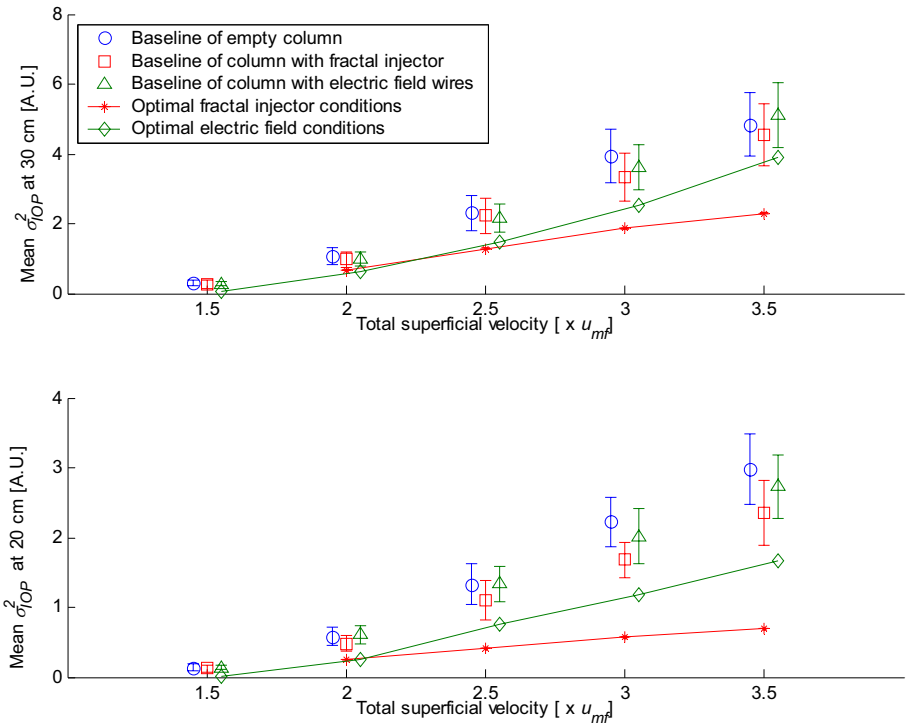

Figure 3-6. The pressure fluctuation analysis method applied to the EF and FI measurements at the optimal electric field or secondary flow ratios, as a function of total flow rate. The σ^2_{IOP} is a measure of the mean bubble size. The three baseline measurements show larger bubble sizes than the EF and FI measurements. Data points have been slightly offset along the horizontal axis for clarity and lines were drawn to guide the eye. Error bars denote 95% confidence intervals.

behaviour in the EF system is not discernable. When active, both systems are able to reduce bubble size considerably, as already shown in Table 3-1. The EF system is more effective at the lower flow rates; the FI system gives a larger bubble size reduction at the higher flow rates.

At this point it is most interesting to compare the bubble hold-up of both systems because of the large influence on the effectiveness of the system. A larger amount of gas in the bubble phase means less contact between catalyst particles and gas, usually reducing conversion. Conversely, when the average bubble size decreases, and the average number of bubbles in the system increases, an equal or lower bubble hold-up means an increase in the emulsion phase flow (as larger bubbles rise more quickly than small ones, which leads to a lower hold-up). The changes in bubble hold-up of the EF and FI systems are compared in Figure 3-7. It is again clear that the EF system is most efficient within the electrified region, leading to a large

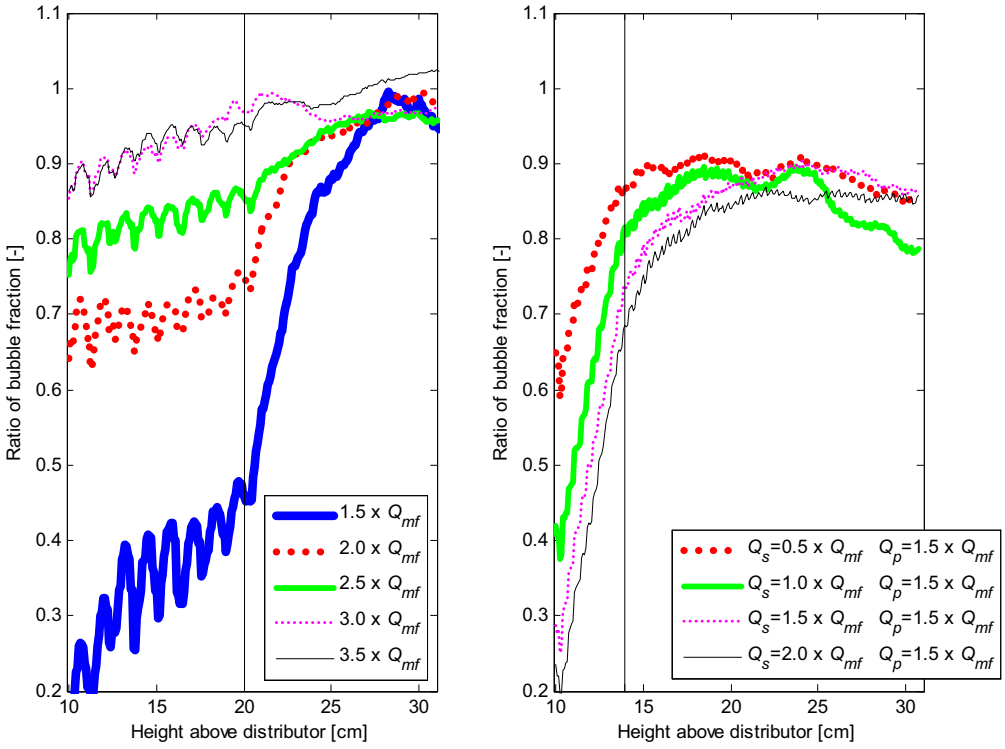

Figure 3-7. Comparison of the improvement in bubble hold-up in the EF (left) and FI (right) systems. The vertical lines indicate the top of the internals. The EF and FI internals both decrease bubble hold-up and increase emulsion phase flow. The electric field has only limited influence on the region above the electrodes, while the FI shows a longer lasting effect. A decrease in bubble hold-up, combined with more and smaller (slower travelling) bubbles, implies an increase in emulsion phase flow.

decrease in bubble hold-up in the lower 20 cm of the column, especially at low flow rates. The bubble hold-up in the same region in the FI column appears to decrease the most at *high* flow rates (large secondary flow), but this is because the total flow at this point is much lower than the reference situation, in which the total flow is all primary flow.

In the region of 20 to 30 cm above the distributor, the influence of the electric fields quickly decays - the bubble hold-up is 90-100% of the baseline values, with some overshoot at the highest flow rate. However, the FI appears to maintain its effect by keeping the bubble hold-up to 80-90% of the baseline values. This difference in bubble hold-up is high, and the increase in emulsion flow may contribute only part of the decrease. A more detailed study of the influence of the changes in RH on bubble size, and a better experimental control of RH, are required to get a more accurate measure of the increase in emulsion flow. In all, the results of the

bubble hold-up analysis show that the height to which the EF or FI internals extend may be optimised for the desired decrease in hold-up.

At first thought, one may expect the mean residence time of gas in the FI column to be shorter than the baseline case because a portion of the gas is injected higher in the column. However, this is not necessarily the case. In fact, it is expected that the mean residence time will either remain unchanged or only decrease slightly (Cheng et al., 2001, Coppens and van Ommen, 2003). Even if there is a slight decrease in residence time, it is mitigated by the improved gas-solid contact resulting from the injection of gas directly into the emulsion phase, the increased driving force for mass transfer between the bubble and emulsion phases, and the increased fraction of gas in the emulsion phase. In the EF system, the reduction of bubble size and increased flow in the emulsion phase are expected to result in an increased residence time. Detailed residence time distribution measurements will be measured in future work. In both systems, the amount of backmixing is expected to decrease, leading to more plug flow-like behaviour. Since the mass transfer from the bubble to the emulsion phase is typically the rate-limiting step in chemical conversions, it will depend on the rate of mass transfer and the rate of reaction how the combination of changes in residence times and bubble sizes will affect the conversion and selectivity of the system using the electric field enhanced fluidised bed or the distributed secondary gas injection system.

3.6 Conclusions

Both the electric field enhanced fluidised bed and the column with distributed secondary injection by using a fractal injector have been demonstrated to redistribute gas to smaller bubbles and to the emulsion phase. Both systems lead to an increase in particle-gas contact but differ in the mechanism by which this is achieved. In the comparison between electric fields and secondary injection, we find that the reduction of bubble size by the fractal injector is larger at higher flow rates, while the electric fields can force homogeneous fluidisation at lower flow rates. Based on the smaller bubble size, the introduction of dynamic structures by both systems is expected to yield significant increases in conversion and selectivity. However, their different influences on the residence time distributions mean that the optimum choice will differ from application to application. It remains for future experimental work that

includes chemical reactions to demonstrate how the changes in bubble size and residence time can be used to the greatest advantage.

3.7 Notation

d_p particle diameter, m

E_0 electric field strength, V/m

P dipole moment, C m

Q gas flow, m^3/s

u superficial velocity, m/s

ε_c relative dielectric constant of air, -

ε_p relative dielectric constant of a particle, -

σ_e electrical conductivity, S

σ^2_{IOP} incoherent variance, Pa^2

Subscripts

$_0$ total fluidizing gas flow

$_{mf}$ minimum fluidization

$_p$ primary

$_s$ secondary

3.8 References

Cheng, Y., van den Bleek, C.M., and Coppens, M.-O., 'Hydrodynamics of gas-solid fluidized beds using a fractal injector', in: Proc. 10th Int. Conf. on Fluidisation, United Engineering Foundation, NY (2001), 373-380.

Colver, G.M., 'An interparticle force model for ac-dc electric fields in powders', *Powder Technol.*, **112** (2000), 126-136.

Coppens, M.-O. and van Ommen, J.R., 'Structuring chaotic fluidized beds', *Chem. Eng. J.*, **96** (2003), 117-124.

Cybulski, A. and Moulijn, J.A., 'Structured catalysts and reactors', Dekker, New York (1998).

Dudukovic, M.P., Larachi, F., and Mills, P.L., 'Multiphase Reactors – Revisited', *Chem. Eng. Sc.*, **54** (1999), 1975-1999.

Kaart, S., Schouten, J.C., and van den Bleek, C.M., 'Improving conversion and selectivity of catalytic reactions in bubbling gas–solid fluidized bed reactors by control of the nonlinear bubble dynamics', *Catal. Today*, **48** (1999), 185-194.

Kleijn van Willigen, F., van Ommen, J.R., van Turnhout, J., and van den Bleek, C.M., 'Bubble size reduction in a fluidized bed by electric fields', *Int. J. Chem. Reactor Eng.*, **1**: A21 (2003). http://www.bepress.com/ijcre/vol1/A21.

Kleijn van Willigen, F., van Ommen, J.R., van Turnhout, J., and van den Bleek, C.M., 'Bubble size reduction in electric-field-enhanced fluidized beds', *J. Electrostat.,* **63** (2005), 943-948.

Kunii, D. and Levenspiel, O., 'Fluidization Engineering' (2nd edn.), Butterworth-Heinemann, Boston (1991).

Levenspiel, O., 'G/S reactor models – packed beds, bubbling fluidized beds, turbulent fluidized beds and circulating (fast) fluidized beds', *Powder Technol.*, **112** (2002), 1-9.

Rhodes, M.J., Wang, X.S., Nguyen, M., Stewart, P., and Liffman, K., 'Onset of cohesive behaviour in gas fluidized beds: a numerical study using DEM simulation', *Chem. Eng. Sci.*, **56** (2001), 4433-4438.

Seville, J.P.K. and Clift, R., 'The effect of thin liquid layers on fluidisation characteristics', *Powder Technol.*, **37** (1984), 117-129.

Saxena, S.C. and Wu, W.Y., 'Hydrodynamic characteristics of magnetically stabilized fluidized admixture beds of iron and copper particles', *Can. J. Chem. Eng.*, **77** (1999), 312-318.

Van den Bleek, C.M., Coppens, M.-O., and Schouten, J.C., 'Application of chaos analysis to multiphase reactors', *Chem. Eng. Sc.*, **57** (2002), 4763-4778.

Van der Schaaf, J., Schouten, J.C., Johnsson, F., and van den Bleek, C.M., 'Non-intrusive determination of bubble and slug length scales in fluidized beds by decomposition of the power spectral density of pressure time series', *Int. J. Multiphas. Flow*, **29** (2002), 865-880.

3.9 Acknowledgements

F. Kleijn van Willigen and J.R. van Ommen thank C.M. van den Bleek and J. van Turnhout for their long-term support. D. Christensen and M.-O. Coppens thank the Dutch National Science Foundation, NWO, for support via a Young Chemist award (NWO/Jonge Chemici).

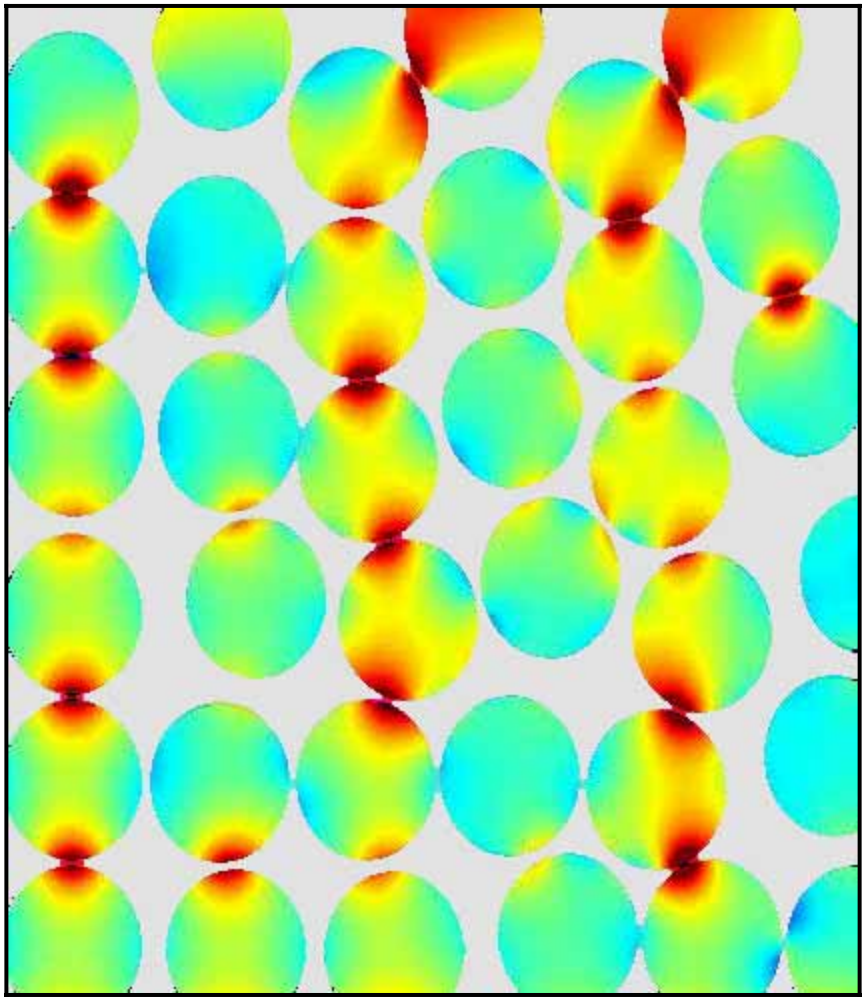

Finite element simulation of insulating particles in a vertical electric field. The colouring shows, locally, the degree of polarization. The effect of the disturbance fields of particles on the polarization of one another is qualitatively demonstrated.

4. Surface Polarization

In Chapters 2 and 3 the bubble behavior in fluidized beds – the mesoscopic scale - was reported. Besides the strong decrease in the size of bubbles due to the electric fields, it was found that the relative humidity of the fluidized gas has a strong influence on the effectiveness of the electric fields. When the fluidized air is bone-dry, the bubble size is reduced significantly less than when the air is humidified to, e.g., 40% RH. Also, the minimum field strength at which the change in bubble size is discernible and reproducible is lower at raised humidities. Clearly, the electric field induced interparticle forces are larger at a higher humidity.

In this chapter, the underlying mechanism responsible for the influence of the relative humidity on the dielectric response of the particles is investigated. Raising the relative humidity increases the surface conductivity of the particles slightly, e.g. from 10^{-9} – 10^{-7} S/m. The Maxwell-Wagner theory of surface polarization is used to model and explain the influence of both conductivity and particle size on the degree of polarization and the optimal field frequency at which this occurs. The qualitative results of this model agree well with the experimental observations reported in Chapters 2 and 3, and show the relative humidity to be an essential component in the effectiveness of electric fields in controlling and reducing bubble size.

This chapter was published as:

Kleijn van Willigen, F., van Ommen, J.R.,van Turnhout, J., and van den Bleek, C.M., 'Bubble Size Reduction in Electric-Field-Enhanced Fluidized Beds', *J. Electrostat.* **63** (2005), 943-948.

4.1 Abstract

Fluidized beds are a common form of a chemical reactor, in which a deep layer of solid particles is set in motion by a stream of gas blowing upward. However, the appearance of gas bubbles can significantly limit the selectivity, conversion, and product properties of gas-solid fluidized beds. We present results on the application of low-intensity electric fields in fluidized beds for reducing the bubble size up to 85% while maintaining the free movement of particles so essential to fluidization, at an energy cost as low as 50 W/m^3.

An analysis is presented of the qualitative response of particles to electric fields, including both drift and diffusion of charges. On this basis, the influence of particle size and particle conductivity on the overall dipole moment, and therefore the interparticle forces, is discussed. Experimental results in a two-dimensional bed show the predicted response to changes in particle size, while variations in optimal frequency response can be explained on the basis of particle conductivity. A maximum reduction in bubble diameter of 25% is achieved with small particles (77 μm), while for large particles (700 μm) the bubble diameter can be reduced by as much as 85%.

Keywords: enhanced fluidization, electric fields, bubble size reduction, interfacial polarization, Debye length, interparticle forces

4.2 Introduction

Gas-solid fluidized beds are one of the workhorses in the chemical process industry, with a vast range of applications in both physical and chemical processes. They are typically employed when pressure drop, temperature control, and replacement of the solid material are important issues. However, the appearance of gas bubbles lowers the mass transfer, and therefore the conversion, in bubbling fluidized beds. A reduction in bubble size by a factor of four can almost double the conversion (Levenspiel, 2002). Furthermore, in the case of parallel and/or series reactions (which occur in almost every realistic situation) smaller bubbles lead to a higher selectivity for the desired product (Kaart, 2002). In this paper we report on the application of electric fields to fluidized beds, with the goal of controlling the bubble size in order to

achieve a significantly higher efficiency from fluidized beds. This is done by stringing thin wire electrodes through the fluidized bed. Fluidizing semi-insulating glass particles of various sizes by air and applying a moderate strength (0-5 kV/cm), low frequency (1-100 Hz) electric field, a significant decrease in gas bubble sizes is measured. A qualitative analysis of the dielectric response of particles to an electric field, based on interfacial polarization and the diffusion of charges, is first given. While this does not directly describe a decrease of bubbles in a fluidized bed (this is determined by interparticle forces that result from the polarization), it does allow us to predict the optimal parameters resulting in the largest interparticle forces, which in turn leads to the largest decrease in bubble size. In the second part, experimental results are described and compared to the theory.

4.3 Complex dielectric constant and conductivity

Variations in interparticle forces on fluidization behavior have been shown, both in experiments and in models, to lead to a more stable fluidization regime *i.e.* fewer bubbles. The attractive and repulsive interparticle forces in this work arise from a polarization of electrostatically neutral particles (see Figure 4-1). In this section, a qualitative analysis will be given of the dominant mechanisms in the response of the particles to the applied electric fields, as well as the parameters that influence this response.

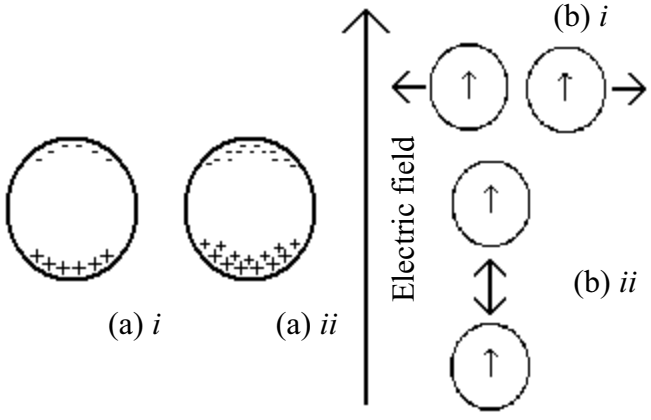

Figure 4-1. The distribution of charges (ions) when drift (a) *i*, and drift and diffusion (a) *ii* play a role. Arrows represent the repulsive (b) *i*, and attractive (b) *ii*, interparticle forces between polarized particles.

In heterogeneous media consisting of materials of different dielectric permittivities or conductivities, interfacial polarization, also known as Maxwell-

Wagner polarization, appears when the system is subjected to electric fields. Our system consists of a mixture of particles and air; the latter is electrically inactive. At low frequencies, the free ionic charges in the particles can follow the change in the electric field easily, resulting in a significantly larger polarization than expected on the basis of electronic, atomic, and molecular polarization. The free charges will drift to the boundaries of the particles, and should be considered to be a surface charge. The interfacial polarization manifests itself as a large increase in the dielectric constant versus frequency and a peak in the dielectric loss. If the concentration of free charges (ions) is not negligible then the dimensions or sizes of the particles can play an important role. This is because the surface charges are in fact not just surface charges, but are distributed over a charge layer, which can be characterized by the Debye diffusion length. The diffusion counteracts the outward drift of the ions and thus decreases the effective dipole moment. This introduces a dependence of the dipole moment on the size of the particle. The important parameters that can be varied in electric-field-enhanced fluidized beds which influence the dielectric response are the particle size and the conductivity. The influence of variations in these parameters will now be outlined.

Using Einstein's relation for the diffusion coefficient and introducing the particle conductivity, σ_p, and the relaxation time of the conductivity, τ_c, we can derive the Debye length, λ, which describes the thickness of the charge layer:

$$\lambda = \sqrt{(D \cdot \varepsilon_0 \cdot \varepsilon_\infty / \sigma_p)} \qquad [4 - 1]$$

where D is the diffusion coefficient, ε_0 the permittivity of free space, and ε_∞ the permittivity of the particle at high frequency. The relaxation time of the particle conductivity equals:

$$\tau_c = \varepsilon_p \cdot \varepsilon_0 / \sigma_p \qquad [4 - 2]$$

The complex dielectric response, including both the drift and diffusion in a plane geometry, is given by Boersma and van Turnhout (1998):

$$\varepsilon^*(\omega) / \varepsilon_\infty = (1 + i \cdot \omega \cdot \tau_c) / (i \cdot \omega \cdot \tau_c + \tanh(y)/y) \qquad [4 - 3]$$

in which $y(\omega) = (d_p / \lambda) \cdot \sqrt{(1 + i \cdot \omega \cdot \tau_c)}$, d_p is the particle diameter, and ω is the radial frequency. The complex permittivity ε^* is defined as

$$\varepsilon^*(\omega) = \varepsilon' - i\varepsilon'' \qquad [4 - 4]$$

The dielectric permittivity, ε', and loss, ε'', are shown in Figure 4-2 for various particle diameters. See Table 4-1 for the relevant values of other parameters.

The trend is for both the rise in ε' and the maximum of ε'' to shift to lower frequencies for larger particle sizes. When calculating characteristic time constants for particles in flows, such as those based on inertia, a similar trend is noticed: larger particles have longer characteristic times than smaller particles. Also, the influence of variations in conductivity on the particle response is significant. Firstly, a higher conductivity gives much larger net dipole moments – this results in larger interparticle forces. Secondly, a higher conductivity and accompanying stronger dielectric response, show a shift to *higher* frequencies of the interfacial dielectric response. This is illustrated in Figure 4-3, and shows that changes in the conductivity may lead to quite different responses of the electric-field-enhanced fluidized bed to the applied field.

Table 4-1. Parameters and constants used for a qualitative analysis of the dielectric behavior of particles in an electric field.

Constant / parameter	Typical value
ε_∞	7
D	10^{-10} m^2/s
σ_p	10^{-7} – 10^{-9} S/m
d_p	70 – 700 μm

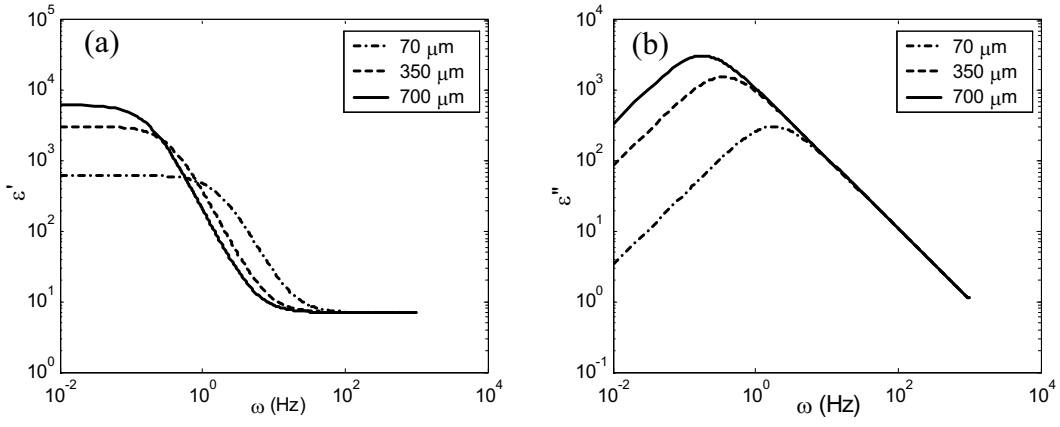

Figure 4-2. Frequency response of dielectric permittivity (a) and loss (b) to changes in particle size.

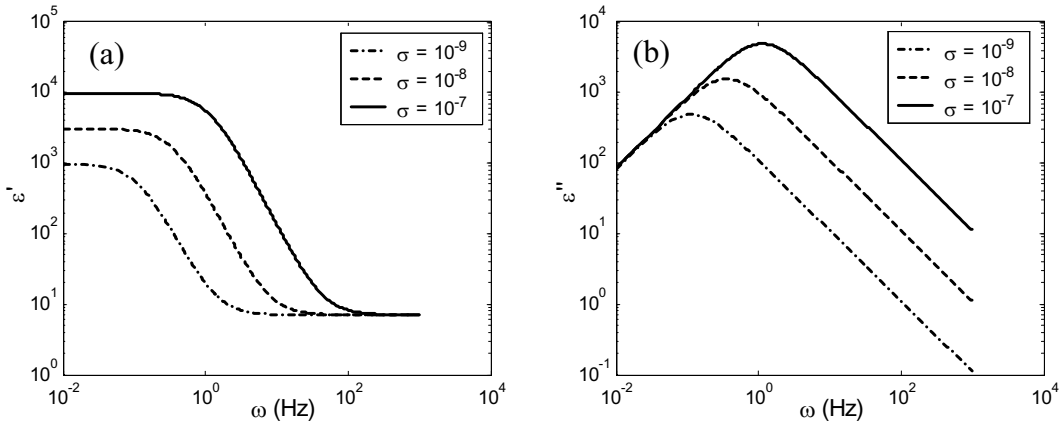

Figure 4-3. Frequency response of dielectric permittivity (a) and loss (b) for a 350μm particle of various conductivities, including both drift and diffusion of the ionic charges.

4.4 Experimental

A two-dimensional fluidized bed, consisting of two vertical flat plates, in between which the particles are fluidized, was equipped with thin wire electrodes placed such that highly non-uniform cross-flow and co-flow electric fields exist in the bed (Kleijn van Willigen et al., 2003). Analysis of high frequency (up to 200 Hz) pressure fluctuations was used as a quantitative indicator of the size of bubbles in the fluidized bed (Van der Schaaf et al., 2002). The influence of the electrodes (diameter 250 μm) when unenergized on bubble behavior was not measurable using the employed technique. The experiments were conducted in a temperature-controlled cabinet, and the settled bed height was typically 300mm. Glass beads of Geldart type A (d_p = 77 μm, u_{mf} = 1.0 cm/s, u_0 = 3 u_{mf}) and type B (d_p = 700 μm, u_{mf} = 33 cm/s, u_0 = 1.5 u_{mf}) were fluidized in dry air (relative humidity lower than 2%).

Typical results are presented in Figure 4-4 as a fractional decrease in bubble diameter for various field strengths and frequencies. During fluidization with and without electric field, it was observed both visually and in pressure fluctuation data that the behavior of the particle phase is very similar and that fluidity was conserved. However, while individual particle movement remains unchanged, the effect on bubbles is significant: up to 25% for the small particles and up to 85% for the large particles. This is in agreement with the qualitative observation made above that

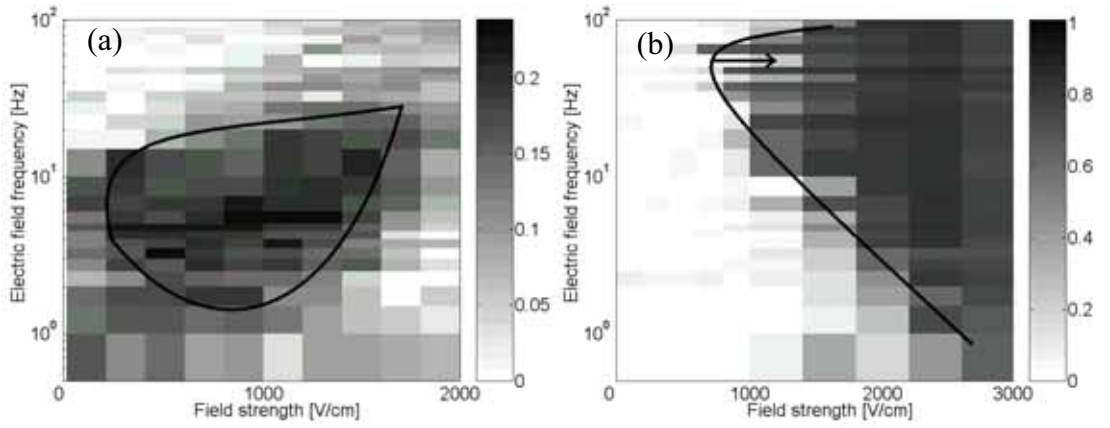

Figure 4-4. Bubble size decreases at 190 mm (63% of bed height), determined using pressure fluctuation analysis. The grayscale shows the fractional change in bubble diameter as a function of frequency and field strength. Bed material: (a) 77 µm glass beads, (b) 700 µm glass beads. The black lines denote the region of optimal electric field strength and frequency (Kleijn van Willigen et al., 2003).

interfacial polarization is more significant for larger particles. The optimal frequency ranges observed (~5 Hz for small particles, ~50 Hz for large particles) suggests that the large particles are more conductive than the small particles.

4.5 Conclusions

A qualitative analysis of the dielectric response of fluidized particles to electric fields, including both drift and diffusion of charges, was presented. The particle diameter, the particle conductivity, and the applied field frequency are parameters that can influence the net dipole behavior of the particles, and therefore they determine the effects of the electric fields on the bubble behavior in the fluidized bed. In this chapter, the response of particles to the electric field is described; the hydrodynamics involved in the decrease of bubble size due to the electric-field-induced interparticle forces will be the subject of future work.

In an experimental electric-field-enhanced fluidized bed, the maximum bubble size reduction was demonstrated to be greater for the large particles, and was shown to occur at lower frequencies for the small particles. The clarification of the effect of these parameters allows for an optimal engineering of systems for the most efficient fluidization regime.

4.6 Notation

D diffusion coefficient, m^2 / s

u_0 superficial velocity, m/s

u_{mf} minimum fluidization velocity, m/s

ε_∞ permittivity of the particle at high frequency, -

ε_p relative dielectric constant of a particle, -

ε_0 permittivity of free space, 8.854 10^{-12} F / m

ε^* complex permittivity, -

ε' dielectric permittivity, -

ε'' dielectric loss, -

λ Debye length, m

σ_p particle conductivity, S

τ_c relaxation time of the conductivity, s

ω radial frequency, 1 / s

4.7 References

Boersma, A., and van Turnhout, J., 'Dielectric study on size effects in polymer laminates and blends', *J. Polym. Sci., Part B: Polym. Phys.*, **36** (1998), 2835-2848.

Kaart, S., Schouten, J.C., and van den Bleek, C.M., 'Improving conversion and selectivity of catalytic reactions in bubbling gas–solid fluidized bed reactors by control of the nonlinear bubble dynamics', *Catal. Today*, **48** (1999), 185-194.

Kleijn van Willigen, F., van Ommen, J.R., van Turnhout, J., and van den Bleek, C.M., 'Bubble size reduction in a fluidized bed by electric fields', *Int. J. Chem. Reactor Eng.*, **1**: A21 (2003). http://www.bepress.com/ijcre/vol1/A21.

Levenspiel, O., 'G/S reactor models – packed beds, bubbling fluidized beds, turbulent fluidized beds and circulating (fast) fluidized beds', *Powder Technol.*, **112** (2002), 1-9.

Van der Schaaf, J., Schouten, J.C., Johnsson, F., and van den Bleek, C.M., 'Non-intrusive determination of bubble and slug length scales in fluidized beds by

decomposition of the power spectral density of pressure time series', *Int. J. Multiphas. Flow*, **29** (2002), 865-880.

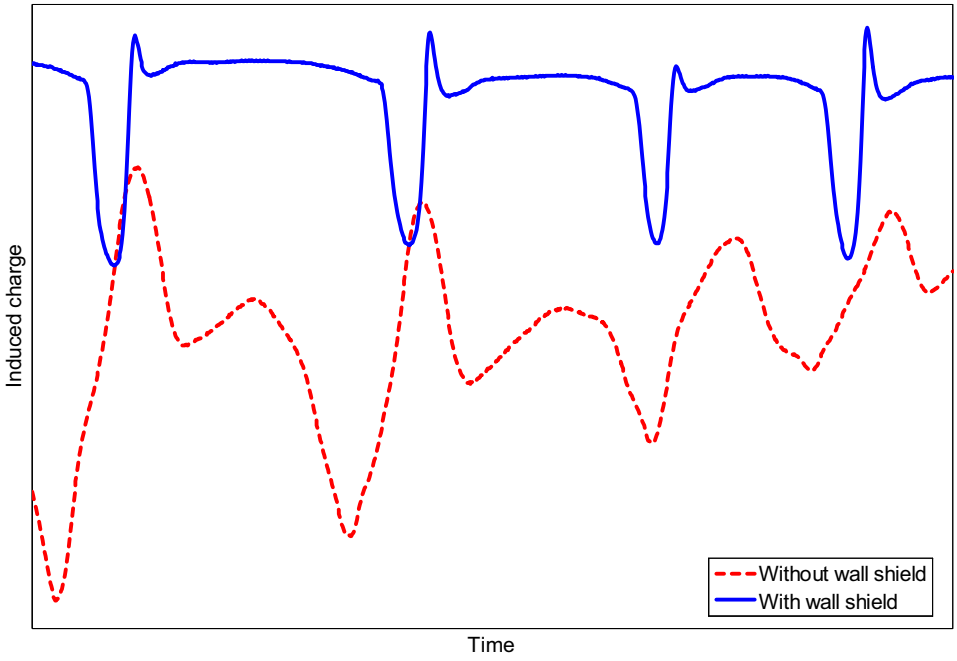

The measurements of electrostatic charge distribution presented in this chapter would not have been possible without the good shielding of the induction probe, as illustrated in the figure above.

5. Mapping the Electrostatic Charge Distribution around Bubbles

The effect of an electric field on particles, such as the response in an electric field enhanced fluidized bed, may be described as an electrodynamic response. The oscillating electric fields induce a periodic electric polarization of the particles, where the charge created at one pole is equal and opposite to the charge on the other pole. That is, the net charge on the particle remains unchanged.

This chapter is different from the other chapters of this thesis in that it treats *electrostatics*. Triboelectric charging occurs in most, if not all, fluidized beds. However, when the rate at which the charge can dissipate or discharge is lower than the rate of triboelectric charging, a surplus charge builds up inside the bed. Here, it is studied how this charge distributes through the bed and around bubbles.

Instead of *applying* electric fields, we now *measure* the fluctuations in the electric field originating from the charged bed mass. A novel induction probe design allows an accurate, localized measurement of the charge of particles in the bed. Using the center of a bubble as a zero-charge reference point, it is found that the net charge on the bed mass is negative, and a more negative charge builds up on the particles in the wake of the bubble.

This chapter was accepted for publication as:
Chen, A., Bi, H.T., Grace, J.R., Kleijn van Willigen, F., and van Ommen, J.R., 'Measurement of charge distribution around a rising bubble in a 2-D fluidized bed', *AIChE J.*, **52** (2006), 174-184.

5.1 Abstract

A technique has been developed to determine the charge distribution around single rising bubbles in a two-dimensional fluidized bed. Four induction probes positioned flush with the outside wall of the column and connected to charge amplifiers record induced charge signals as bubbles pass. The charge distribution surrounding a single bubble is then reconstructed with the assumption that the bubble is symmetrical and that the charge around the bubble remains constant as it rises. The emulsion phase far from the bubble in a two-dimensional fluidized bed of glass beads was found to be charged negatively and, contrary to our previous assumptions, the charge density decreased gradually toward the bubble-dense phase interface with a nearly zero charge density inside the bubble. The wake of the bubble is more negatively charged than the emulsion phase, supporting our previous speculations.

Keywords: tribo-electric charging, particles, electrostatics, gas-solid fluidized beds, bubbles, induction probes.

5.2 Introduction

Electrostatic charging in gas-solid fluidized beds is unavoidable. When the discharging rate of the particles is low compared to the charging rate, the negative effects on fluidization can induce problems such as particle agglomeration, changes in the hydrodynamic behavior of the bed, adhesion of particles to the walls, interference with instruments, nuisance discharges or explosions, and undesirable by-products.

The source of charge generation in fluidized beds is the contact and separation between particles, the fluidizing gas, and the reactor wall in which they are contained. This process is known as triboelectrification (Harper, 1967). When the particles are insulators (such as sand, glass, FCC catalyst, polymers, many pharmaceutical materials) and the fluidizing gas has low conductivity (i.e. low relative humidity in the case of air) the discharge rate is typically much lower than the charging rate, leading to a buildup of electrostatic charge in the system. In fluidization, we can differentiate between particle-particle and particle-wall contact. Because particle-particle collisions result only in a separation of charge, the net charge over the two particles is conserved. Which particle gains or loses charge is difficult to predict when they are

similar in size and material. This is different when fluidizing dissimilar materials (that is, blends of particles of binary particle sizes); there will usually be a clear preference for one group to be charged differently than the other group in a process known as bipolar charging (Zhao et al., 2003).

The collision particles with the reactor wall, on the other hand, always occurs dissimilar materials. When this is the case, there is typically a net flow of charge to or from the walls. Thus, whereas particle-particle interaction does not lead to an overall charge build-up in a fluidized bed, particle-wall collisions will. Charging by the fluidizing gas is generally considered to be low (Mehrani et al., 2005) unless ionized gas is used. Despite the negative effects of charge buildup, the mechanisms of charge generation and dissipation remain poorly understood.

The build-up of net charges in the bed has been studied using Faraday pails (see Chen et al., 2003a, for an overview) or induction systems (Murtomaa et al., 2003). However, a bubbling fluidized bed consists of two distinct phases: a dense phase (also known as emulsion phase) and a dispersed bubble phase. The reactant concentration is usually higher in bubbles and the region surrounding bubbles, leading to faster reaction near the bubbles than elsewhere in the dense phase. Particles in the region surrounding a rising bubble tend to move more quickly than particles in the elsewhere in the dense-phase region of the bed. Particle-particle and particle-wall collisions are more vigorous among particles surrounding bubbles, potentially leading to higher rates of charge generation arising from particle-particle contact charging. It is therefore expected that particles around bubbles may carry higher charges than those further away.

Until recently, there have only been two studies in the open literature on electrostatic charges around bubbles in fluidized beds. Based on the signals from an induction probe, Boland and Geldart (1971) speculated that the front and wake of bubbles carry charges of opposite signs. A collision probe inside a two-dimensional column was used by Park et al. (2002a) to explore charge induction and transfer when a single bubble passed. Park et al. (2002b) and Chen et al. (2003b) developed a theoretical model to explain the electrical current signals generated by the passing of single gas bubbles. The model, which assumes that there is a charge distribution in the region adjacent to the bubble and much higher charge density in the wake region of the same sign as the front region of the bubble, correctly predicted the trend of charge signals registered by a sensitive collision probe when bubbles passed. Testing

of the quantitative predictions from this model requires information on the distribution of specific charge density surrounding rising gas bubbles in gas-solids fluidized beds. Examining the distribution of charges in the vicinity of rising bubbles can assist in understanding electrostatic charge generation, charge separation, dissipation, and accumulation in fluidized bed reactors.

The purpose of this study was to develop a technique to measure the charge distribution surrounding a single rising bubble in two-dimensional gas-solids fluidized beds. The new technique is independent of net charge build-up in the bed, not influenced by charge transfer such as with collision probes, and allows the reconstruction of the complete charge distribution around bubbles, unlike the line traces or averages available from other techniques. Induction probes, which have been widely used for the measurement of surface charge distribution with high spatial resolution (Taylor, 2001), were selected to measure the charge distribution around rising bubbles in two-dimensional columns made of transparent materials. A number of induction probes were placed flush with the outer surface of the column to eliminate probe interference with the motion in the bed and charge transfer arising from collisions between particles and the probe. These induction probes are sensitive to *changes* in electric field as a bubble passes, and as such are not influenced by residual charge on the column wall. Signals from the probes are analyzed using an image-reconstruction technique to map the charge distribution around the bubble, which is independent of a priori knowledge of the bubble size or location. The resolution of the reconstruction is affected by the size and number of probes. In this paper, four probes were used.

5.3 Measurement technique

Tests on the static charge around bubbles were conducted with induction probes in a two-dimensional fluidized bed. The column, made of Plexiglas®, has an inner thickness of 14 mm, a width of 280 mm, and a height of 1.24 m. The windbox volume is 800 cm^3. Glass beads of diameter 0.560 mm and density 2500 kg/m^3 were used as the bed material. The settled bed height was approximately 700 mm. The bed was fluidized at an air flow rate of Q_{air}= 1.78 m^3/s, leading to a regular pattern of independent bubbles with few particles raining through them. Bubbles were approximately 80 mm in diameter and had rise velocities of about 0.26 m/s. Figure

5-1 shows a schematic of the column and probes. Copper tape on both the front and rear walls was connected to ground to maintain a zero potential on the column wall. The resistivity between the left and right sides of the column was measured to be $3.8 \times 10^7\ \Omega\ m^{-1}$. Four induction probes were placed 520 mm above the perforated plate distributor. The distance between adjacent probes was 13 mm. A Canon digital video camera, operating at 30 frames/s, was used to record the rise of bubbles through the column and to ensure that measurements were performed on single bubbles not directly influenced by others. Bubbles whose center passed probe 1 and whose edge passed probe 4 were selected for further analysis. The video was thus always synchronized to the charge measurements.

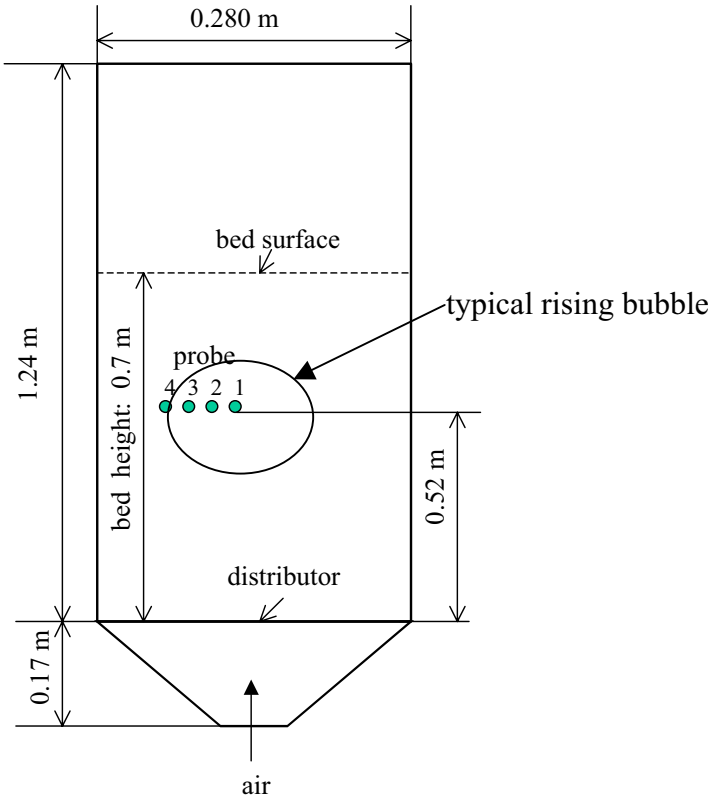

Figure 5-1. Front view of the two-dimensional fluidization column, showing the optimal location and size of a bubble rising by the induction probes.

Induction probes (see Figure 5-2) constitute the simplest type of field meters. Each induction probe consists of an insulated, circular copper disc (10 mm diameter), connected to the core of a coaxial cable, embedded in a Teflon® cylinder, and wrapped with a single strip of conducting copper tape. The shielding of the coaxial cable is connected to the shielding around the probe and to common ground that,

together with the coated and grounded walls of the column, minimizes distortion of the signal from charges above, below, or to the side of the probe. The metal sensor is charged by induction attributed to the electric field generated by the charged particles.

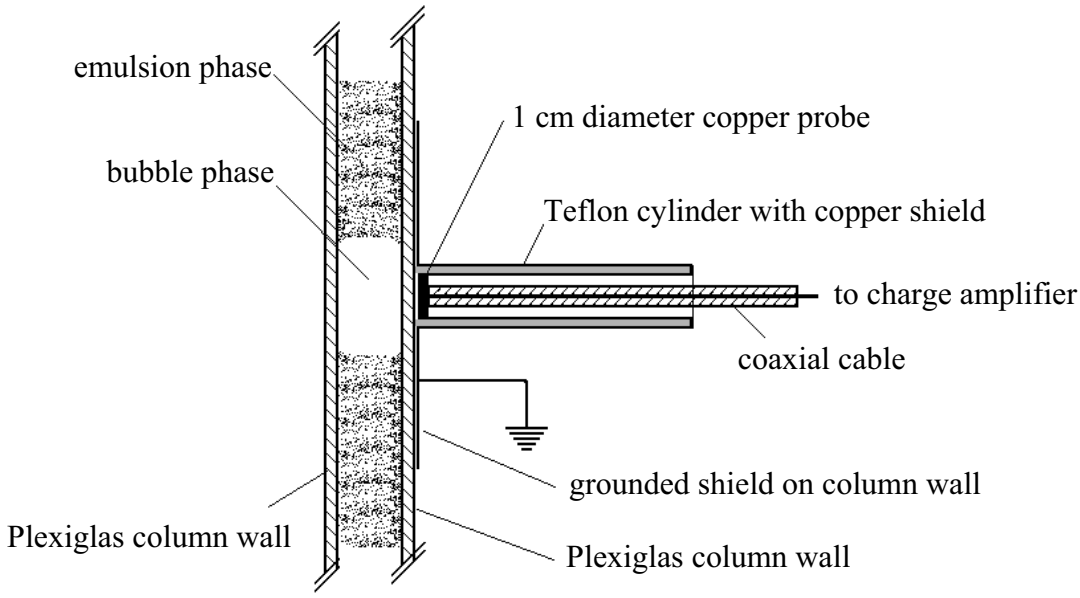

Figure 5-2. Induction probe. The probe is placed flush with the outside wall of the column (as shown). Around the probe and on the column wall is the grounded shielding. When a bubble is in front of the probe, little or no charge is induced on it. When the bubble passes past the probe, the charge of the emulsion phase is measured.

Each induction probe is connected to a separate Kistler charge amplifier (model 5011B or 5015) by a coaxial cable. Although the induction probe is simple in concept, in practice it is susceptible to drift, charging, and distortion. Charge amplifiers and Teflon® insulation minimized the first two of these problems. Through the use of conductive shields, field distortion was minimized. Grounding of these shields, in combination with the very low potential of the probe, enabled optimal measurement of the fields generated by the charged particles. The outputs of the Kistler charge amplifiers were synchronously recorded using an LMS-Difa APB220 data-acquisition system at a sample rate of 200 Hz.

The four probes described above can measure induced charges during the passage of bubbles. Figure 5-3 shows typical experimental results for a bubble with its center passing probe 1 and the outer edge of the bubble passing probe 4. The

measurement shows the change in induced charges, which has the opposite sign to the change in charges in front of the probe. When the bubble is far from the probes, the signals are constant. When the bubble nose approaches the probe, the induced charges began to decrease until a minimum was reached when the center of the bubble reaches the probe. Induced charges then increased as the bubble moved away from the probe. Maximum charges occurred after the bubble passed the three central probes 1, 2 and 3, but not probe 4. All induced charges reached stable values after the bubble left the probes far behind. Note that the zero level of charge is arbitrary – an absolute value cannot be determined using this technique. The purpose of this article is to reconstruct the charge distribution surrounding the bubble from the induced charge signals recorded from all four probes.

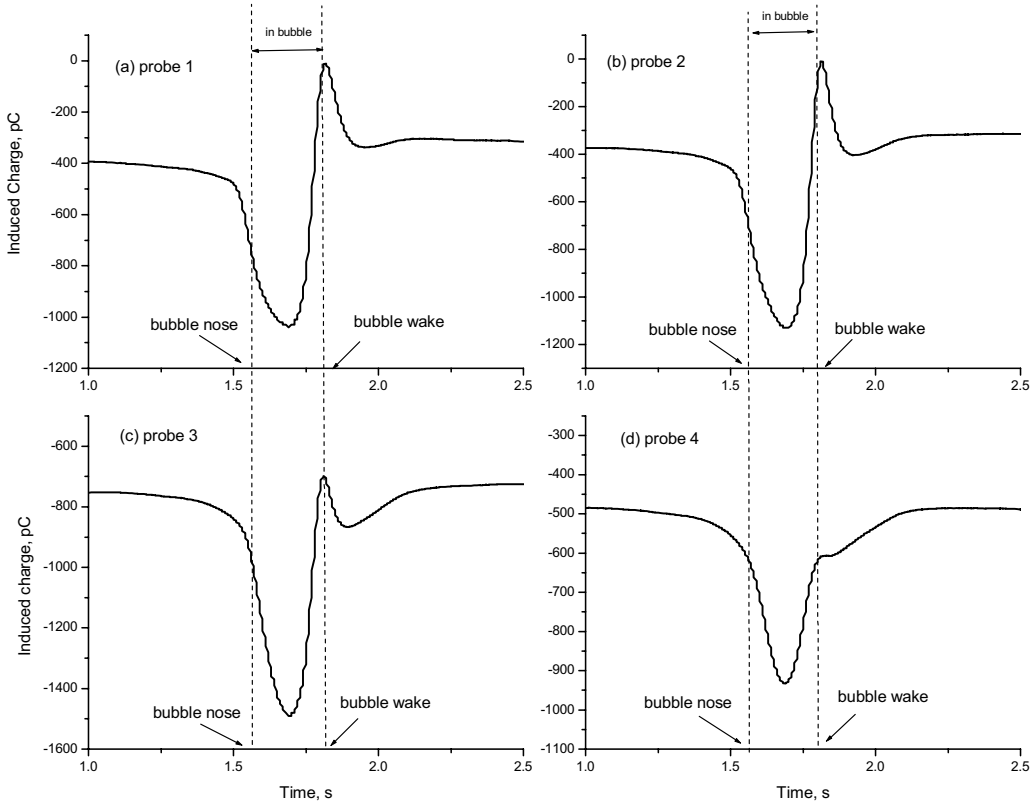

Figure 5-3. Induced charges measured by the four probes as a single bubble passed. Approximate time of the passage of the bubble nose and wake are shown. The signal from probe 4 is weaker than the others because it was on the edge of the bubble.

5.4 Reconstruction of charge distribution

The region around the bubble is first divided into a number of pixels, as shown in Figure 5-4. Combining Gauss's law with the definition of electric field and potential (Cross, 1987), the electrostatic field E and potential V are given by:

$$\text{div } E = \frac{q}{\Pi} \qquad [5 - 1]$$

and

$$E = \text{-grad } V \qquad [5 - 2]$$

where q is the volume charge density and Π is the permittivity of the medium, assumed to be uniform in the region of interest.

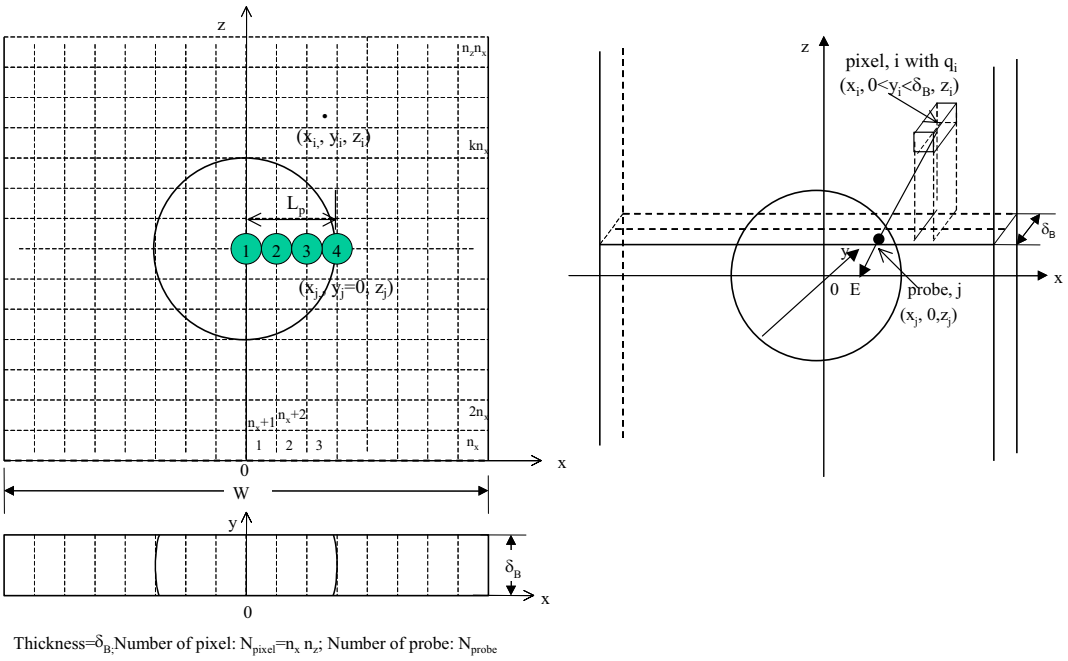

Figure 5-4. Geometric positions of the probes and pixel grid reconstruction.

From Eq. 5 - 1 and Eq. 5 - 2

$$\text{div}(\text{grad } V) = \nabla^2 V = \frac{\partial^2 V}{\partial x^2} + \frac{\partial^2 V}{\partial y^2} + \frac{\partial^2 V}{\partial z^2} = -\frac{q}{\Pi} \qquad [5 - 3]$$

It is assumed that there are charges only in pixel i with constant charge density, q_i, in the y direction, and with no charges in other regions. Hence

$q = q_i$ at $x = x_i$, $0 < y < \delta_B$ and $z = z_i$,

$q = 0$ in all other regions.

Because the permitivity Π of the medium in the bed is taken to be uniform in all directions, and letting $v' = -\frac{\Pi V}{L_p^2 q_i}$, $x' = x/L_p$, $y' = y/L_p$, $z' = z/L_p$, then the dimensionless form is

$$\frac{\partial^2 v'}{\partial x'^2} + \frac{\partial^2 v'}{\partial y'^2} + \frac{\partial^2 v'}{\partial z'^2} = q' \qquad [5 - 4]$$

where

q' =1 at $x' = x_i/L_p$, $0 < y' < \delta_B / L_p$ and $z' = z_i / L_p$,

q' = 0 in all other regions.

The boundary conditions are:

at the "left" and "right" sides: $x' = -W / 2L_p$ and $x' = W / 2L_p$: $v' = 0$

at the front and rear walls: $y' = 0$ and $y' = \delta_B / L_p$: $v' = 0$

at $z = 0$ and $z = H_{bed} / L_p$: $\frac{\partial v'}{\partial z'} = 0$.

Eq. 5 - 4 can be solved to obtain v' and hence V.

For an infinitesimal element of the probe at (x_j, $y_j = 0$, z_j), the electric field perpendicular to the wall can be estimated by

$$E_\perp = E_y = -\frac{\partial V}{\partial y}\Big|_{x=x_j, y=0, z=z_j} \qquad [5 - 5]$$

Then the induced charge on an infinitesimal element ds of the probe is

$$\sigma_{ij} = \Pi \; E_\perp \, ds = -\Pi \; \frac{\partial V}{\partial y}\Big|_{x=x_j, y=0, z=z_j} ds = q_i L_p \frac{\partial v'}{\partial y'}\Big|_{x'=x_j/L_p, y=0, z=z_j/L_p} ds \qquad [5 - 6]$$

The total charge on probe j is

$$\sigma_{ij,total} = \iint_{\text{surface of probe j}} \sigma_{ij} \, ds \qquad [5 - 7]$$

If the probe is a circular plate of radius r_{probe} with its center at (x_{j0}, 0, z_{j0}), the total charge of probe j from the i^{th} pixel can be expressed as

$$\sigma_{ij,total} = \iint_{\text{surface of probe j}} \sigma_{ij} \, ds$$

$$= q_i L_p \int_{x_{j0}-r_{probe}}^{x_{j0}+r_{probe}} \int_{z_{j0}-[r_{probe}^2-(x_j-x_{j0})^2]^{0.5}}^{z_{j0}+[r_{probe}^2-(x_j-x_{j0})^2]^{0.5}} \frac{\partial v'}{\partial y'}\Big|_{x'=x_j/L_p, y'=0, z'=z_j/L_p} dz_j dx_j \qquad [5 - 8]$$

Let

$$\omega_{ij} = L_p \int_{x_{j0}-r_{probe}}^{x_{j0}+r_{probe}} \int_{z_{j0}-[r_{probe}^2-(x_j-x_{j0})^2]^{0.5}}^{z_{j0}+[r_{probe}^2-(x_j-x_{j0})^2]^{0.5}} \frac{\partial v'}{\partial y'}\Big|_{x'=x_j/L_p, y'=0, z'=z_j/L_p} \mathrm{d}z_j \mathrm{d}x_j \qquad [5 - 9]$$

Eq. 5 - 8 is used to calculate the induced charge on probe j attributed only to pixel i having a charge density q_i. The induced charge from all pixels to probe j is then obtained by

$$Q_j = \sum_{i=1}^{N} \sigma_{\mathrm{ij,total}} = \sum_{i=1}^{N} \omega_{ij} q_i \ (j = 1, 2, \ldots, \mathrm{M}) \qquad [5 - 10]$$

Theoretically, if the charge induced on probe Q_j can be measured, q_i for each pixel can be reconstructed using multiple probes. The quality of the reconstruction is influenced by the number of measurements and the number of probes. For good reconstruction, measurements should be taken inside, on the border and outside the bubble. The larger the number of probes, the better the reconstruction.

In our experiments, only four probes were fixed horizontally on the wall and many (10,000) pixels had to be employed in the reconstruction (see Figure 5-4) to gain sufficient resolution. Ideally, one should install many probes surrounding the rising bubble to reconstruct the charge density distribution. For the current case with only four fixed probes, it is assumed that each bubble is symmetrical and that the charge around the bubble does not vary as the bubble passes through the measurement region. The latter assumption means that the rising of the bubble past the probes provides the vertical resolution, and the number of probes limits only the horizontal resolution. Thus, although there were only four probes, the induced charge measured at different vertical locations relative to the bubble can be obtained and used to solve Eq. 5 - 10.

5.5 Simulation results

The model was implemented in Fortran using Visual FORTRAN Professional Edition 5.0. Simulations were performed using a line charge and various charge distributions around bubbles to test the model and ascertain how effective it is in reconstructing the charge distribution.

First, the electric field around a line of charge leading from the front wall to the back wall of the column of $-q/\Pi$=1 C / F mm^2, situated at x = 10 mm and z = 10

mm, was determined. The rest of the domain is uncharged. The result is presented in Figure 5-5. Figure 5-5 a shows the electric potential from the side – it is clear that the potential distribution is very narrow at z = 10 mm. Figure 5-5b shows the electric field from the front. Based on this simulation it is concluded that the charge induced on a properly shielded probe situated flush with the wall arises primarily from charges in the region directly in front of it. This implies that matrix ω_{ij}, required to reconstruct the charge distribution q_i in Eq. 5 - 10, is singular as a result of the sharp gradient in the electric field. To solve Eq. 5 - 10, matrix ω_{ij} was calculated and then inverted. The LSGRR subroutine was used to invert the matrix directly, but if the matrix was determined to be mathematically singular or ill-conditioned, a least-squares routine or the singular value decomposition routine provided by Visual FORTRAN Professional Version 5.0 was used to obtain approximate results.

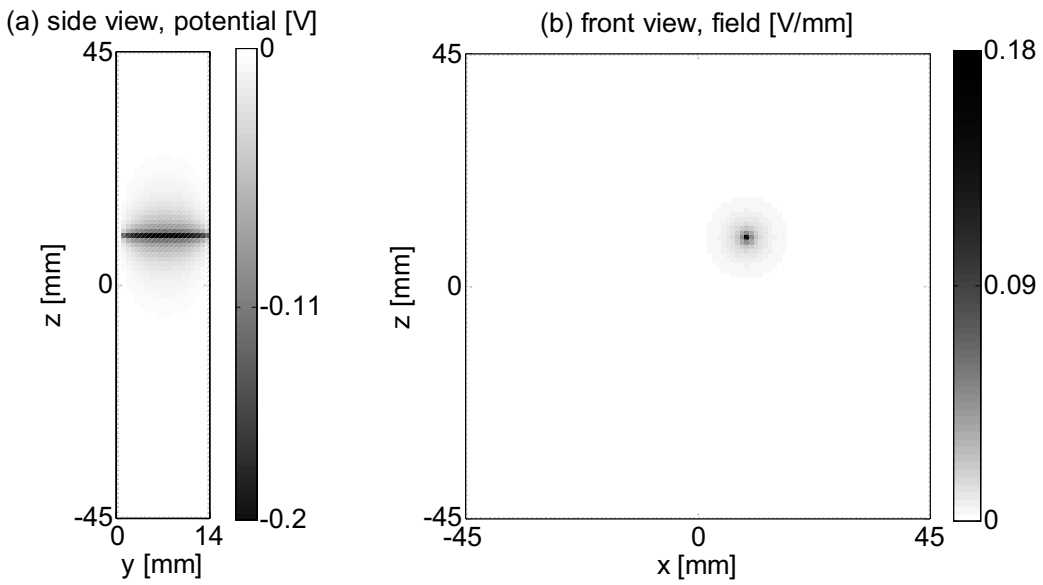

Figure 5-5. Electric potential over the cross section of the column (a) and the electric field perpendicular to the wall (b) resulting from a simulated line charge $-q$ / Π = 1 C/(F mm^2) located at x=10 mm and z=10 mm.

Next, a bubble with its associated charge distribution passing the probes was simulated, and the induced charge was used to reconstruct the original charge distribution. The diameter of the bubble was set at 80 mm for four probes of diameter 10 mm located horizontally, as shown in Figure 5-1. The distance between adjacent

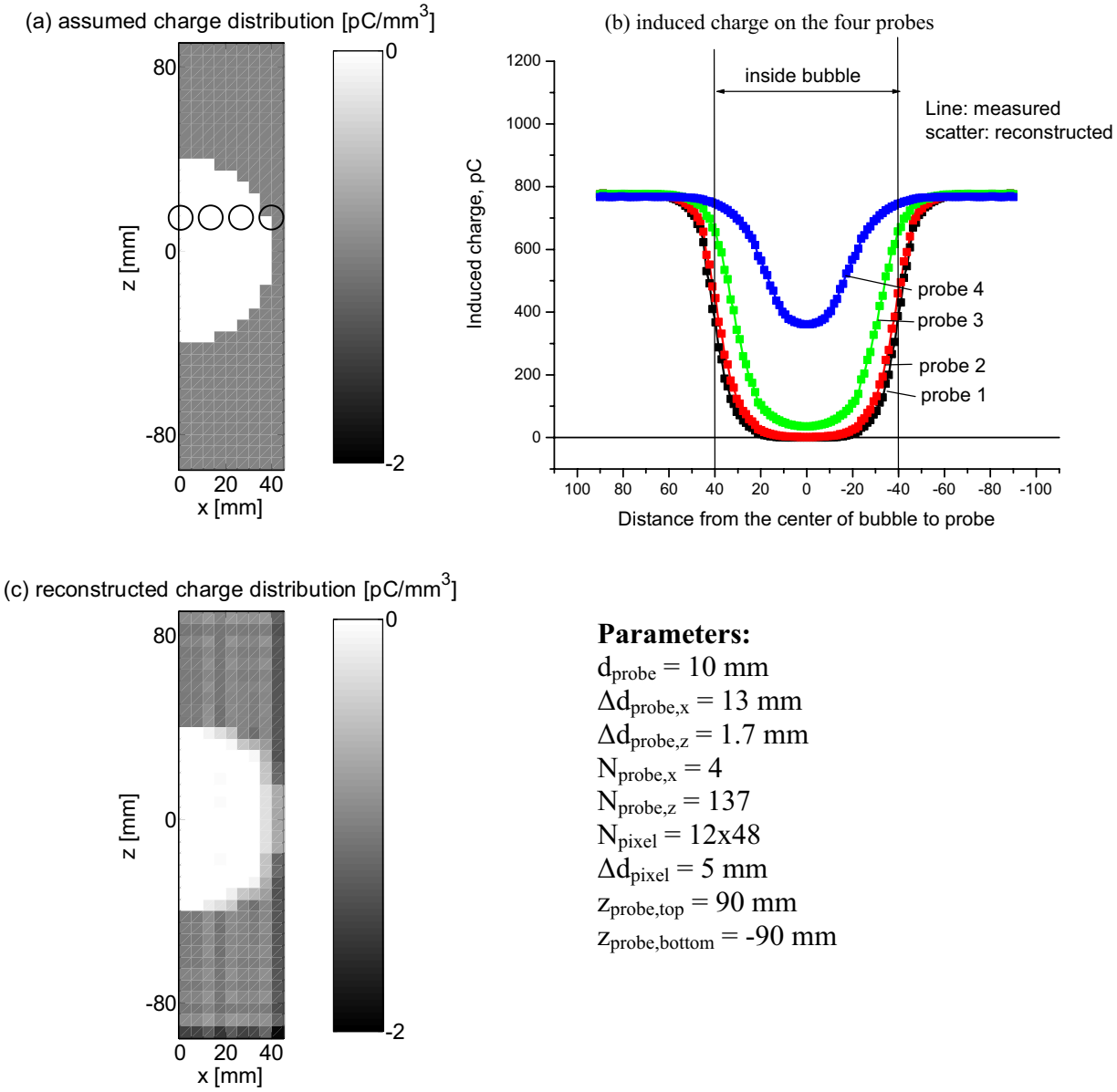

Figure 5-6. Simulation of a rising bubble (d_B = 80 mm) with a uniform charge of 1 pC/mm^3 assumed in the emulsion phase. The simulated induced charges (b) are used to reconstruct the charge distribution (c). The positions of the induction probes are shown in (a).

probes is 13 mm, as in the experiments. It was assumed there is a uniform charge distribution in the emulsion phase (around the bubble) of q = 1 pC/mm^3 and that the inside of the bubble was uncharged. The simulated and reconstructed charges are presented in Figure 5-6. The charges induced on the four probes, shown in Figure Figure 5-6b, are seen to be symmetric and to have the same value when the bubble is far away. When the simulated bubble approaches the probes, the induced charges

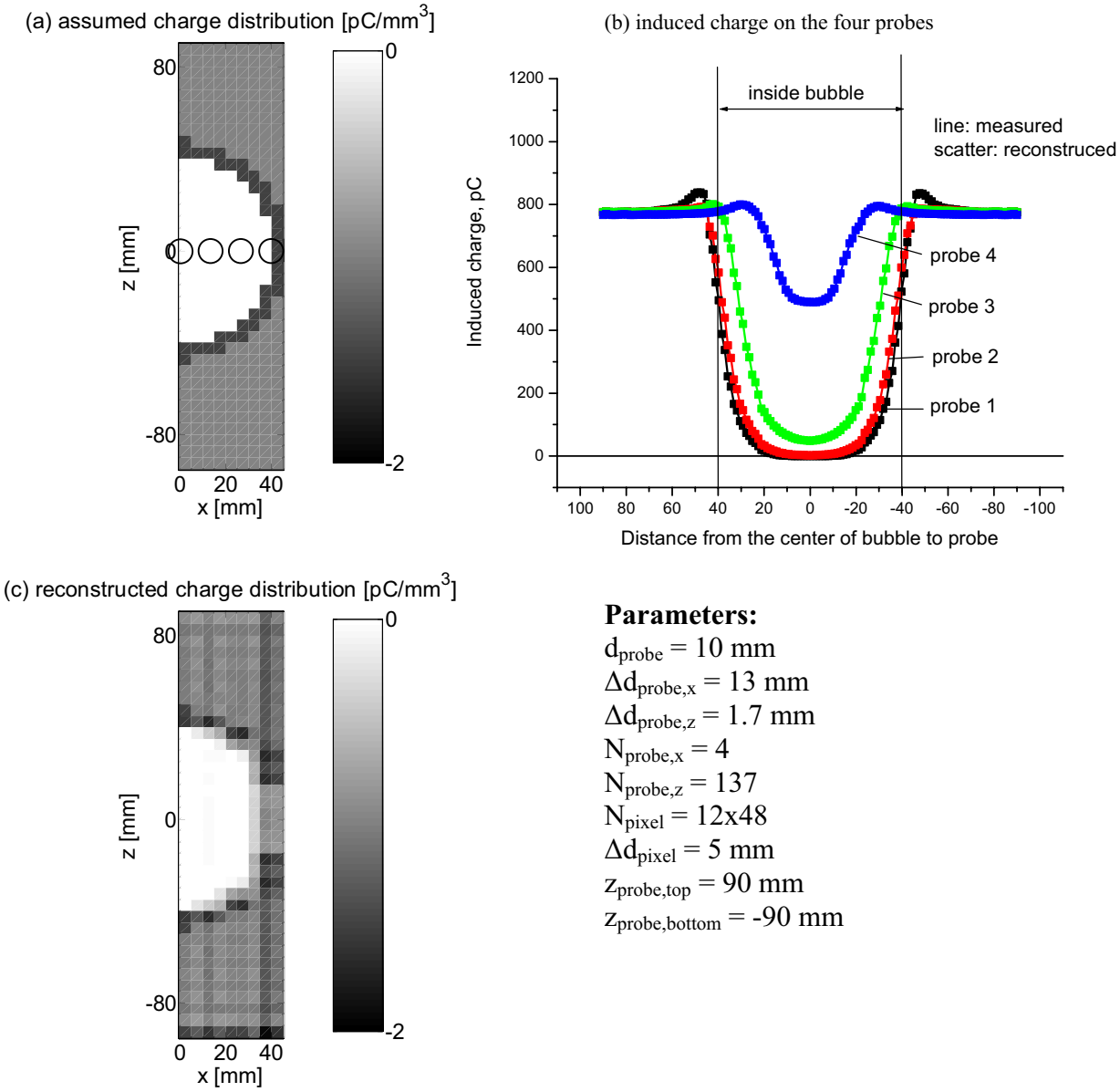

Figure 5-7. Second simulation of a rising bubble (d_B = 80 mm) with a uniform charge of 1 pC/mm^3 assumed in the emulsion phase, but now with a thin layer of highly charged particles (2 pC/mm^3) around the bubble. The simulated induced charges (b) are used to reconstruct the charge distribution (c). The positions of the induction probes are shown in (a).

begin to decrease, reaching a minimum when the bubble is directly in front of the probes. As the edge of the bubble approaches the probes, the induced charges again increase. The induced charges for probes 1 and 2 are 0 and for probe 3 are close to 0 when probes are at the center of the bubble because of zero charge inside the bubble. The induced charge for probe 4, which is at the edge of the bubble, is not zero. Using these four calculated induced charges, the charge distribution around the bubble is

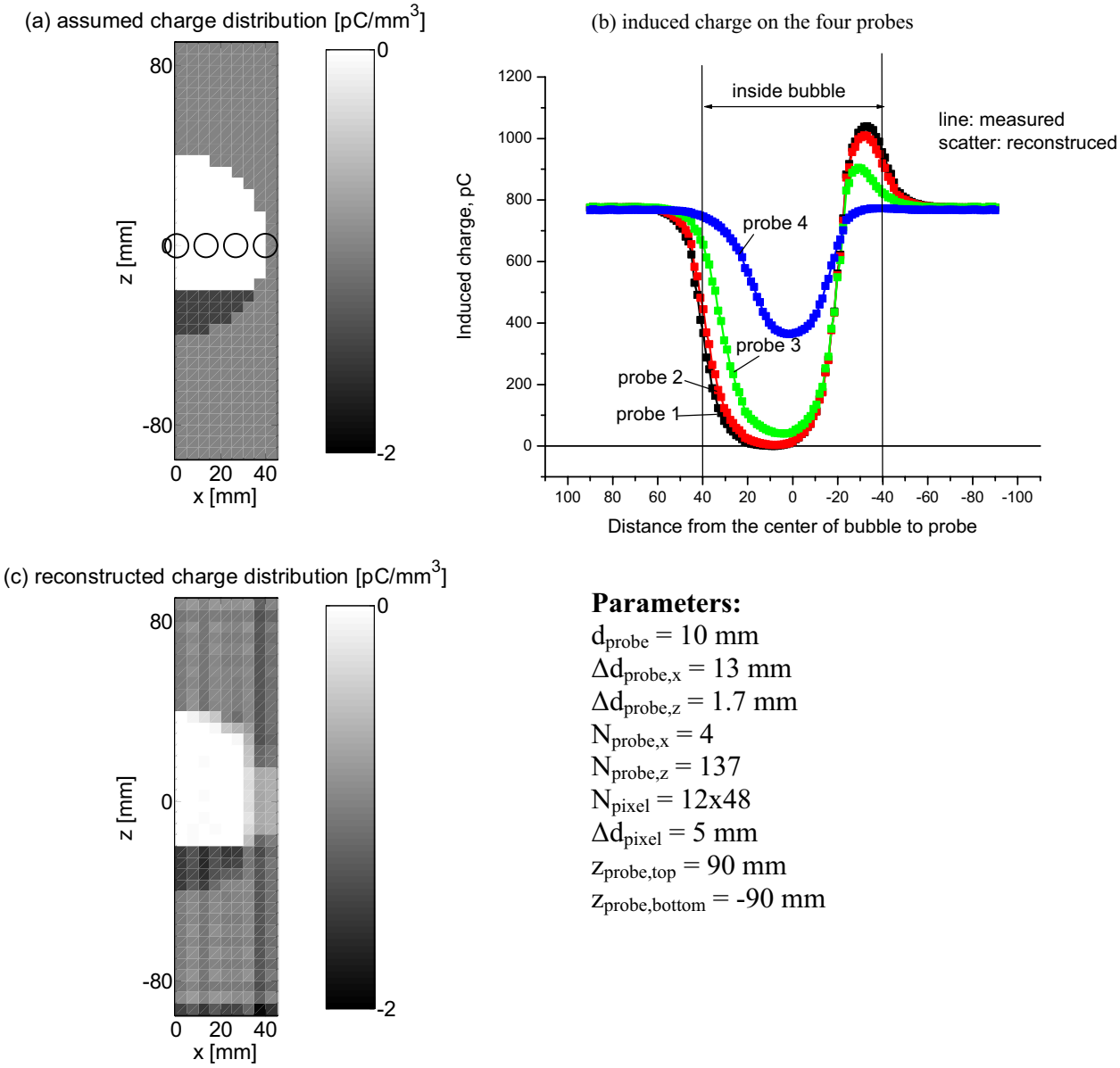

Figure 5-8. The third simulation of a rising bubble (d_B=80 mm), with a uniform charge of 1 pC/mm^3 assumed in the emulsion phase and a highly charged wake (2 pC/mm^3). The simulated induced charges (b) are used to reconstruct the charge distribution (c). The positions of the induction probes are shown in (a).

reconstructed with the above model and shown in Figure 5-6c. It can be seen that there is reasonable agreement between the assumed and reconstructed charge distributions. The distortion at the edge, around probe 4, is largely a result of the ill-defined matrix ω_{ij} while solving Eq. 5 - 10.

In the second simulation, we test whether the reconstruction can accurately reproduce a thin highly charged layer of particles around the bubble. In a two-dimensional view, this means that a ring of particles surrounds the bubble with a

higher charge than that of the emulsion phase. Figure 5-7 shows the induced charges for the four probes (Figure 5-7b) and the reconstructed charge profile (Figure 5-7c) with the distribution assumed to have a thin, highly charged layer around the bubble (Figure 5-7a). It can be seen in Figure 5-7b that there are peaks when the simulated bubble reaches and leaves the probes and that the induced charges for probes 1, 2, and 3 are close to zero when the center of the bubble passes the probes. The induced charge for probe 4 when the bubble center passes is larger than the others because the probe is right at the edge of the bubble. It can also be seen from Figure 7c that there are differences between the reconstructed charge and the assumed charge distribution, especially in the highly charged layer around the bubble. Because there is no probe in the region outside the bubble, the charge reconstruction is poor for $x > 40$ mm. Adding one or two probes outside the bubble would substantially improve the reconstruction.

When a higher charge density is assumed in the wake region of the bubble, as shown in Figure 5-8a, it can be seen from Figure 5-8b that the calculated induced charges for probes 1, 2, and 3 reach maxima as the wake of the bubble passes the probe. All the induced charges approach the same base value after the bubble moves away. These induced charge profiles are very similar to the preliminary experimental results shown in Figure 5-3. Again, the induced charges for probes 1, 2, and 3 are zero when the center of the bubble passes the probes, whereas the induced charge for probe 4 has values greater than zero. The higher charge density in the bubble wake region is captured in the reconstructed profile in Figure 5-8c, although discrepancies still exist between the assumed and reconstructed charge distributions.

5.6 Reconstruction of experimental signals

Typical induced charge measurements using the experimental setup are presented in Figure 5-3. We now reconstruct the charge distribution in the same way as in the simulated cases presented above, but with experimentally measured charge signals as the input.

The baseline of the measured induced charge (that is, charge of the emulsion phase) cannot be measured using the induction probes, but must be determined to reconstruct the charge distribution around bubbles. This is based on observations in the previous section that (1) induced charges from the four probes have the same base

value when the bubble is far from the probes; (2) the minimum charge induced on the probes as the bubble passed (probes 1, 2, and 3) may reach zero; and (3) the induced charge for a probe on the edge of, or outside, the bubble (probe 4) should be nonzero. Lines for all four probes after the bubble advanced far beyond the probes are first set to zero as shown in Figure 5-9a. The minimum induced charge for probe 2 while the center of the bubble passes the probe is found to have the lowest value. Thus, the scale is adjusted so that the minimum induced charge of probe 2 is set to zero. The final rearranged induced charge signals are shown in Figure 5-9b. All induced charges from the four probes have the same base value of approximately +820 pC when the bubble is far from the probes.

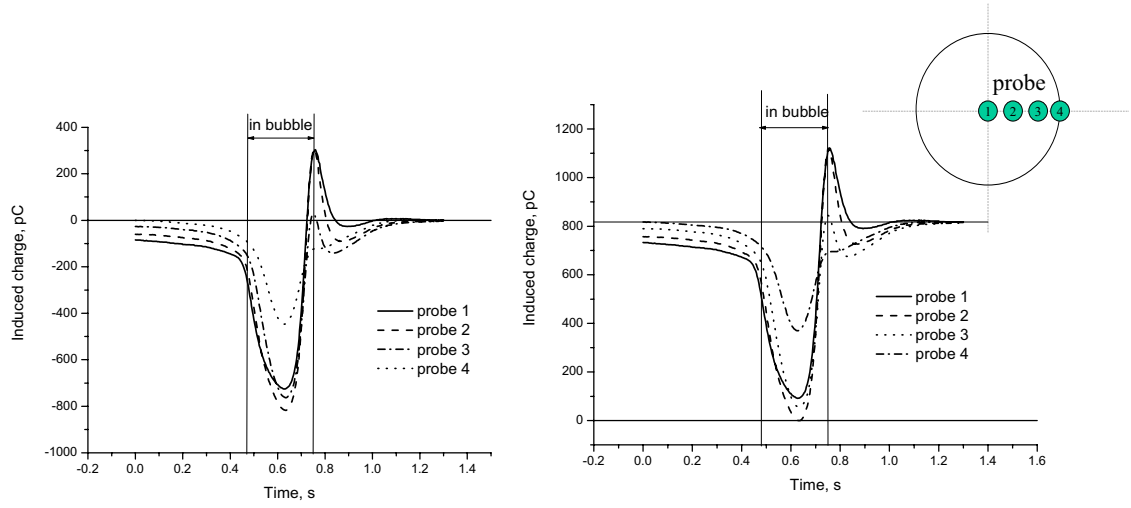

(a) (b)

Figure 5-9. Scaling of the measured induced charges to a common base line. (a) Charges for all four probes after the bubble has advanced far beyond the probes are set to zero. (b) The minimum induced charge for probe 2 while the probe is at the center of the bubble is set to zero.

In the reconstruction model presented above, it is assumed that a bubble is symmetric and that the charge around the bubble does not change as the bubble rises. Therefore, the induced charge as a function of time can be converted into a series of induced charges varying with vertical distance between the center of the bubble and the probe. Here, data from 0.45 to 0.85 s, or the vertical distance between the center of bubble and the probe from 90 to -90 mm, are chosen for the reconstruction.

Figure 5-10a shows the reconstruction results for the induced charges shown in Figure 5-9. It can be seen that the charge inside the air bubble is almost zero, whereas the charges in the dense phase remote from the bubble is negative. There is a

more negatively charged wake, confirming the postulate based on measurements with a single collision probe (Park, 2002a, and Chen, 2003b). However, there is no layer of higher charge density in the boundary region around the bubble-dense phase interface, contrary to the assumption of a surface charge distribution made in the models used to interpret the collision probe data (Park, 2002a, and Chen, 2003b). The charge density outside the bubble in the dense phase is approximately -0.9 pC/mm^3 or -3.6 × 10-7 C/kg. The charge in the wake is about -1.7 pC/mm^3 or -6.8 × 10-7 C/kg. Figure 5-10b compares measured induced charges with those calculated from the reconstructed charge density in Figure 5-10a. As expected, the differences are not significant.

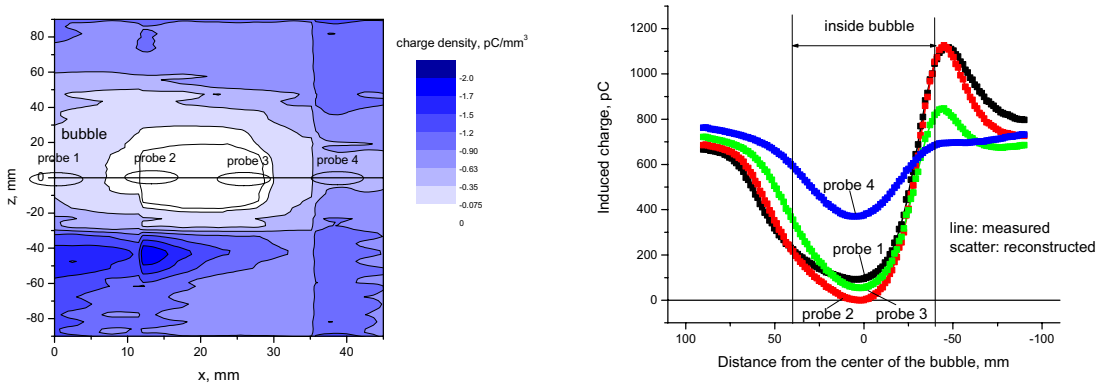

d_{probe}=10mm, $\Delta d_{probe,x}$=13 mm, $\Delta d_{probe,z}$=1.3mm, $N_{probe,x}$=4, $N_{probe,z}$=137
N_{pixel}=12x48, Δd_{pixel}=5mm, $z_{probe,top}$=90 mm, $z_{probe,bottom}$=-90mm

Figure 5-10. (a) Reconstructed charge distribution and (b) comparison of measured induced charge signals and simulated induced charge signals based on reconstructed charge distribution. Case 1, H_{mf} = 0.7 m, d_B = 0.08 m, u_B = 0.26 m/s, d_p = 565 µm, ρ_p=2500 kg/m^3, Q_{air}=1.78 m^3/s .

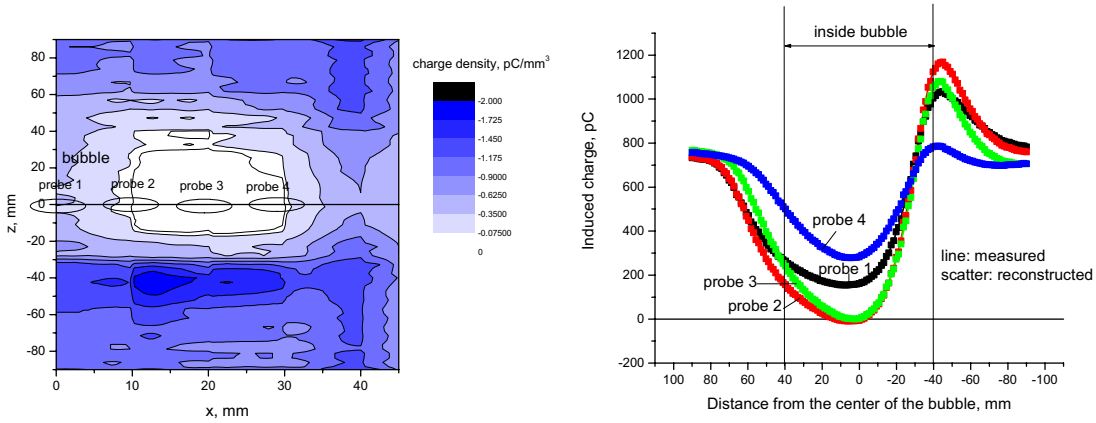

d_{probe}=10mm, $\Delta d_{probe,x}$=13 mm, $\Delta d_{probe,z}$=1.3mm, $N_{probe,x}$=4, $N_{probe,z}$=137
N_{pixel}=12x48, Δd_{pixel}=5mm, $z_{probe,top}$=90 mm, $z_{probe,bottom}$=-90mm

Figure 5-11. (a) Reconstructed charge distribution and (b) comparison of measured induced charge signals and simulated induced charge signals based on reconstructed charge distribution (Case 2, H_{mf} = 0.7 m, d_B = 0.08 m, u_B = 0.26 m/s, d_p = 565 µm, ρ_p = 2500 kg/m^3, Q_{air} = 1.78 m^3/s).

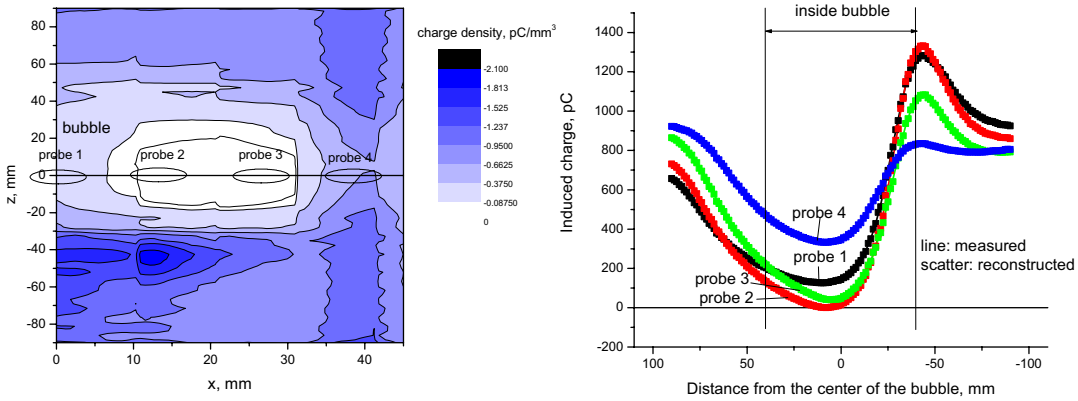

d_{probe}=10mm, $\Delta d_{probe,x}$=13 mm, $\Delta d_{probe,z}$=1.3mm, $N_{probe,x}$=4, $N_{probe,z}$=137
N_{pixel}=12x48, Δd_{pixel}=5mm, $z_{probe,top}$=90 mm, $z_{probe,bottom}$=-90mm

Figure 5-12. (a) Reconstructed charge distribution and (b) comparison of measured induced charge signals and simulated induced charge signals based on reconstructed charge distribution (Case 3, H_{mf} = 0.7 m, d_B = 0.08 m, u_B = 0.26 m/s, d_p = 565 µm, ρ_p = 2500 kg/m^3, Q_{air} = 1.78 m^3/s).

The reconstruction of other typical bubbles (see Figure 5-11 and Figure 5-12) gives similar charge density distribution profiles, confirming that the emulsion phase with glass beads is negatively charged with a more negatively charged wake.

5.7 Conclusions

A technique has been developed to determine the charge distribution around a single rising bubble in a two-dimensional fluidized bed using a number of induction probes positioned flush with the outer wall of the Plexiglas® column. With the probes at the same level, the vertical resolution is obtained by the rise of the bubble under the assumption that the charge distribution does not change during the bubble passage. The method currently uses four probes of 10-mm diameter, but the resolution of the charge density distribution reconstruction can be improved by reducing the probe size and increasing the number of probes. The reconstruction technique does not require any a priori model or knowledge about the charge distribution or density.

Reconstructed images from experimental data show that the emulsion phase far from the bubble was charged negatively for the glass beads used in the experiments. There is a decrease of charge density moving inward from the emulsion phase bubble interface, with essentially zero charge density inside the air bubble. However, the charge distribution has been shown to be nontrivial for this system in that the particles in the wake are strongly charged. It remains for future work to demonstrate the effect of this on the general charging of the bed mass, as well as to show the influence of material properties.

5.8 Notation

d	diameter, m
Δd	differential distance, m
E	electric field, V/m
$E_{\perp}$	electric field perpendicular to wall, V/m
H_{bed}	fluidized bed height, m
H_{mf}	packed bed height, m
L_p	distance between probe 1 and 4 (see Figure 5-4), m

M	number of pixels
N	number of probes
q	volumetric charge density, C/m^3
Q	induced charge on probe from all pixels, C
Q_{air}	air flowrate, m^3/s
r	radius, m
s	area, m^2
u	velocity, m/s
v'	$-\frac{\Pi V}{L_p^2 q_i}$
V	electric potential, V
W	width of two-dimensional bed, m
x, y, z,	Cartesian coordinates, z = vertical, y = horizontal, x = width, m
x', y', z'	normalized coordinates, $x' = x/L_p$, $y' = y/L_p$, $z' = z/L_p$

Greek letters

δ_B	thickness of two dimensional column, m
σ	induced charge on probe from one pixel, C
Π	permittivity of medium, F/m
ρ	density, kg/m^3
ω	matrix in Eq. 5 - 10

Subscripts

B	bubble
i	ith pixel
j	jth probe
x, y, z	x, y, z directions
p	particle

5.9 Acknowledgements

The authors are grateful for support from the Natural Sciences and Engineering Research Council of Canada (NSERC) and Nova Chemicals of Canada. Flip Kleijn van Willigen is also grateful for the support from Profs. J. van Turnhout and C.M. van den Bleek (Delft University of Technology) for his work at the University of British Columbia.

5.10 References

Boland, D. and D. Geldart, 'Electrostatic charging in gas fluidized beds,' *Powder Technol.*, **5** (1971/1972), 289-297.

Chen, A.H., H.T. Bi and J.R. Grace, 'Measurement of particle charge-to-mass ratios in a gas–solids fluidized bed by a collision probe,' *Powder Technol.*, **135-136** (2003a), 181-191.

Chen, A.H., H.T. Bi and J.R. Grace, 'Effects of charge distribution around bubbles on charge induction and transfer to a ball probe in gas-solid fluidized beds,' *J. Electrostat.*, **58** (2003b), 91-115.

Cross, J., 'Electrostatics: Principles, Problems and Applications,' Hilger, Bristol (1987).

Harper, W.R., 'Contact and Frictional Electrification,' Oxford University Press, London (1967).

Mehrani, P., H.T. Bi, and J.R. Grace, 'Electrostatic charge generation in gas-solid fluidized beds,' *J. Electrostat.*, **63** (2005), 165-173.

Murtomaa, M., E. Räsänen, J. Rantanen, A. Bailey, E. Laine, J.-P. Mannermaa, and J. Yliruusi, 'Electrostatic measurements on a miniaturized fluidized bed,' *J. Electrostat.*, **57** (2003), 91-106.

Park, A.-H., H.T. Bi, J. R. Grace and A. Chen, 'Modeling charge transfer and induction in gas-solid fluidized beds,' *J. Electrostat.*, **55** (2002a), 135-168.

Park. A.-H., H.T. Bi., and J. R. Grace, 'Reduction of electrostatic charges in gas-solid fluidized beds,' *Chem. Eng. Sci.*, **57** (2002b), 153-162.

Taylor D. M., 'Measuring techniques for electrostatics', *J. Electrostat.*, **51** (2001), 502-508.

Zhao, H., G.S.P. Castle, I.I. Inculet, and A.G. Bailey, 'Bipolar charging of poly-disperse polymer powders in fluidized beds,' *IEEE T. Ind. App.* **39** (2003), 612-618.

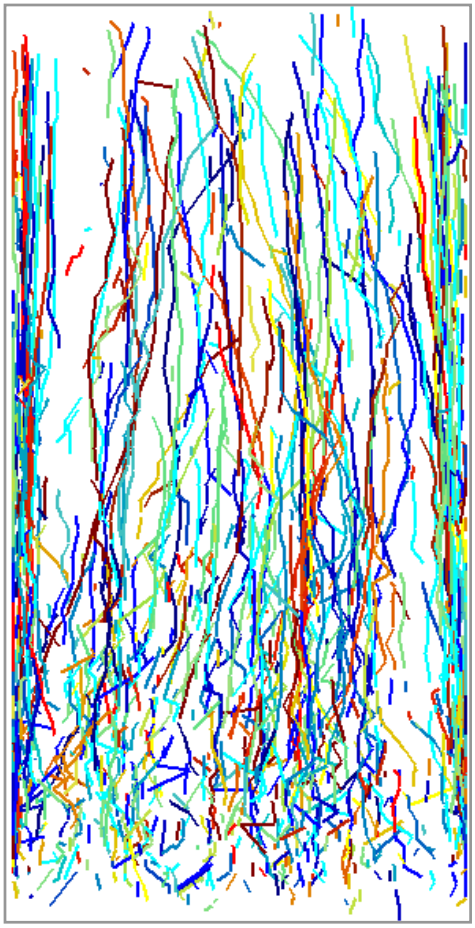

The chaotic tracks of bubbles rising through a fluidized bed, when no electric field is applied. The image was generated from the simulations presented in this chapter.

6. Discrete Particle Simulations of an Electric Field Enhanced Fluidized Bed

In this chapter the effects of electric fields on the bubbles in fluidized beds is analyzed numerically by discrete particle simulations. After establishing the polarization mechanism in Chapter Four, the electric field induced interparticle forces are simulated for each particle in a fluidized bed, together with the other forces acting on the particles (drag, gravity) and the fluid flow.

The simulations show a significant effect on the size of bubbles, both with horizontal and vertical electric fields applied. When the field strength is increased to values higher than those used in the experiments, the particles are found to form strings in the direction of the electric field. At very high field strengths, bed defluidization is observed, as was observed in experiments.

Through the analysis of the bubble behavior, it is concluded that moderate strength electric fields distribute gas more evenly at the bottom of the bed. As the bubbles rise through the bed, the coalescence rate is lower because of the guiding paths, or resistance, the particles form due to the field. This results in a smaller average bubble size in the higher region of the bed. The simulations presented in this chapter show *how* and *why* the electric fields reduce bubble size in electric field enhanced fluidized beds.

This chapter is being prepared for publication as:
Kleijn van Willigen, F., Demirbas, B., van Ommen, J.R., Ye, M., Deen, N.G., and Kuipers, J.A.M., 'Discrete particle CFD simulations of electric field enhanced fluidization'.

6.1 Introduction

The application of electric fields to fluidized beds has experimentally been shown to enhance the fluidized bed behavior (Kleijn van Willigen et al., 2003). Using low-energy alternating electric fields, the interaction of particles in the bed is changed, leading to a smaller average size of the bubbles in the fluidized bed. While the agitation by bubbles in a fluidized bed generally enhances the solids mixing of the system, the gas contained in bubbles rises quickly through the bed with little interaction with the solid catalyst particles. Therefore, control and reduction of bubble size is desirable since it leads to higher efficiency in fluidized bed reactors.

When particles in a fluidized bed are subjected to alternating electric fields, they experience a periodically oscillating attractive or repulsive interparticle force, depending on their relative orientation. It has been shown experimentally that this leads to smaller bubbles in both pseudo two-dimensional as well as in circular cross-section beds. Such properties as the size of bubbles, the number of bubbles, their rise velocity, and the total bubble hold-up when electric fields are applied have been measured with a variety of techniques. Although an understanding of the phenomenon of the reduced bubble size and increased hold-up has been reached, the mechanism leading to smaller bubbles is not yet clear.

That varying the interparticle forces between particles has a large effect on fluidization phenomena is well-known – it has been investigated both experimentally and in simulations. Experimentally, the interparticle force has been influenced via liquid bridge forces (e.g., Seville and Clift, 1984) and magnetic forces (e.g., Wu et al., 1997), showing artificially induced homogeneous bubbling in Geldart B material, or cohesive behavior in Geldart A systems. Molerus (1982) has suggested that it is the ratio of interparticle van der Waals force to fluid drag forces that defines the Geldart B/A and A/C transitions in the Geldart classification, although other interparticle forces may also have a significant influence on fluidization behavior.

Artificially changing the interparticle forces in discrete particle simulations has shown (Rhodes et al., 2001, Ye et al., 2004) qualitatively that an increased cohesive interparticle force helps promote homogeneous fluidization for systems that normally would not show such a behavior. Typically, a system that displays homogeneous fluidization behavior at lower flow rates will form smaller bubbles at higher flow rates than a system in which no homogeneous fluidization is possible.

Larger interparticle forces lead to cohesive behavior, whereby large agglomerates of particles build up.

However, the control of interparticle forces in experiments is difficult. On a small scale, in a controlled environment, and at high energy costs, such methods as liquid bridging using thin oil films (Wright and Raper, 1998) and magnetic fields (e.g., Wu et al., 1997, Rhodes et al., 2001) can be used, but these methods are often not practical in a large scale system.

The application of electric fields is an alternative method of altering the bubble behavior in fluidized beds. However, the interparticle force induced by the electric fields differs from the cohesive forces discussed above in that the electric field induced force is either attractive or repulsive depending on the particle orientation. In addition, because the applied field is alternating, the force it induces also varies periodically.

The aim of this work is to incorporate the understanding of the microscopic electric field induced interparticle forces into a discrete particle CFD model (DPM) to obtain more insight in which way the bubble behavior is influenced. Specifically, we want to know *why* the electric field, and the interparticle forces it induces, leads to a reduction in bubble size.

6.2 Electric Field Induced Forces

In an electric field enhanced fluidized bed, an applied electric field induces electric dipoles in the particles, leading to electric field induced interparticle forces. When a non-conductive particle is placed in an electric field, a charge separation occurs and the particle becomes polarized (cf. Figure 6-1). This charge separation can be from the scale of electrons or molecules to the scale of particles, under certain conditions. Note that such a charge separation does not lead to a build-up of charge on the particle, as, for example, triboelectric charging of the particles with the walls can. The particles in our application and simulations remain electrostatically neutral.

The particles used in electric field enhanced fluidized beds are insulating particles (e.g., glass beads, silica or alumina catalyst particles) with a slightly conductive bulk and/or surface layer (since the fluidized air is slightly humidified), and the electric field alternates at frequencies ranging from 1 to 100 Hz. The dielectric response of such a system can be described by the Maxwell-Wagner theory

of interfacial polarization (e.g., Boersma and van Turnhout, 1998). This means that the degree of polarization, and the ensuing particle interaction, is not dictated by the particle and gas permittivities, but rather by the particle and gas conductivities. The polarization is now not mainly due to dipoles on the atomic or molecular scale, but rather due to the migration of charges in the particle, often restricted to a thin layer within or on the particle, aided by absorbed moisture. For charges to migrate over such large distances, rather slow electric fields are required, i.e. the 1-100 Hz alternating fields previously mentioned. At higher frequencies, only the (significantly smaller) effect of the material dielectric permittivity on the polarization is active. In the simulations described in this paper, the field frequency effect on the degree of polarization of a particle is ignored – it has been described before by Kleijn van Willigen et al. (2005), and the focus here is on the motion of the particles.

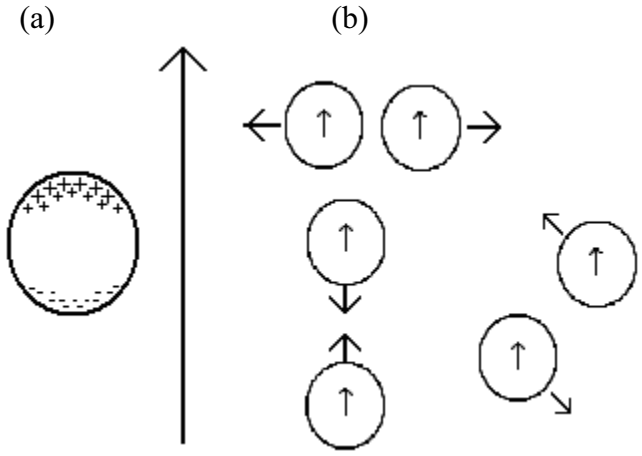

Figure 6-1. (a) Maxwell-Wagner polarization of spherical particles, showing the migration of charge to the poles of the particle. (b) the direction of the electric field induced interparticle force for various particle orientations.

The relative dielectric constant (ε_p) is a measure for the degree of charge separation in a particle in an electric field. When the electric field has induced a small movement of positive and negative charges in opposite directions, the particle has become an electric dipole, quantized in the electric dipole moment p situated at the center of the particle. It is related to the electric field E by:

$$p = \tfrac{1}{2}\, \pi\, \varepsilon_0\, K\, d_p^{\,3}\, E \qquad [6 - 1]$$

where ε_0 is the permittivity of free space, d_p the particle diameter, and K the Clausius-Mossotti function, which provides a measure of the strength of the effective polarization in a spherical particle:

$$K = (\varepsilon_p - \varepsilon_{air}) / (\varepsilon_p + 2\,\varepsilon_{air}) \qquad [6 - 2]$$

The relative permittivity of the particle is ε_p, the relative permittivity of air is approximately $\varepsilon_{air} = 1$.

For the approximation of the electric field induced interparticle force between two particles, $\vec{F}_{ij}$, the assumption of interaction between point dipoles is made:

$$\vec{F}_{ij} = C \cdot \frac{3}{16} \cdot \pi \cdot \varepsilon_0 \cdot \varepsilon_{air} \cdot {d_p}^2 \cdot K^2 \cdot E^2 \cdot \left(\frac{d_p}{a_{ij}}\right)^4 \cdot \left[\left(3\cos^2\theta_{ij} - 1\right)\vec{e}_r + \left(\sin 2\theta_{ij}\right)\vec{e}_\theta\right] \qquad [6 - 3]$$

where C is the multipole correction factor, a_{ij} is the surface to surface separation distance, θ_{ij} is the angle between the center-to-center particle axis and the electric field, and $\vec{e}_r$ and $\vec{e}_\theta$ are the unit vectors in the r and θ directions respectively (cf. Figure 6-2).

Particles oriented with their centers aligned in the direction of the electric field will attract, while particles with their centers perpendicular to the field will repel one another. Particles in any other orientation will experience a torque, and attempt to align to the field. This suggests that particles will tend to form strings or chains in an electric field. Also note that in an infinite matrix of regularly spaced particles, the net force on each individual particle is zero.

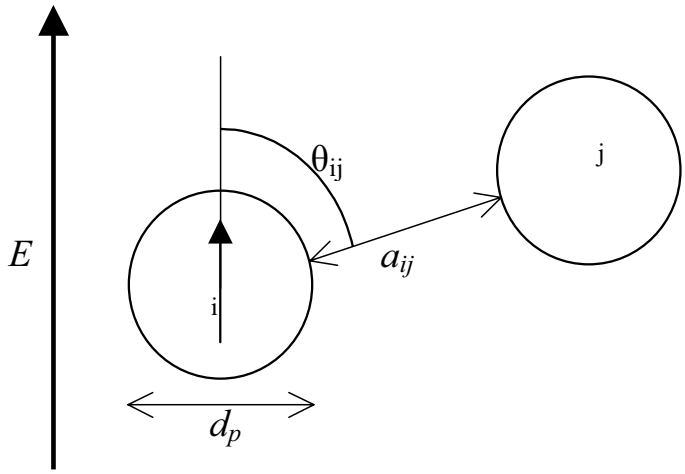

Figure 6-2. Geometric parameters for the calculation of electric field induced interparticle forces.

The assumption of point dipoles is a large simplification because the disturbance fields created by the spheres will further polarize one another, resulting in significantly larger forces. This is shown qualitatively in Figure 6-3., using a finite element calculation of the degree of polarization for a number of particles in an electric field. This sketch is calculated for particles in a homogeneously applied electric field by solving the Maxwell equations. The particles are clearly influenced by each other's local fields in a complex fashion; also, the particle's response is not homogeneous. This illustrates the fact that, formally, Eq. 6 - 3 is only strictly valid in the limit where $K \rightarrow 0$, or $a_{ij} / d_p \rightarrow \infty$. The nature of the discrete particle simulations done here, however, is qualitative, and it is more important to have a good description of the direction of the forces than of the magnitude of the force. While the direction of the force is relatively accurate, ignoring the multipole contributions results in a calculated force that is typically an order of magnitude less than the real force experienced by a particle (Chen et al., 1990). To limit the computational load, this discrepancy is corrected for by the factor C in Eq. 6 - 3. In the simulations described below, the factor is always set at $C = 10$.

In Figure 6-4 the forces experienced by one particle of a two particle system are shown, as a function of their relative orientation and separation. When the

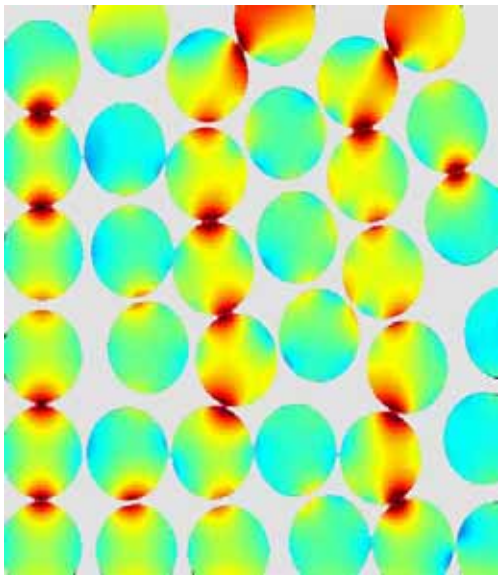

Figure 6-3. Finite element simulation qualitatively showing the effect of the disturbance fields of particles on the polarization of one another. The color intensity shows the degree of polarization. The influence of the polarized particles on each other leads to stronger polarization at the poles. This effect strongly increases the tendency to form strings or chains of particles.

particle-particle axis is parallel to the electric field, the attractive force between the particles is largest, as the head of one dipole is aligned to the tail of the other. At a 90˚ angle, the repulsive force is largest. In this orientation, the heads and the tails of the dipoles are next to each other, but now separated further than in the 0˚ position due to the diameter of the particle. The largest repulsive force is thus always smaller than the largest attractive force. Interestingly, the range of angles over which the net force is attractive is larger than the range of angles over which the force is repulsive, suggesting that the formation of chains will preferably be in the direction of the electric field.

The fourth power of the particle separation distance in the numerator of Eq. 6 - 3 dictates that, as the particles move away from each other, the interparticle force decreases very quickly (cf. Figure 6-5). At a separation of four times the particle diameter, the maximum interparticle force is two orders of magnitude less than when the particles are separated by the equivalent of one particle diameter, and four orders of magnitude less than when the particles are separated by 10% of the particle diameter.

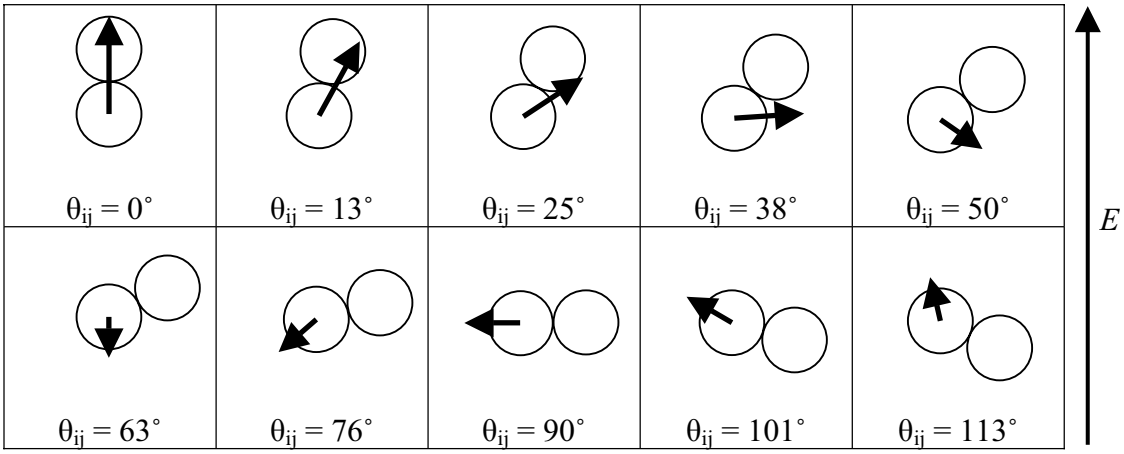

Figure 6-4. Both the angle and the direction of the electric field induced interparticle force varies as the angle between the particles and the electric field, θ_{ij}, varies. The largest attractive force occurs when the particles are aligned to the field.

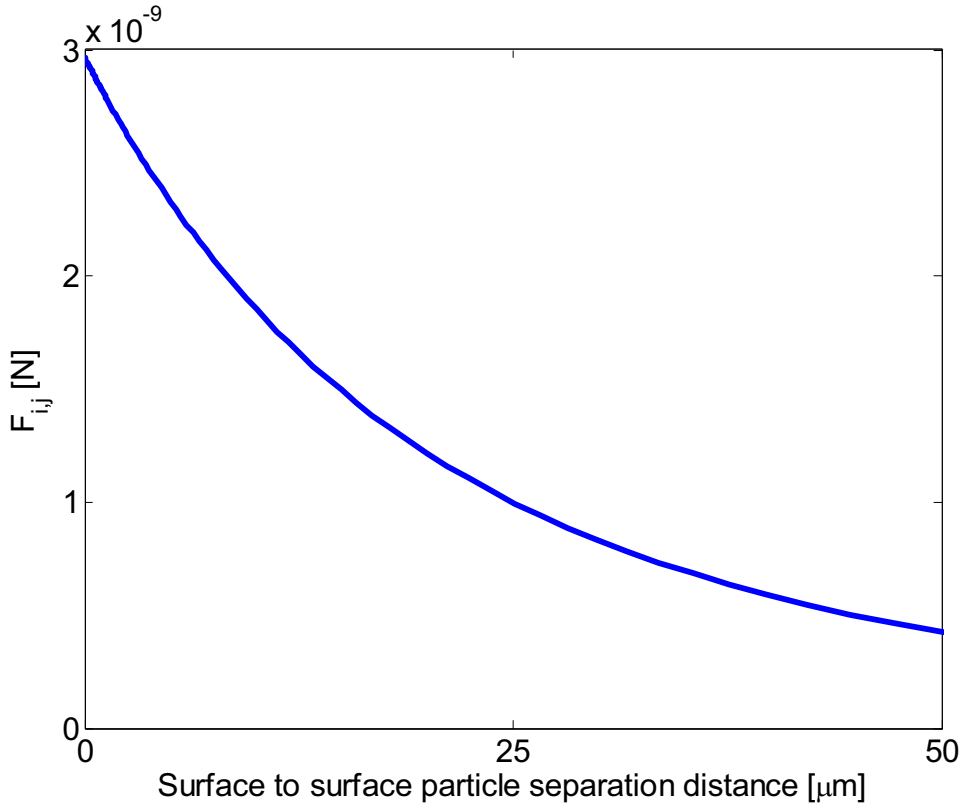

Figure 6-5. The maximum electric field induced interparticle force is strongly dependent on the particle separation distance, a_{ij}. Parameters: d_p=200 µm, ε_p=7, ε_{air}=1, E=10^5 kV/m, C=10.

6.3 Electric Fields

The alternating electric field applied in the simulations is either horizontal (cross-flow) or vertical (co-flow). In addition, the field is considered to be homogeneous. This is a simplification of the design of our electric field enhanced fluidized bed reactors, where the electric fields are non-homogeneous. Instead, in the experiments a multipole design is used such that the field density can be made as high as possible without requiring very high potentials (cf. Figure 6-6). The scale of the unit cell of this heterogeneous design is approximately twice as large as the current simulation volume. In a significant area of the cell there is little or no electric field, and therefore no electric-field induced interparticle force, due to the combined effect of the horizontal and vertical components. Using homogeneous fields, and considering the vertical and horizontal effects seperately, allows us to focus on the effect of interparticle forces on bubbles on a small scale.

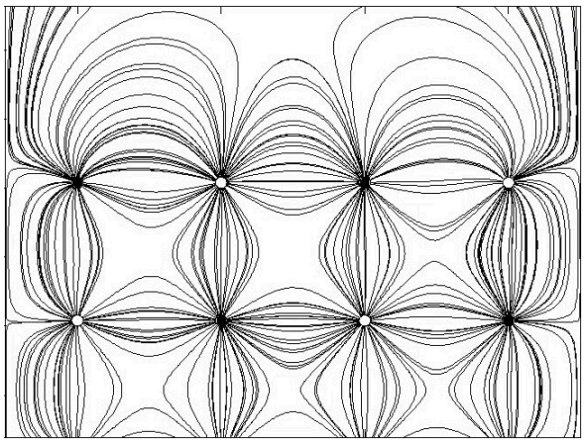

Figure 6-6. Electric field lines in an experimental, pseudo two-dimensional electric field enhanced fluidized bed with thin wire electrodes. The nodes are alternately, both horizontally and vertically, grounded and live electrodes. Note that the field strength on the diagonals between nodes is zero, and the strongest field is in the region between two nearby electrodes.

6.4 Model Description

The 2D soft-sphere discrete particle model (DPM) used here is the same as that described by Ye et al. (2004), where it was used to describe the influence of (artificially increased) van der Waals forces on homogeneous fluidization. The gas flow is modeled by the volume-averaged Navier-Stokes equations.

Continuity equation gas phase:

$$\frac{\partial(\varepsilon\rho_g)}{\partial t} + \left(\nabla \cdot \varepsilon\rho_g u\right) = 0 \qquad [6 - 4]$$

Momentum equation gas phase:

$$\frac{\partial(\varepsilon\rho_g u)}{\partial t} + \left(\nabla \cdot \varepsilon\rho_g uu\right) = -\varepsilon\nabla p_g + S_p - \nabla\cdot(\varepsilon\tau) + \varepsilon\rho_g g \qquad [6 - 5]$$

where ε is the porosity, and ρ_g, u, τ, and p_g are the density, velocity, viscous stress tensor, and the pressure of the gas phase, respectively. The source term S_p is a function of the drag coefficient β (Hoomans et al., 1996). To calculalate the drag coefficient, the well-known Ergun equation (Ergun, 1952) is used for porosities lower than 0.8 and the Wen and Yu correlation (Wen and Yu, 1966) for porosities higher than 0.8.

The equations of motion of the particles follow from Newton's second law, extended with the electric field induced interparticle force:

$$\frac{m_i d^2 r}{dt^2} = F_{cont,i} + \frac{V_i \beta}{1-\varepsilon}\left(u - v_i\right) - V_i \nabla p_g + m_i g + \sum_j F_{ij} \,, \qquad [6 - 6]$$

$$I_i \frac{d^2 \Theta}{dt^2} = T_i \qquad [6 - 7]$$

where m_i is the mass of the particle, $F_{cont,i}$ the contact force, T_i the torque, I_i the moment of inertia, Θ the angular displacement, and F_{ij} the electric field induced interparticle force. The contact force between two particles, or two particles and a side wall, is calculated by use of a linear-spring and dashpot model for soft-sphere particle interaction (Cundall and Strack, 1979). These equations are solved using a standard first-order time-integration scheme.

6.5 Numerical Simulation

In the simulations we consider a system consisting of 10,011 monodisperse spheres (141 rows of 71 particles when the bed is square-packed) with a diameter of 200 μm, a density of 2000 kg/m^3, and a relative dielectric constant of $\varepsilon_p = 7$. The electric field applied to the bed is sinusoidal, with varying frequency and strength depending on the simulation. The direction of the field is either horizontal (cross-flow) or vertical (co-flow). The input parameters are given in Table 6-1.

The electric field configuration parameters for the different simulations are summarized in Table 6-2. Each simulation runs for four seconds in real time, of which the first second is discarded to allow the system to adjust to the input conditions. Halve a second was found to be sufficient in most cases for the simulation to reach steady state, but one second gives a sufficient safety margin. Four different reference cases without electric field were generated by raising the gas velocity to 0.04, 0.07, 0.10, and 0.50 m/s for 0.5 s (making the total length of these reference case simulations 4.5 s; the last three seconds of these simulations are evaluated).

The normal relative gas velocity, $u_f = 0.20$ m/s, was chosen at approximately five times the minimum fluidization velocity so as to encourage the formation of larger bubbles.

Table 6-1. Simulation parameters.

Particle diameter, d_p	200 μm
Particle density, ρ	2500 kg / m^3
Normal restitution coefficient, e_n	0.95
Tangential restitution coefficient, e_t	0.95
Friction coefficient, μ_f	0.15
Normal spring stiffness, k_n	7 N m
Tangential spring stiffness, k_t	2 N m
Gas time step	1×10^{-5} s
Particle time step	1×10^{-6} s
Column height, H	42.3 mm
Column width, L	14.2 mm
Numerical grid height, Δy	492 μm
Numerical grid width, Δx	473 μm
Number of particles	10011
Superficial gas velocity, U_f	0.2 m / s
Shear viscosity of gas, μ	1.8×10^{-5} Pa s
Gas temperature, T	298 K
Particle relative permittivity, ε_p	7
Gas relative permittivity, ε_{air}	1
Multipole factor, C	10

Table 6-2. Overview of the simulations run under varying field strengths and frequencies.

	Number of simulations	Electric field direction	Field strength (kV/mm)	Field frequency (Hz)
Set 1				
Reference case	4	n.a.	0	0
Set 2				
Varying field frequency	10	Horizontal	0.5, 0.7	5, 10, 30, 50, 100
Varying field frequency	10	Vertical	0.5, 0.7	5, 10, 30, 50, 100
Set 3				
Varying field strength	8	Horizontal	0.2, 0.3, 0.5, 0.7, 1.0, 1.5, 2.0, 3.0	30
Varying field strength	8	Vertical	0.2, 0.3, 0.5, 0.7, 1.0, 1.5, 2.0, 3.0	30

It was already shown in Figure 6-5 that the electric field induced interparticle force is strongly distance dependent, and that when particles move from a separation distance of 10% to 400% the particle diameter, the force decreases by four orders of magnitude. Because the majority of particles are located much closer, a value of four times the particle diameter is used as a cutoff distance for calculation of the electric field induced force in the DPM simulations. At larger separation distances, the force is considered to be zero.

6.6 Bubble analysis

The aim of this work is to determine the change in bubble behavior due to an applied electric field. It is therefore important to quantify the bubble dimensions and properties in a reliable way during the post-processing. The method employed in this work is based on the determination of the voidage on the scale of the (fluid) grid cells,

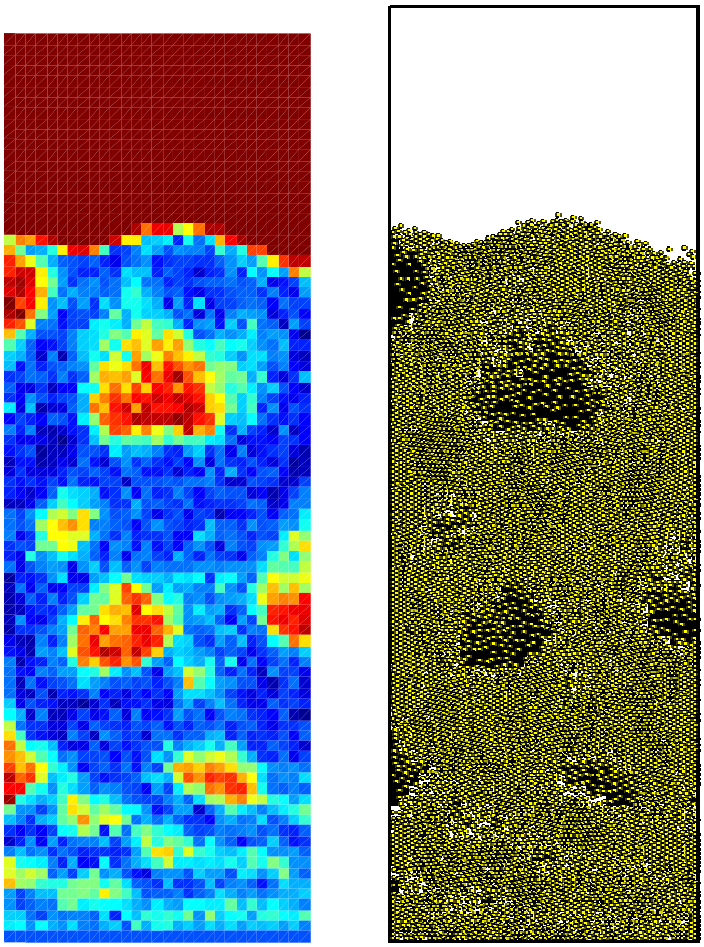

Figure 6-7. (a) Local voidage in the fluidized bed; (b) the cells that surpass the threshold value are marked as 'voids', and are shown here overlayed with the particle locations.

i.e. unit cells with the dimensions of 473×492 μm. Figure 6-7 shows the local voidage (a) and the thresholded voids overlayed with the particle locations (b). When the local voidage in a cell is higher than 0.7, a grid cell is considered to be a void, which can be either a bubble or part of the region above the bed surface. When the local voidage is lower than 0.7, the cell is considered to be emulsion phase. After denoting each cell as either emulsion phase, bubble, or freeboard region, the properties of each were determined. For a region to be considered a bubble, four adjoining cells must have been marked as 'void', corresponding to a minimum bubble size of 0.93 mm^2. The bed height, the average voidage, and the size of the emulsion phase are recorded for each CFD time step. For every individual bubble, its surface area (called 'size' in this chapter), location, width, and height are measured, as well as the average voidage of the bubble phase. By comparing sequential frames, bubbles could be numerically tracked over time, allowing the determination of their lateral and vertical (rise) velocities.

6.7 Results and Discussion

Bubble size and bubble frequency

In Figure 6-8a the bubbling behavior of a normal fluidized bed, *without* any applied electric field, is shown. When a very high strength electric field (3 kV/mm, 30 Hz, horizontal or vertical) is applied to this bed, the change in behavior is very strong (Figure 6-8b and Figure 6-8c). This field strength is the approximate theoretical limit for the field strength without electric breakdown when air is used as fluidizing gas. In the simulations, however, this is not an issue and we can use such high field strengths to demonstrate the extreme case effects. The figures demonstrate how strings of particles are formed in the direction of the electric field. The strings in the horizontal field bounce as gas is forced through, but typically do not break apart. The strings formed in the vertical field are separated by small channels to allow the fluidizing gas to pass. Note that in both the horizontal and vertical field simulation, agglomerates are formed (as compared to strings of single particles) when two particle strings are at a slight offset to each other. Many strings are 3-5 particles thick, but in some regions much larger groups of closely-packed particles are observed. This is especially

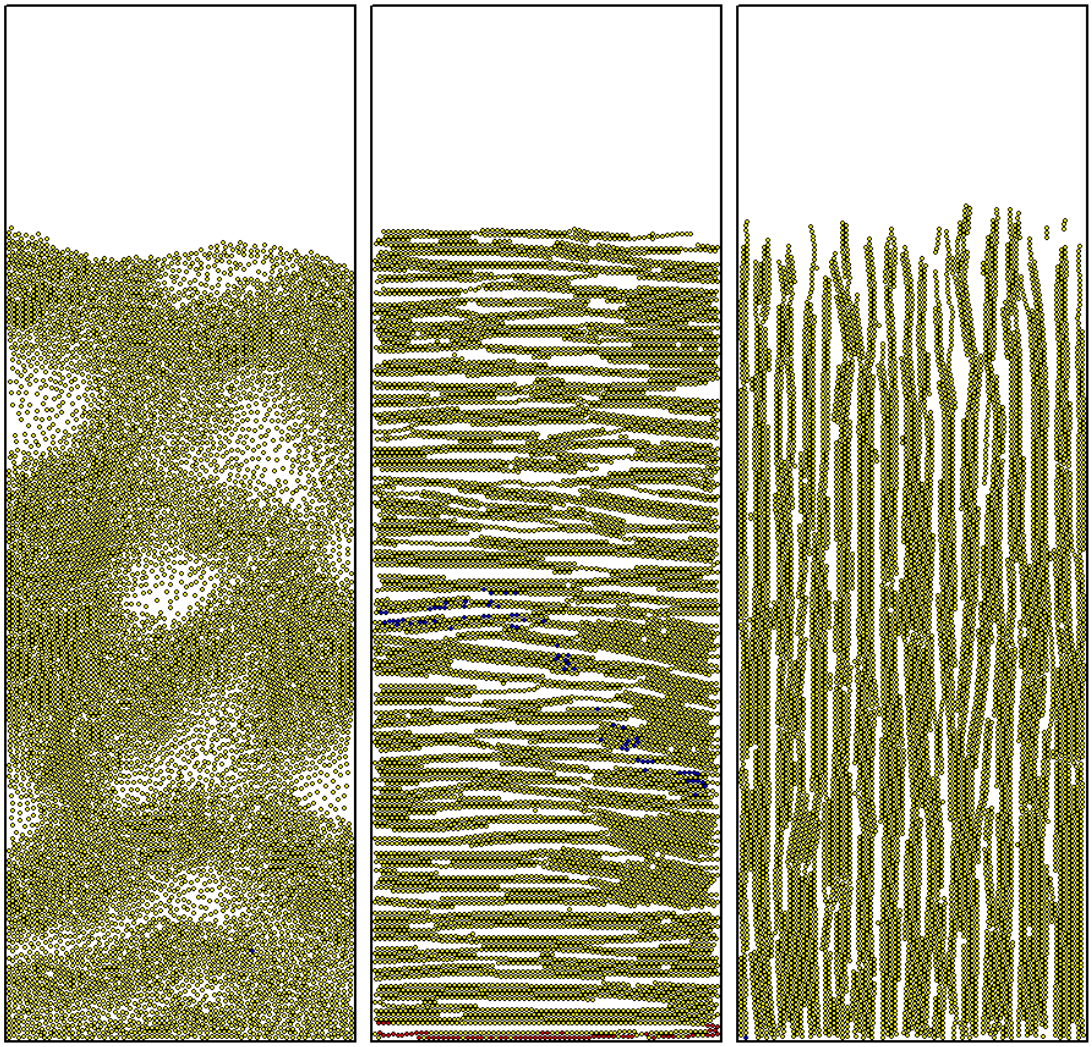

Figure 6-8. a: Freely bubbling bed, no electric field. b: Horizontal electric field applied (3 kV/mm, 30 Hz). c: Vertical electric field applied (3 kV/mm, 30 Hz).

evident on the right-hand side of Figure 6-8b. A freezing and complete defluidization has previously been reported for experimental observations of electric field enhanced fluidized beds with very strong or, more often, DC fields (Dietz and Melcher, 1978).

However, the *fluidity* of the system in these two high field strength simulations is clearly not preserved – particles are not free to move, and one can not consider the voids in these systems to be bubbles in a fluidized bed. There is little advantage to be gained from employing such a system – the mass and especially heat transfer will be lower than in a bubbling fluidized bed, mixing of the emulsion phase is virtually non-existent, and the efficiency of the reactor will not benefit. We are interested in modifying only the bubble behavior in the fluidized bed, while conserving the fluidized state of the emulsion.

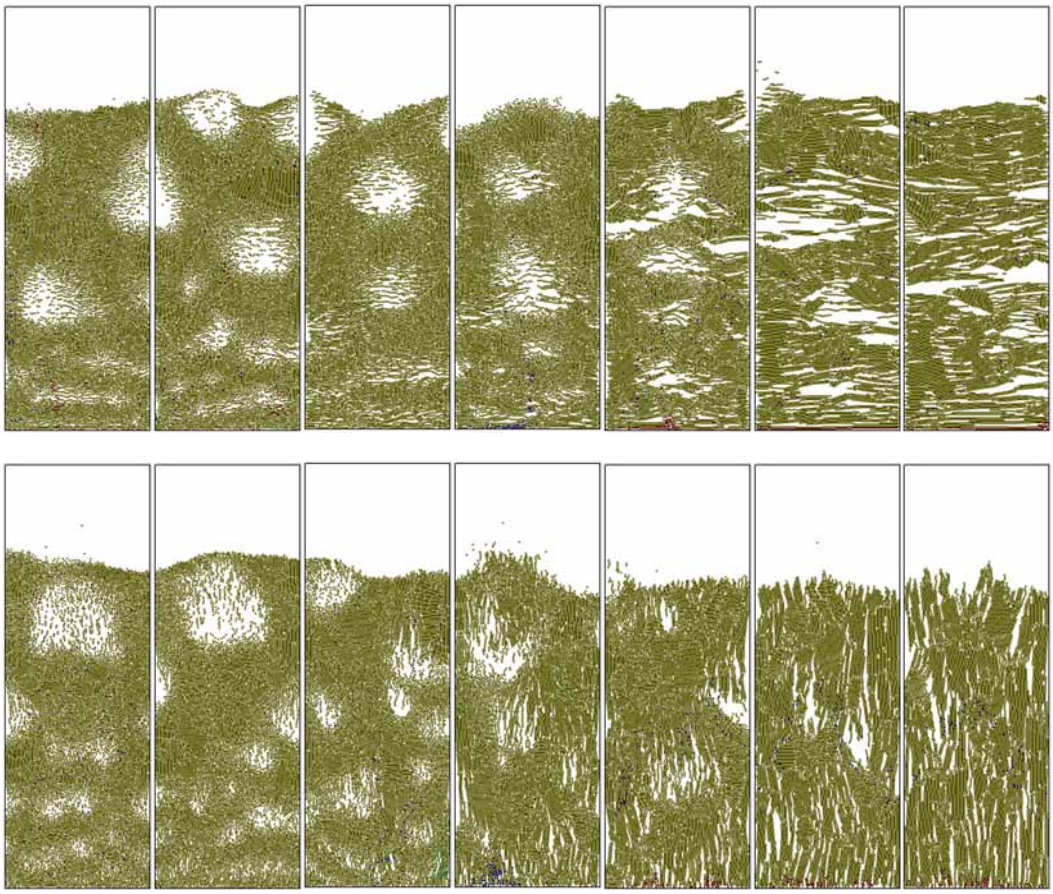

Figure 6-9. Influence of a horizontal (top) or vertical (bottom) electric field of 0.2, 0.3, 0.5, 0.7, 1.0, 1.5, and 2.0 kV/mm at 30 Hz on the bubble and particle behavior.

The effect of decreasing the field strength, resulting in smaller electric field induced interparticle forces, on the fluidization behavior is shown qualitatively in the snapshots shown in Figure 6-9. Visual observation of the bed behavior shows that 1.5 and 2.0 kV/mm the balance between attractive and repulsive forces is such that slugging occurs, which was not seen in the 3.0 kV/mm simulation. Visually, the freedom of particles to move in the emulsion phase appears to decrease significantly when the field becomes stronger than 1.0 kV/mm.

However, the most important property to examine is the bubble size and the number of bubbles in the column. These results are shown in Figure 6-10 for vertical electric fields and Figure 6-11 for horizontal fields. A vertical field of 0.3 kV/mm or less has little influence on either the bubble size or the number of bubbles in the bed, but as the strength is increased to 0.7 or 1.0 kV/mm the maximum bubble size decreases by 30 or even 55%. The number of bubbles in the system increases by approximately 20% at the bottom of the column. The bubble size decreases even

more for the highest field strengths, but as already observed, this is at the cost of a significant decrease in the freedom of particles to move. At 3.0 kV/mm, the size of 'detected bubbles' is barely above the detection limit, but because of their 'frozen' state there are many of them, especially in the top of the bed.

Figure 6-11 shows the effect of the same electric field strengths, but now in the horizontal direction. The slight resistance to rising bubbles due to the tendency of particles to form strings in the bed leads to a slightly larger bubble size in the lower part of the column. When the bubbles are slightly larger, they have enough momentum to 'break through' this resistance, but while the bubbles rise through the bed, their rate of coalescence is lower than in the freely bubbling situation.

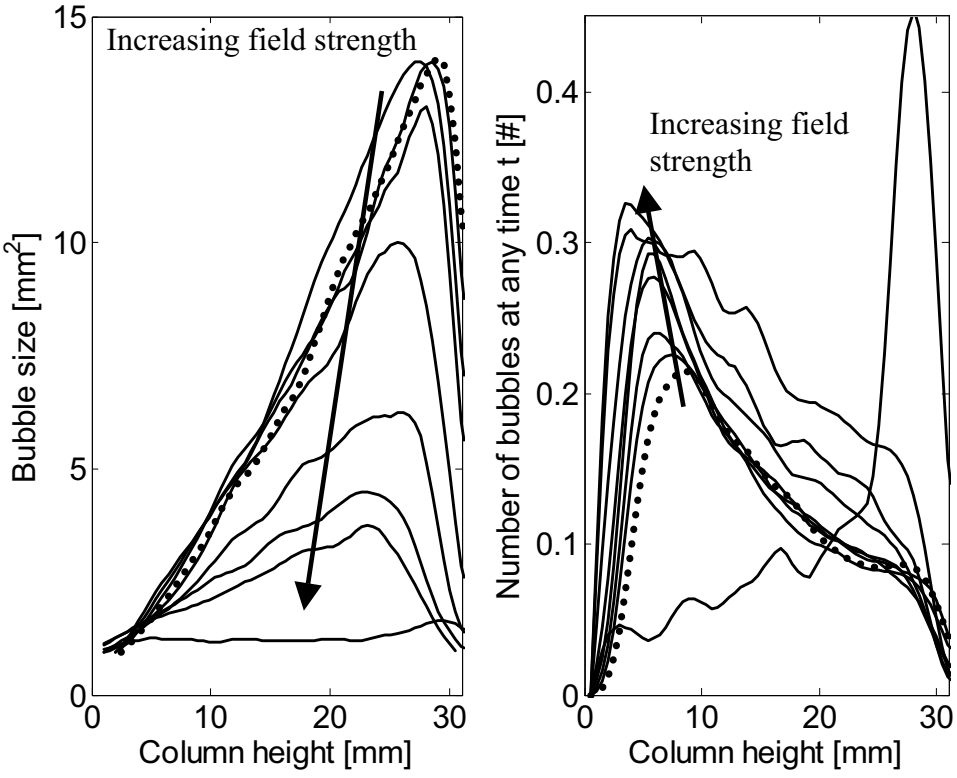

Figure 6-10. Bubble area and frequency as function of height, with a vertical electric field (0.0 to 3.0 kV/mm, 30 Hz). The dashed line is the reference case (0 kV). Curves are smoothed by a five-point (2.5mm) moving average. The mean bubble size decreases at the top of the bed due to the fact that bubbles that have reached the surface are considered part of the freeboard. The large peak in the bubble occurrence plot corresponds to a complete freezing of the bed under the highest field strength (3.0 kV/mm).

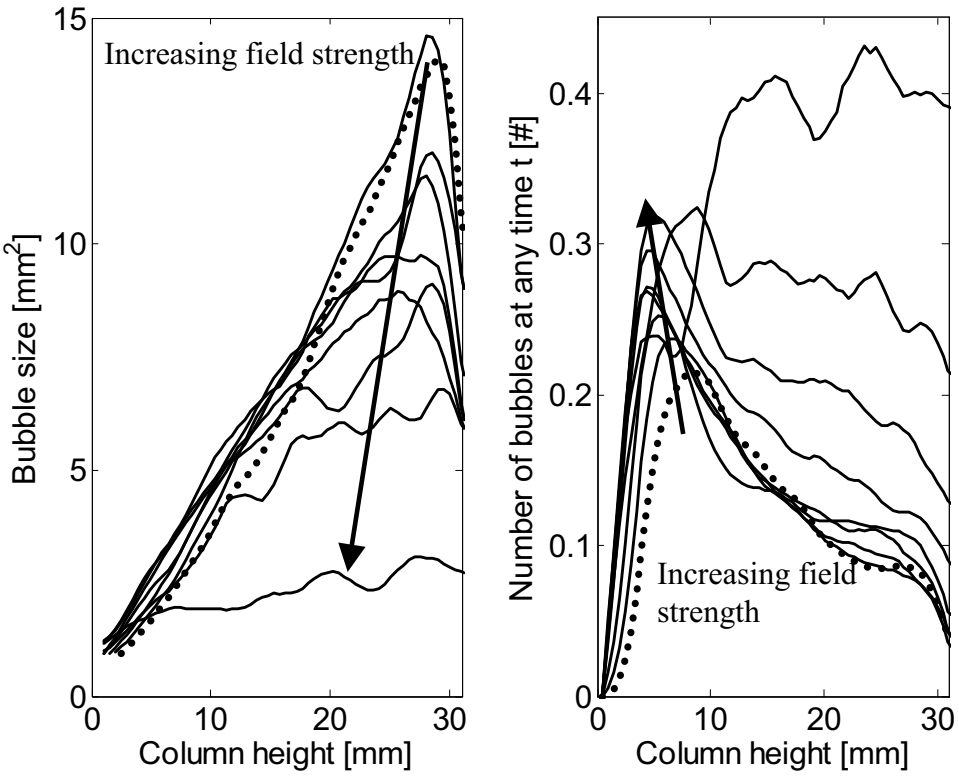

Figure 6-11. Bubble size and frequency as function of height, with a horizontal electric field (0.0 to 3.0 kV/mm, 30 Hz). The dashed line is the reference case without electric fields. Curves are smoothed by a five-point (2.5mm) moving average. As with the vertical fields, the highest field strength (3 kV/mm) shows a large number of bubbles, breaking the trend of the more moderate field results.

Voidage, bubble hold-up, and bed height

It was already shown how, on average, the attractive forces on particles are larger than the repulsive forces. Besides leading to (the tendency for) chain-formation in the bed, this also leads to a decrease in the porosity of the emulsion phase, irrespective of the direction of the electric field. During simulations, the average voidage of the emulsion phase decreased from 0.45 for the reference case to 0.42 for the 1 kV/mm simulations. When the field strength was larger than 1.5 kV/mm, the voidage again increases, because the narrow and elongated volumes between the chains of particles is considered to be 'emulsion phase' gas.

The average bubble phase voidage, on the other hand, appears to increase slightly. That is, bubbles become slightly emptier of particles. However, the scale of the simulations prohibits any concrete conclusions on the amount of particles in the bubbles.

The height of the bed (including the bubbles within the bed) and the bubble hold-up (that is, the fraction of the bed in bubbles) show opposite trends, depending on the direction of the field. The horizontal electric field leads to an expansion of the bed, through an increased fraction of bed in bubbles. This is substantiated by the observation that the bed with a horizontal electric field has a tendency to show slugging behavior. The vertical field, on the other hand, leads to a lower average bed height as well as a lower bubble hold-up. This difference suggests a difference in the rise velocities of bubbles.

Bubble velocities

If the effect of the electric field is to 'guide' bubbles along (vertical field) or resist their rise (horizontal field), it follows that the bubble rise velocity will be influenced. This is indeed seen when the bubbles are tracked over a series of time steps. Figure 6-12 shows the horizontal velocities of bubbles, as function of field frequency at a constant field strength of 0.5 or 0.7 kV/mm. The horizontal field, with the tendency

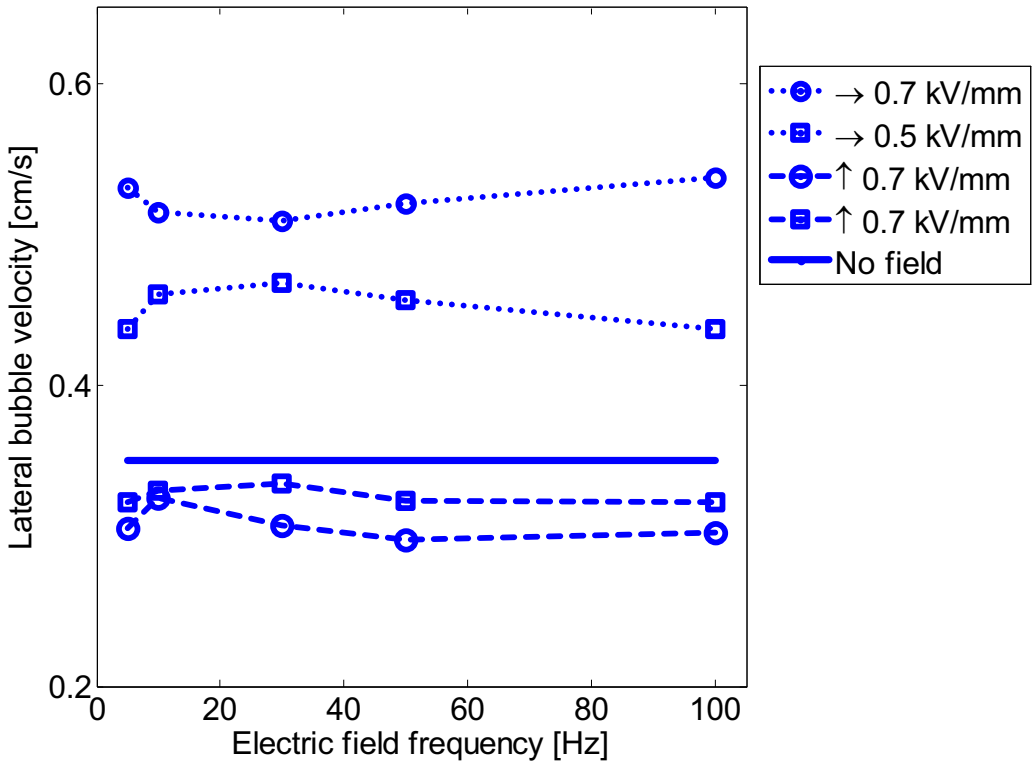

Figure 6-12. Lateral (horizontal) velocity of bubbles, under the effect of horizontal and vertical fields of various frequencies. Absolute values of the displacements were taken; the mean velocities were approximately zero in all simulations. Without an electric field, the average horizontal bubble velocity is 0.35 cm/s. Lines drawn to guide the eye.

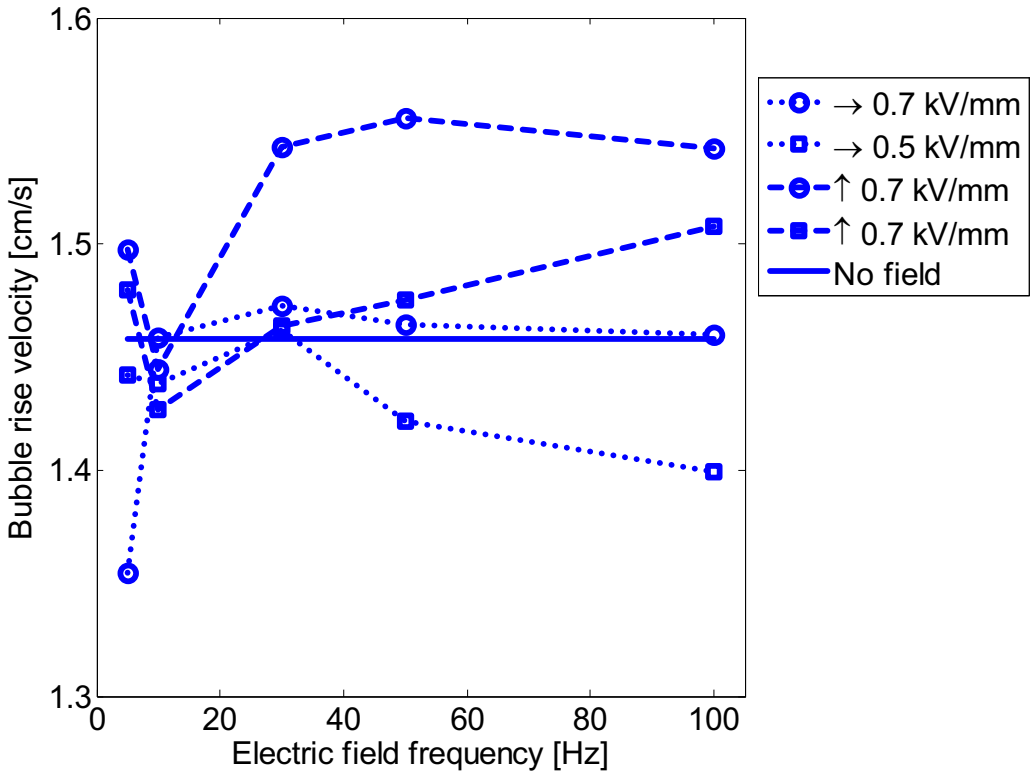

Figure 6-13. Rise (vertical) velocity of bubbles, under the effect of horizontal and vertical fields of various frequencies. Without an electric field, the average rise velocity is 1.46 cm/s. Lines draw to guide the eye.

of particles to form horizontal strings, causes bubbles to move from side to side more than bubbles in the freely bubbling system do. The stronger the field strength, the larger this effect is. Conversely, the vertical electric field guides bubbles up along straight paths, and therefore the lateral bubble movement is significantly less. However, if the bubbles are guided upwards, then they should have a higher rise velocity – despite their smaller size. This is confirmed in Figure 6-13. The bubbles rising through the horizontal electric field, on the other hand, show relatively little difference in rise velocity, due to their larger size in the lower halve of the bed.

The lateral velocities and rise velocities plotted in Figure 6-12 and Figure 6-13 have been averaged over all voids that were identified as bubbles in a simulation and could be correlated for 2 or more time steps. While in the bubble size and bubble frequency plots no dependence on the electric field frequency could be seen, this is seen in the rise velocities. The fluctuations within a series of constant field strength

were determined not to be statistically reliable enough to relate the field frequency to bubble velocities.

Bubble aspect ratio

The distortion of the bubbles when an electric field is applied follows from the tendency to form (at lower field strengths), or the actual formation (at high field strengths), of strings of particles. This effect is shown in Figure 6-14. Under the effect of a vertical electric field, bubbles become more elongated, or narrower. The horizontal fields have a less clearly defined influence on the aspect ratio than moderate vertical fields, whereas a significant flattening of bubbles would be expected. This was also seen in the rise velocities of bubbles. It appears that the majority of the bubbles recognized in the bubble thresholding are large bubbles that have reached the critical size to pass through the horizontal barriers, and when they do so, the bubbles return to there 'natural' shape.

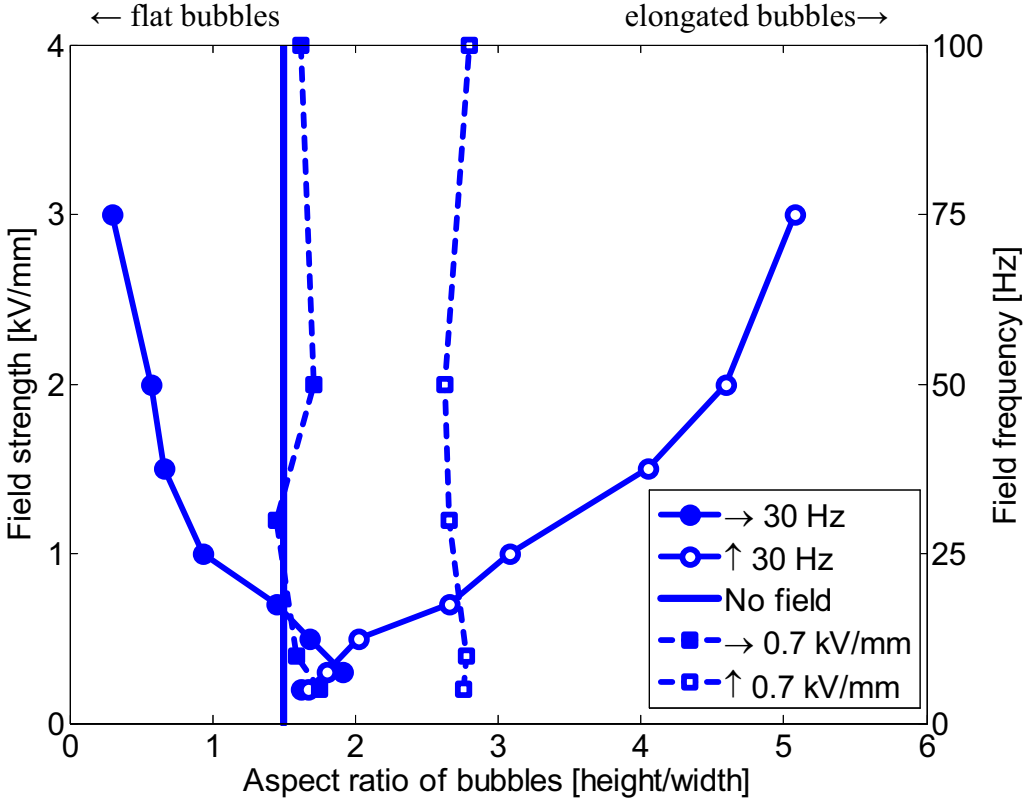

Figure 6-14. The flatness of bubbles depends strongly on the direction of the field, as well as the field strength (solid lines, on the primary y-axis, with a constant field frequency of 30 Hz). The field frequency (dashed lines, on the secondary y-axis, with a field strength of 0.7 kV/mm) appears to have little effect. 'Normal' bubbles have a h/w ratio of ~1.5, as shown by the vertical solid line. Very strong fields lead to very flat or elongated bubbles.

Frequency

Two types of electric field frequency effects can be distinguished. Firstly, the periodic nature of the attractive and repulsive forces on the particles could lead to a harmonic effect in the macroscopic features, such as bubble size, bed height, or voidage. For example, if the electric field frequency is 5 Hz, one might expect the bed height to oscillate in phase with the electric field. Such an effect was not found over the range of frequencies at which the simulations were done.

However, experimental results (Kleijn van Willigen et al., 2003) have shown a strong frequency effect on the bubble phenomena, notably size, that is not immediately reflected in the simulation results. The results of the simulations show no relation between frequency and bubble phenomena at constant field strengths, with the exception of the bubble velocities. Both the lateral and the rise velocities of bubbles, both with horizontal and vertical fields, show a different trend at 5 and 10 Hz when compared to the higher the field frequencies, without any corresponding visible effect on other bubble properties. Because the data at low frequencies are not consistent, further simulations are required to determine whether a causal relation between electric field frequency and bubble phenomena exists. As has been described above, however, the electric field frequency strongly influences the *degree* of polarization, which in turn determines the magnitude of the electric field induced interparticle force, and this effect was *not* included in these simulations. Thus, it may be concluded that the frequency dependence determined experimentally is a polarization effect and not a particle-motion correlation.

6.8 Conclusions

The simulations show a clear influence of the electric field induced interparticle force on the behavior of bubbles in a fluidized bed. At moderate field strengths, the macroscopic behavior is not strongly modified – the bed maintains its ‘fluidity’. At very high field strength, the particles form visible strings throughout the bed, and show little free movement. It has been shown how the electric field, whichever orientation it has, leads to a better distribution of gas into a larger number of bubbles in the bottom of the bed. As these bubbles rise through the bed, the coalescence rate is lower because of the guiding paths the particles form (or tend to form) due to the field. In the higher region in the bed, this leads to a smaller mean bubble size.

A comparison to experimental results should be done with care. There are two main reasons for this. The electric field applied to experimental columns is a combination of horizontal and vertical fields, setup in such a way that it leads to a cell-like structure in the bed, with the highest field strengths on the ribs. The size of such cells is typically comparable to the size of the simulated column discussed in this paper. Secondly, the simulations are limited by the number of particles in the system. These two scaling issues make it difficult to make quantitative comparisons of the effects of electric fields. However, the simulations do indicate an answer to *how* the electric fields lead to a smaller bubble size, namely by distributing gas into small bubbles in the bottom of the bed and decreasing the coalescence rate. This insight can help in the design of future generations of electric field enhanced fluidized beds.

6.9 Notation

a_{ij} center to center particle separation distance, m
C multipole correction factor, -
d_p particle diameter, m
e_r, e_θ unit vectors in the r and θ directions, -
e_n normal restitution coefficient, -
e_t tangential restitution coefficient, -
E electric field strength, V/m
$F_{cont,a}$ contact force, N
F_{ij} electric field induced interparticle force, N
H column height, m
I_a moment of inertia, kg m^2
k_n normal spring stiffness, N m
k_t tangential spring stiffness, N m
K Clausius-Mossotti function, -
L column width, m
m_a mass of particle, kg
p dipole moment, C m
p_g gas pressure, N / m^2
r particle position vector, m
S_p reaction force to the drag force, N / m^3

t	time, s
T	temperature, K
T_a	torque, N m
u	velocity, m / s
U_f	superficial gas velocity, m / s
V_a	particle volume, m^3
x	numerical grid width, m
y	numerical grid height, m

β	volumetric interphase momentum transfer coefficient, kg / m^3s
ε	porosity, -
ε_0	permittivity of free space, 8.854 10^{-12} F / m
ε_{air}	relative dielectric constant of air, -
ε_p	relative dielectric constant of a particle, -
Θ	angular displacement, rad
μ	gas viscosity, Pa s
μ_f	friction coefficient, -
ρ	particle density, kg / m^3
ρ_g	gas density, kg / m^3

6.10 References

Boersma, A., and van Turnhout, J., 'Dielectric study on size effects in polymer laminates and blends', *J. Polym. Sci. Part B: Polym. Phys.* **36** (1998), 2835–2848.

Chen, Y., Sprecher, A.F., and Conrad, H., 'Electrostatic particle-particle interactions in electrorheological fluids', *J. Appl. Phys.*, **70** (1991), 6796-6803.

Cundall, P.A., and Strack, O.D., 'A discrete numerical model for granular assemblies', *Geotechnique*, **29** (1979), 47 - 65.

Dietz, P.W., and Melcher, J.R. 'Interparticle electrical forces in packed and fluidized beds', *Ind. Eng. Chem. Fundam.*, **17** (1978). Pp. 28-32.

Ergun, S., 'Fluid flow through packed columns', *Chem. Eng. Prog. Symp. Ser.* **48** (1952), 89-94.

Hoomans, B.P.B., Kuipers, J.A.M., Briels, W.J., and van Swaaij, W.P.M., 'Discrete particle simulation of bubble and slug formation in a two-dimensional gas-fluidised bed: a hard-sphere approach', *Chem. Eng. Sci.* **51** (1996), 99-118.

Kleijn van Willigen, F., van Ommen, J.R., van Turnhout, J., and van den Bleek, C.M., 'Bubble Size Reduction in a Fluidized Bed by Electric Fields', *Int. J. Chem. Reactor Eng.*, **1**: A21 (2003). http://www.bepress.com/ijcre/vol1/A21.

Kleijn van Willigen, F., van Ommen, J.R.,van Turnhout, J., and van den Bleek, C.M., 'Bubble Size Reduction in Electric-Field-Enhanced Fluidized Beds', *J. Electrostat.* **63** (2005), 943-948.

Molerus, O., 'Interpretation of Geldart's type A, B, C, and D powders by taking into account interparticle cohesion forces', *Powder Technol*. **33** (1982), 81-87.

Seville, J.P.K., and Clift, R., 'The effect of thin liquid layers on fluidisation characteristics', *Powder Technol.* **37** (1984), 117-129.

Rhodes, M.J., Wang, X.S., Forsyth, A.J., Gan, K.S., and Phadtajaphan, S., 'Use of a magnetic fluidized bed in studying Geldart Group B to A transition', *Chem. Eng. Sci.* **56** (2001), 5429-5436.

Wen, C.Y., and Yu, Y.H., 'Mechanics of fluidization', *Chem. Eng. Prog. Symp. Ser.* **62** (1966), 100-111.

Wright, P.C., and Raper, J.A., 'Role of liquid bridge forces in cohesive fluidization', *T. I. Chem. Eng.-Lond.* **76A** (1998), 753-760.

Wu, W.Y., Navada, A., and Saxena, S.C., 'Hydrodynamic characteristics of a magnetically stabilized air fluidized bed of an admixture of magnetic and non-magnetic particles', *Powder Technol.* **90** (1997), 39-46.

Ye, M., van der Hoef, M.A., and Kuipers, J.A.M., 'A numerical study of fluidization behavior of Geldart A particles using a discrete particle model', *Powder Technol.* **139** (2004). Pp 129-139.

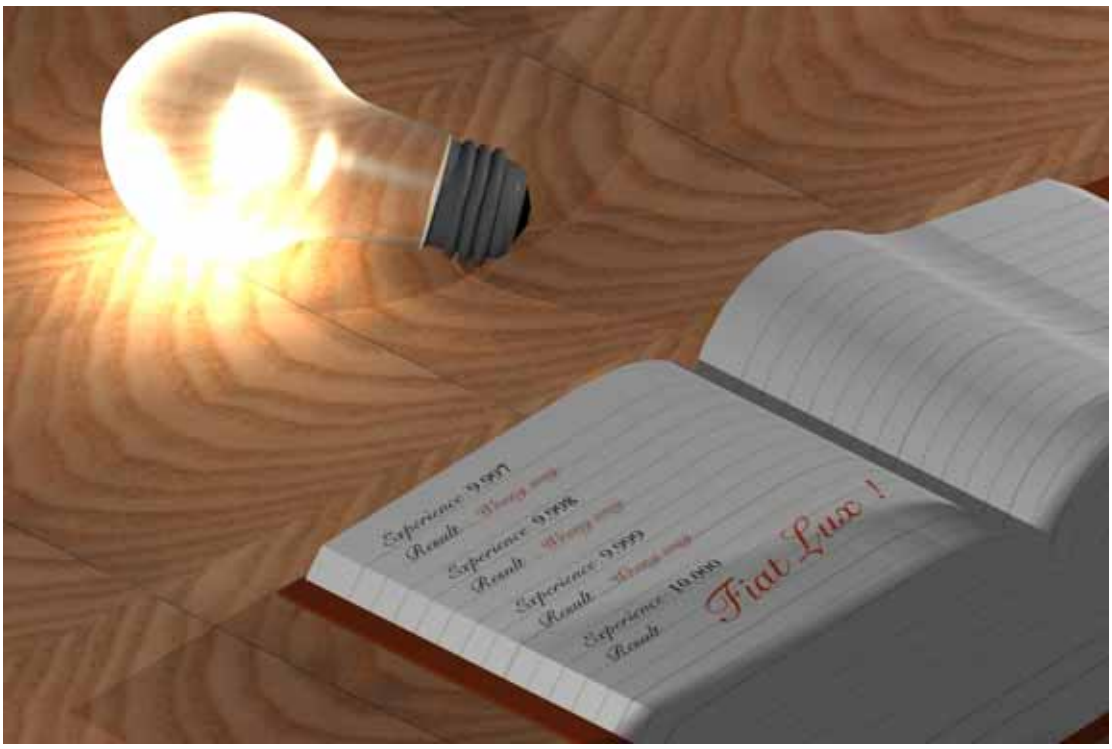

An ‘Edison’ experiment is the one single experiment out of a (very) long series that finally ‘works’ – in the case of Thomas Edison finding the material that could be used as a filament in a light bulb. The working title of the ozon decomposition experiments from this chapter was the ‘Edison Experiment’. (Image by Alfredo Roberto Marins, jr.)

7. Proof of Principle: Conversion in Electric Field Enhanced Fluidized Beds

In the previous chapters, it was shown how electric fields can be used to decrease the size of bubbles in a fluidized bed. In this chapter, we demonstrate that a smaller bubble size is beneficial to the conversion in a fluidized bed. Two proofs are presented. First, the fluidization model developed by Kunii and Levenspiel (Levenspiel, 1992), extended with a variable bubble size, is used to show how the conversion can be significantly increased, especially for reactions with a high reaction rate. The influence of reaction rate and flow velocity is studied.

The second proof is experimental: using the decomposition of ozone, it is demonstrated that a low-energy electric field leads to an increase in the conversion of ozone to oxygen by as much as 15%. Both untreated alumina particles and particles impregnated with 0.5% wt/wt iron to increase their activity were used. The system with the impregnated particles benefited more when the bubble size was reduced by the applied electric field than the untreated particles.

7.1 Introduction

Fluidized beds have many desirable features for chemical and physical processes. The free movement of the solid particles gives a good heat transfer throughout the bed and an optimal contact between the particles and the surrounding gas. This contact is important both to heterogeneously catalyzed reactions as well as to noncatalytic gas-solid reactions and physical processes such as drying and mixing.

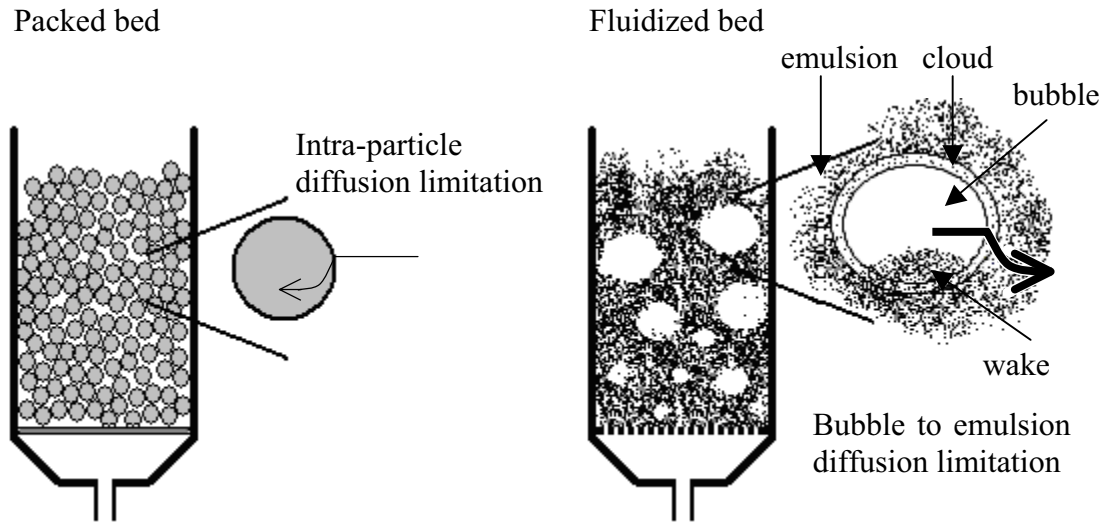

Figure 7-1. Two reactor types for gas-solids contacting: the packed bed and the (bubbling) fluidized bed. The efficiency of packed bed reactors is limited by intraparticle mass- and heat-diffusion lengths due to the larger particles (inset left). The smaller particles in the fluidized bed hardly suffer from this limitation, but now the appearance of large gas bubbles limits the interchange of the gas in these bubbles to the particles in the emulsion phase (inset right).

The appearance of gas bubbles, however, is a limiting factor to the conversion and selectivity which can be achieved in fluidized bed reactors. In fact, the overall conversion in a bubbling fluidized bed is considerably less than the conversion in a comparable packed bed due to the bypassing of gas through the bubbles. Yet, fluidized beds are often preferred over packed beds for heterogeneously catalyzed reactions because they can take greater advantage of better and more reactive catalysts. Hydrodynamically, the smaller particles used lead to better distribution and mixing, in combination with a low pressure drop, in a fluidized bed. Due to shorter intraparticle diffusion distances, the catalyst particles are used more efficiently than the larger particles of packed beds, and heat exchange, both from particle to gas as well as to heat exchanger tubes, is more effective. The risk of local hot-spots is

decreased because of the constant mixing, and it is easier to add or remove particles from a fluidized bed than from a packed bed.

Despite these advantages, the conversion in a fluidized bed is substantially lower than in a comparable packed bed. This is because, for a wide range of particle sizes and densities known as Geldart A and B materials, most or virtually all the gas blown into a fluidized bed beyond that required for minimum fluidization, is present as bubbles (cf. Figure 7-1). These voids, containing the gaseous reactants and products, rise through the particles, pushing them aside both laterally and radially. Within the bubbles are very few catalyst particles, and surrounding the bubble is a region with a lower particle concentration (the cloud). As the bubble size increases, the interchange of the gas in these bubbles to the emulsion phase with the catalyst particles decreases significantly. Especially when the reaction kinetics are fast, the transfer from the bubble phase to the particle phase will be the rate limiting step. Reducing or eliminating the bubbles from the system would significantly enhance the conversion in the reactor. On the other hand, a certain amount of bubbling enhances mixing in the bed, so a tuning of bubble behavior to the specific process is desirable.

Many methods have been explored to reduce or control the average bubble size in bubbling fluidized beds in a variety of ways. Internals such as baffles, trays, and heat exchanger pipes have been studied (Dutta and Suciu, 1992), as well as external means such as fractal injection (Cheng et al., 2001), pulsed flow (Coppens and van Ommen, 2003), chaos control (van den Bleek et al., 2002), mechanical vibration (Kwauk, 1994), and magnetic fields (Rosensweig, 1995). The method of injecting gas into the system, i.e. the gas distributor, has also been shown to influence the bubble size and bubble size distribution (Svensson et al., 1995). The applicability of many of these designs is limited, either because they influence the hydrodynamics of the bed negatively, because the lifetime of the system is very limited, or because the energy input is so great that the system becomes economically unfeasible.

In this paper, the bubble size is controlled using electric fields (Kleijn van Willigen et al., 2003). The application of alternating electric fields has been shown to be a low energy method capable of reducing the size of bubbles in bubbling fluidized beds of Geldart B materials by as much as 80%. Fundamentally, the method depends on a surface polarization of the particles, leading to interparticle forces (Kleijn van Willigen et al., 2005). The magnitude and direction depend on the relative locations

of the particles, the strength and frequency of the electric field, and the conductivity of both the particles and the gas.

First, the influence of a change in bubble diameter is qualitatively investigated with the Kunii and Levenspiel model. The three-phase model (consisting of the bubble, cloud, and emulsion phases) is extended with the Darton equation for bubble growth and a electric field efficiency factor. As such, the model is used to demonstrate the influence of such parameters as reaction rate and gas flow rate on the conversion both under normal circumstances and with an electric field induced smaller bubble size.

The second method of demonstrating that the change in hydrodynamics, i.e. bubble size, is beneficial to the efficiency of the electric field enhanced fluidized bed is experimental. Using the decomposition of ozone as a test reaction, we experimentally confirmed the influence a change in bubble size due to applied electric fields has on the conversion attainable in an electric field enhanced fluidized bed. The decomposition of O_3 to O_2 has frequently been used in experimental studies of catalyzed reactions in fluidized beds (see Kunii and Levenspiel, 1991, for an overview). This reaction is practically first order in ozone concentration, and, runs easily at temperatures close to room temperature. In addition, both the generation and the analysis of ozone are practical in laboratory setups. A porous alumina catalyst carrier, Sasol Puralox® was used. This study was intended as a proof of principle that smaller bubbles induced with applied electric field actually leads to a higher conversion, not as an exhaustive experimental study into all of the many possibilities of chemical reactions in electric field enhanced fluidization.

7.2 Three-phase fluidized bed model

The Kunii and Levenspiel model (Kunii and Levenspiel, 1968, 1990) gives an elegant and instructive description of the three phase behavior of a bubbling fluidized bed. Its accuracy in describing systems without significant axial dispersion has been attributed to its good estimates of the interchange rate coefficients (Chavarie and Grace, 1975). The adaptation of the simple model used here is based on the following assumptions:

1 – the bubbles are all spherical, and follow the Davidson model for bubble behavior. Thus, bubbles rise through the bed with a velocity higher than the emulsion phase flow rate, and are surrounded by thin clouds. The

(upward) flow through the clouds is considered to be negligible. The wake is considered part of the cloud.

2 – the (mean) size of bubbles is derived using the Darton relation, and therefore bubbles grow in size as they rise through the bed. When an electric field is used to reduce bubble size, this is assumed to give a linear decrease in bubble size throughout the bed through the electric field efficiency factor, *E*. The consequence of this is that the bubble fraction, δ, changes through the height of the bed, as larger bubbles rise faster. In the original model by Kunii and Levenspiel, the bubble size remains constant, allowing (together with the assumption that the emulsion phase is stagnant, see point 3 below) for an analytical solution.

3 – the emulsion phase stays at minimum fluidization conditions, i.e. the porosity does not change, neither with height in the bed nor with the application of electric fields. Contrary to the original model, flow through the emulsion phase is included.

These adaptations to the original model, which was analytically solvable, means the model must be solved numerically. A schematic representation of the model is shown in Figure 7-2.

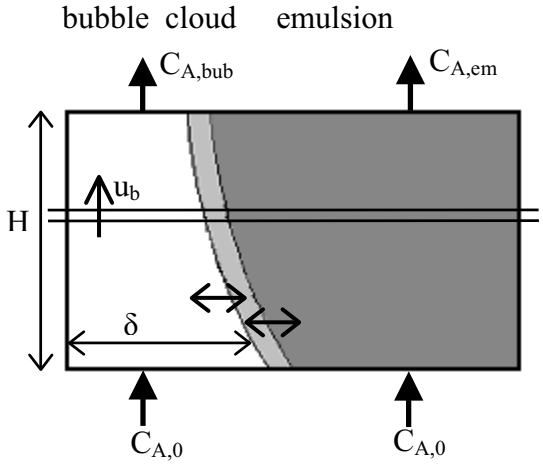

Figure 7-2. The adapted Kunii and Levenspiel model for three-phase flow through a fluidized bed. The flow rate through the emulsion phase is that required for minimum fluidization, the flow through the bubble phase is the excess gas flow [adapted from Levenspiel, 1999].

Hydrodynamics

The bubble size is described by the Darton relation (Darton et al., 1977) for a porous plate gas distributor, extended with an electric field efficiency factor E:

$$d_b = \frac{0.54\left(u_0 - u_{mf}\right)^{0.4} h^{0.8}}{g^{0.2}} \cdot E \qquad [7 - 1]$$

Without the electric field present, E is 1. When the field is applied by $E < 1$, the electric field decreases the bubble diameter.

The bed fraction in bubbles, δ, can be derived as follows for the regime considered here ($u_{mf} / \varepsilon_{mf} < u_b < 5\ (u_{mf} / \varepsilon_{mf})$. The bed fraction in bubbles varies with height, as larger bubbles have a higher rise velocity:

$u_{br} = 0.711(g\ d_b)^{1/2}$ single bubble rise velocity *at* u_{mf} [7 - 2]

$u_b = u_0 - u_{mf} + u_{br}$ rise velocity of bubbles in bubbling bed [7 - 3]

$\delta = (u_0 - u_{mf}) / u_b$ bed fraction in bubbles [7 - 4]

The volume of solids in the bubble phase is based on experimental estimates given in the literature (Rowe and Partridge, 1965); the volume of solids in the cloud and the emulsion phase can be derived from the bed fraction in bubbles:

$$f_{bub} = 0.001 \qquad [7 - 5]$$

$$f_{cl} = \delta(1 - \varepsilon_{mf})\left[\frac{3u_{mf} / \varepsilon_{mf}}{u_{br} - u_{mf} / \varepsilon_{mf}} + \alpha\right] \qquad [7 - 6]$$

$$f_{em} = (1 - \varepsilon_{mf})(1 - \delta) - f_c - f_b \qquad [7 - 7]$$

$$f_{bub} + f_{cl} + f_{em} = f_{total} = 1 - \varepsilon_f \qquad [7 - 8]$$

where f_{bub} is the volume of solids in the bubble over the volume of the bed, f_{cl} the volume of solids in the could and wake over the volume of the bed, f_{em} the volume of solids in the emulsion phase over the volume of the bed, and f_{total} the total volume of solids in the bed over the volume of the bed.

The diffusion of gas between bubble and cloud, and from cloud to emulsion phase, is derived from Davidson's theoretical expression for bubble-cloud circulation and Higbie's theory for cloud-emulsion diffusion.

$$K_{bub\text{-}cl} = 4.5\ (u_{mf} / d_b) + 5.85\ (D^{0.5} g^{0.25} d_b^{1.25}) \qquad [7 - 9]$$

$$K_{cl\text{-}em} = 6.77\ (\varepsilon_{mf} D\ u_{br} / d_b^3)^{0.5} \qquad [7 - 10]$$

The height of the bubbling fluidized bed, H_{bfb}, is determined by the weight of the particles, W, the cross-sectional area of the column, A, and the porosity of the fluidized bed:

$$H_{bfb} = W / [\rho_s A (1-\varepsilon_f)] \qquad [7 - 11]$$

The bed fraction of bubbles, δ, is a function of height, since the bubble size is a function of height. In addition, the solids fractions and gas interchange constants also depend on bubble size, and therefore implicitly on height. A minimum bubble size of 5 mm is used for numerical consistency at low gas velocities; at smaller bubble size the equations for the bed fraction in bubbles no longer hold.

Material balances for bubble, cloud, and emulsion phases

For a first order irreversible reaction,

$$A \rightarrow B,\ r = k\, C_A \qquad [7 - 12]$$

a set of material balances for reactant A can then be derived for every slice of bed *dh*, for the three bubble, cloud, and emulsion phases:

$$\frac{dC_{A,bub}}{dh} = \frac{1}{u_0 - u_{mf}} \cdot \left[C_{A,bub} \left(-k \cdot f_{bub} - \delta \cdot K_{bub-cl} \right) + C_{A,cl} \cdot \delta \cdot K_{bub-cl} \right] \qquad [7 - 13]$$

$$0 = K_{bub-cl} \cdot \delta \cdot (C_{A,bub} - C_{A,cl}) - K_{cl-em} \cdot \delta \cdot (C_{A,cl} - C_{A,em}) - k \cdot f_{cl} \cdot C_{A,cl} \qquad [7 - 14]$$

$$\frac{dC_{A,em}}{dh} = \frac{1}{u_{mf}} \left[K_{cl-em} \cdot \delta \cdot (C_{A,cl} - C_{A,em}) - k \cdot f_{em} \cdot C_{A,em} \right] \qquad [7 - 15]$$

This set of coupled ODE's [Eq. 7 - 13 and Eq. 7 - 15] together with the relevant algebraic equations were solved with the variable order ODE15s solver, as implemented in Matlab™.

The overall conversion in the system, *X*, is calculated based on the recombination of the flow from the emulsion and the bubble phases:

$$X = 1 - \frac{u_{mf} C_{A,em} + (u_0 - u_{mf}) C_{A,bub}}{u_0 C_{A,0}} \qquad [7 - 16]$$

7.3 Model results

In Figure 7-3a typical concentration profiles are shown for the bubble, cloud, and emulsion phases without bubble size reduction, whereas in Figure 7-3b the bubble size is reduced to 25% of the normally occurring size. A reduction in bubble diameter by 75% is not uncommon in experiments, as will be demonstrated later. Shown are

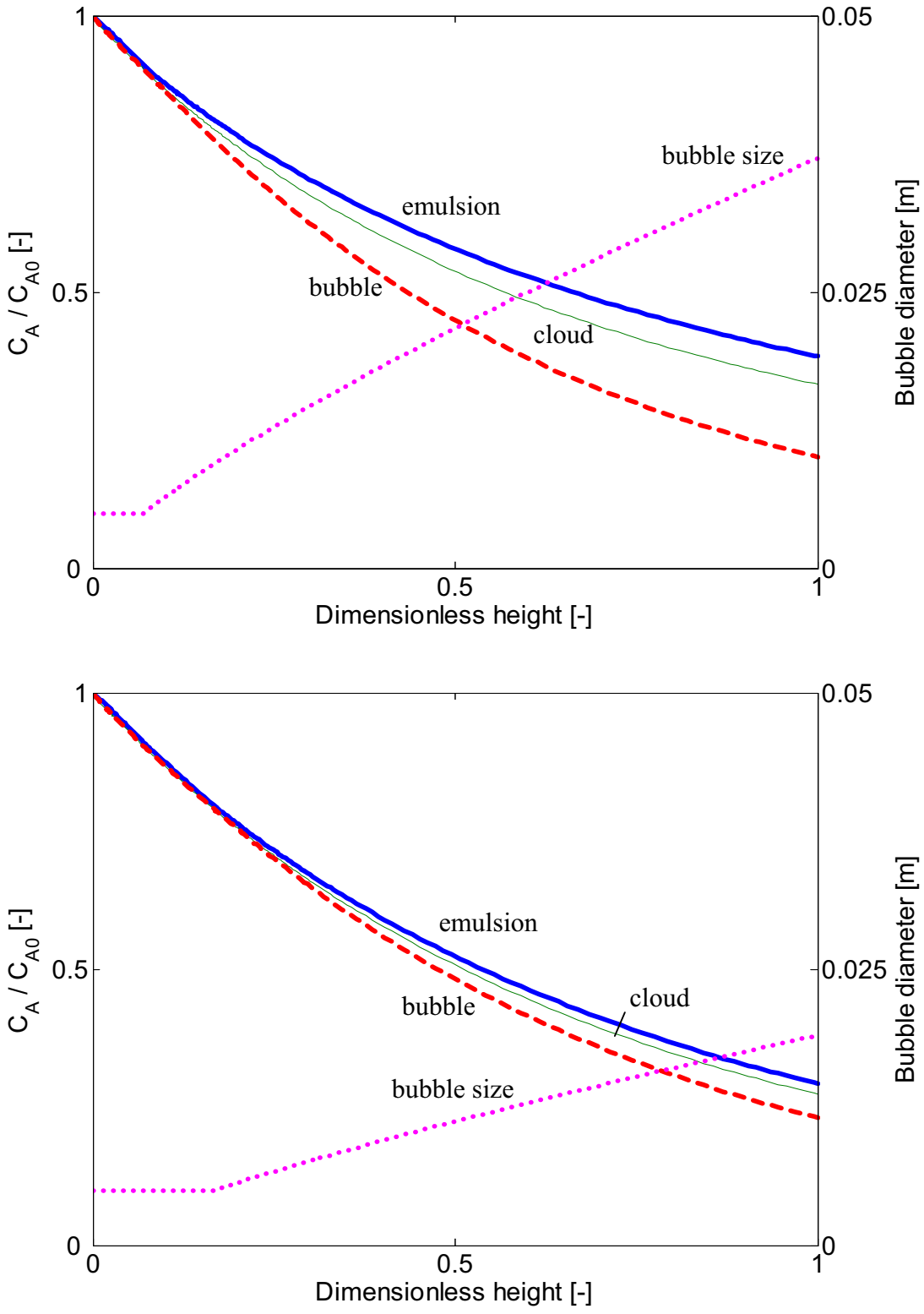

Figure 7-3. (a) Simulation results using the Kunii and Levenspiel model extended with a growing bubble size, showing the concentration profiles for reactant A and the mean bubble size, as function of height. (b) When the bubble size is decreased, i.e. by applying electric fields, the mass transfer resistance from bubble to emulsion is decreased and the net conversion increases. The A → B reaction is first order, k = 0.5 s^{-1}, the $H_{settled}$ / D_{bed} ratio is 3.5, and the flow rate is 2 U_{mf}.

the concentration profiles of reactant A as a function of the height in the bed, at a flow rate of twice the minimum fluidization velocity. The height of the settled beds is the same ($H_{settled}$ / d_{bed} is 3.5), but due to the smaller bubble size in the electrified simulation, the average rise velocity of the bubbles is slower, the total hold-up increases, and the expanded bed height is larger. The plots clearly demonstrate the increased conversion attainable when the bubble size is reduced. In (a), the normal situation, the rate limiting step is in the mass transfer from bubble to emulsion, as shown by the concentration gradient between the bubble and emulsion phases. In (b) the concentrations in bubble, cloud and emulsion are all almost the same: the smaller bubbles lead to a larger mass exchange area. The rate limiting step shifts to the rate of reaction, and the overall conversion increases by 5%.

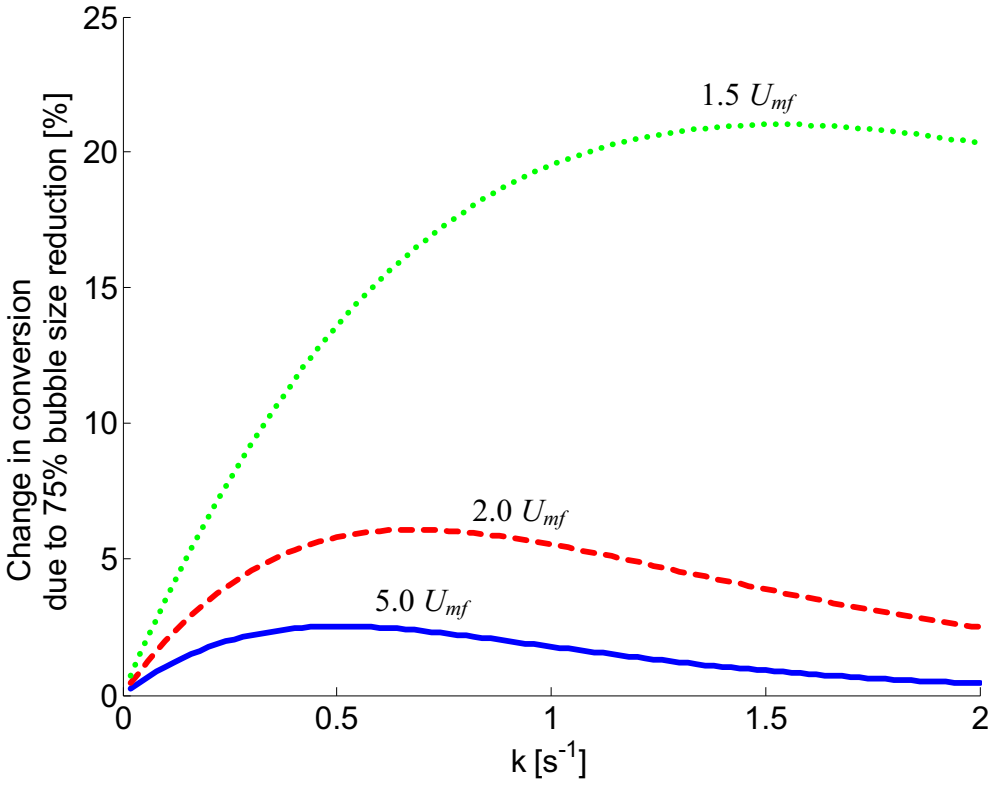

Figure 7-4. The effect of varying the reaction rate on the higher conversion gained by reducing the bubble size. Decreasing the bubble size is most effective in the regime where the mass transfer from bubble to cloud is limiting. As the reaction rate itself becomes faster, or very slow, the change in concentration in the emulsion phase has little effect on the total conversion.

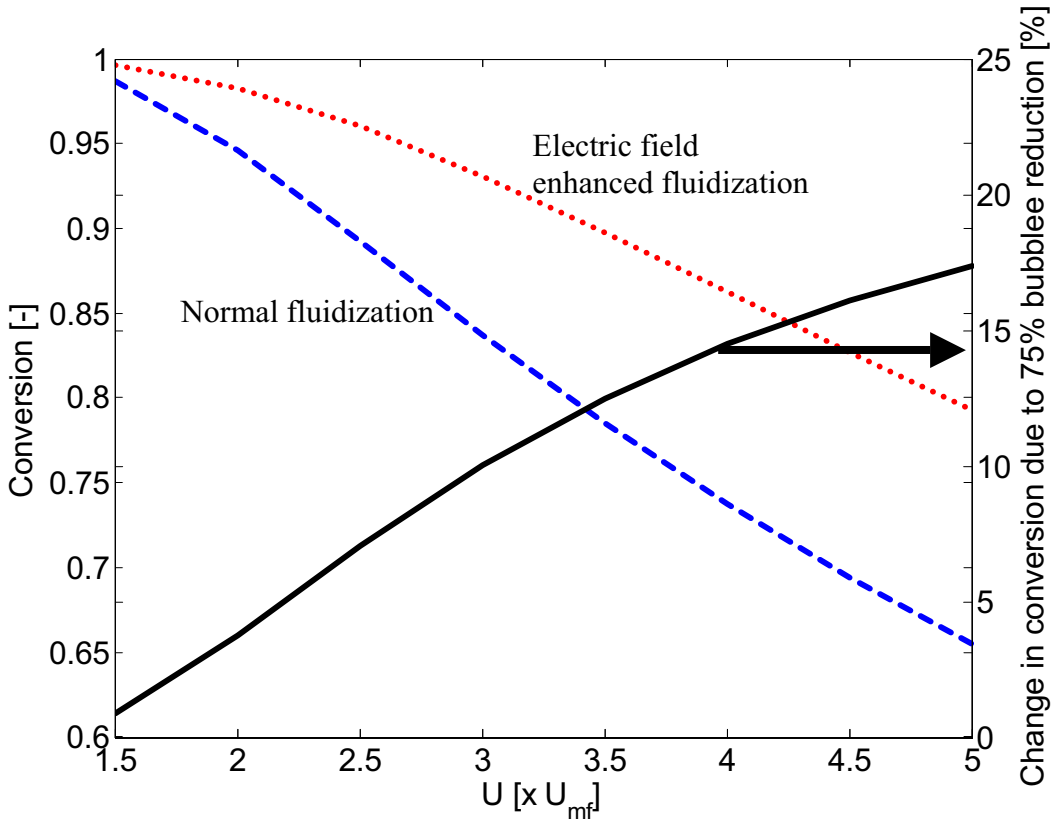

Figure 7-5. The influence of *U* on conversion (left axis), and on the right axis the relative change in conversion, i.e. the increase in reactor efficiency. As the excess flow rate increases, the bubble fraction increases and the overall conversion decreases. By using electric fields to decrease the bubble size, a significantly higher conversion can be achieved at the same flow rate, or a similar conversion at much lower flow rate.

The improvement that can be achieved by reducing the bubble size is influenced by the rate of reaction in the system. As already described for the base case, decreasing the bubble size is efficient as long as the mass transfer from bubble to emulsion is the rate limiting step, or, conversely, if the reaction kinetics in and on the catalyst particles are fast enough to convert any additional reactants brought to the emulsion phase. This effect is illustrated in Figure 7-4. For the parameters used, the reaction rate becomes the rate determining step when the reaction rate is less than approximately 0.5 s^{-1}. That is, reducing the bubble size further is no longer beneficial, because the reaction simply doesn't run faster. At high reaction rates, the overall conversion approaches 100%, and increasing the efficiency has relatively little effect.

The second parameter of interest is the gas flow rate, U_0, and this is shown in Figure 7-5. As the gas flow rate increases, the bubble size also increases. Thus, it follows that when bubbles are decreased in size at a constant flow rate (75% bubble

size reduction, or $E = 0.25$, in this case), the higher flow rate will gain more from the bubble size reduction. At the higher flow rates, the system will be limited by the maximum bubble diameter (i.e. the diameter of the column). However, while the *change in conversion* at high flow rates may be larger, the *change in outlet concentration* will actually be much smaller. Therefore, it will experimentally be easier to determine the effect of bubble size reduction at lower flow rates.

7.4 Ozone decomposition

The influence of bubbles on the conversion in electric field enhanced fluidized beds was shown above using a three-phase model of the fluidized bed. Now, we show in an experimental electric field enhanced fluidized bed setup that the decomposition of ozone can be increased by applying low-strength alternating electric fields.

Experimental setup

Experiments were conducted in a circular cross-section Plexiglas column with an inner diameter of 82 mm and a settled bed height of 300 mm. The column was placed in a thermostrated cabinet to prevent temperature gradients in the reactor. Two compressed air feed lines were used, one enriched with ozone, the other enriched with water vapor in order to regulate the relative humidity of the system. The two flows, of approximately equal magnitude depending on the desired ozone concentration, are mixed in a 100 mm long plastic static mixer with 10 elements. Both the air flows and the column are thermostated to a set temperature of 50 ˚C. Ozone was produced using an OAS Coolflow ozone generator, with a maximum production of 2 g/hr O_3. Water was added to the second feed line using a precision peristaltic pump. To ensure complete evaporation and good mixing of the water, the air and water mixture was passed over a 600 mm packed bed. The dew-point temperature of this flow was measured using a Testo FA200-2. Since both the O_3 production and the amount of water that can be added to the flow are limited by pressure, the pressure in the feed system was kept as low as possible (in practice ~0.4 – 0.6 barg). The O_3 concentration passed over the bed ranged from 40-80 ppm_v; the relative humidity in the bed was 2-10% (dew point temperature –15 to 17 ˚C) , depending on the operating conditions.

Ozone measurements were conducted with an INUSA IN-2000 UV-absorption analyzer (range 0-100 ppm, precision 0.1 ppm). Only one flow at a time can be sampled. From the windbox, a constant flow of 1.8 l/min was withdrawn, and either vented or sampled for O_3 concentration. A same flow was withdrawn from the freeboard so that ozone concentration at the outlet could be recorded. The outlet of the freeboard was slightly restricted to prevent back mixing of air from outside into the system.

At a height of 30, 80, 180, and 280 mm above the support plate, as well as in the wind box, pressure fluctuations were measured using Kistler piezo-electric pressure transducers, type 7261. The charge from the piezo-element was amplified and converted to a voltage using a Kistler amplifier type 5011. The signals were high-pass filtered with a cut-off frequency of 0.16 Hz. The transducers measured the pressure fluctuation relative to the average pressure with an accuracy of 2 Pa, and owing to the high-pass filter, the average of the measured pressure time series is zero. The sensors were connected to the column by 100 mm Teflon tubes (i.d. 4 mm), which were covered with 40 μm mesh wire gauze at the tips to prevent particles from entering. The probe tips were fitted flush with the sidewalls, in the same manner as the pressure drop probe. A 16 channel LMS-Difa Scadas III data acquisition system was used to record the pressure fluctuation measurements, the pressure drop measurement, the O_3 concentration, and the relative humidity measurement.

Electric fields were applied to the system using electrodes of round, 0.25 mm diameter Nichrome wire. The design is similar to that reported earlier (Kleijn van Willigen, 2003). At each 12.5 mm in the vertical direction a continuous wire was strung, creating a grating-like pattern of wire with a spacing of 10 mm. The electrode grating on the next level is rotated by 90˚ (cf. Figure 7-6 for the top view). Each electrode grating thus runs crosswise to its nearest neighbors. The total height of the electrode section was 300 mm. The 'odd' electrodes (i.e. at 12.5, 37.5, 62.5 mm, etc) are the live electrodes; the 'even' are grounded. Optionally, only the wires in the lowest 10 cm of the bed could be electrified, with the wires in the top 20 cm being inactive. The volume density of the electrodes was approximately 0.004%. For safety reasons, the wired inner column was placed in a Plexiglas outer column. A Trek 20/20c high-voltage amplifier was used to generate AC fields with a maximum strength of 8000 V/cm. The LMS-Difa data acquisition system both supplied the input signal and recorded the output voltage and current.

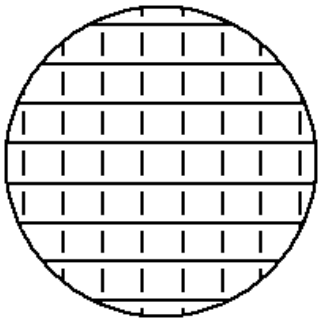

Figure 7-6. Top view of the crosswise strung electrode wires.

The particles used in the experiments were porous Puralox alumina particles, with a mean (sieved) particle size of 250-300 μm. For the experiment with iron-impregnated particles, 40 grams of the particles were impregnated with 0.5 weight percent Fe. This was done by placing the particles in a measured volume and concentration of iron nitrate solution, which was completely absorbed. The particles were subsequently dried overnight at 300 ˚C. The 40 grams of impregnated particles were mixed with non-impregnated particles until the desired bed height was reached.

Table 7-1. Experimental conditions.

Experiment	Bed height	Energized electrode height
1.5 U_{mf} (humidified)	25 cm	10 cm
1.5 U_{mf} (dry)	25 cm	10 cm
2 U_{mf} (humidified)	25 cm	30 cm
2 U_{mf} (dry)	25 cm	30 cm
2 U_{mf}, impregnated with Fe (humidified)	10 cm	10 cm

7.5 Experimental results

The experimental goal is to demonstrate whether a reduction of bubble size through the application of electric fields results in a higher conversion in a fluidized bed. The first step in doing so is to determine how the bubble diameter changes. The analysis of pressure fluctuations is a powerful technique for this, since the fluctuations are closely associated with the properties of bubbles. Using a technique developed by van der Schaaf et al. (2002) and validated by Kleijn van Willigen et al. (2003) for 2-D columns, the time series measured with the probes described earlier are decomposed

into a variance associated with the size of the bubbles passing the probes (the incoherent variance, σ^2_{IOP}), and a variance associated with other process occurring in the bed, such as bubble formation, coalescence, and break-up. This technique requires measuring the pressure fluctuations at both the height under consideration and at a place where there are few or no bubbles, such as the plenum or the very bottom of the bed. The incoherent variance is a good quantitative indicator of a characteristic bubble size. The technique is not influenced negatively by variations in flow rate or measuring height.

Results for the characteristic bubble size are presented in Figure 7-7 and Figure 7-8 at a measuring height of 8 and 18 cm, respectively. It is clear how the bubble size increases with the measuring height and flow rate, although at 1.5 U_{mf} the bubble growth is quite limited – it is possible that at such low flow rates, the frequency of bubble coalescence becomes very low.

When the electric field is applied, a reduction in bubble size is observed for all experiments, varying from just 10% smaller bubbles to as much as 80% reduction. The reduction is stronger when the humidity of the system is raised slightly from the default dry condition. Raising the humidity increases the conductivity slightly, making the macroscopic electric polarization of the particles larger. Also, the bubble size reduction becomes larger when the electric field is utilized over the whole bed.

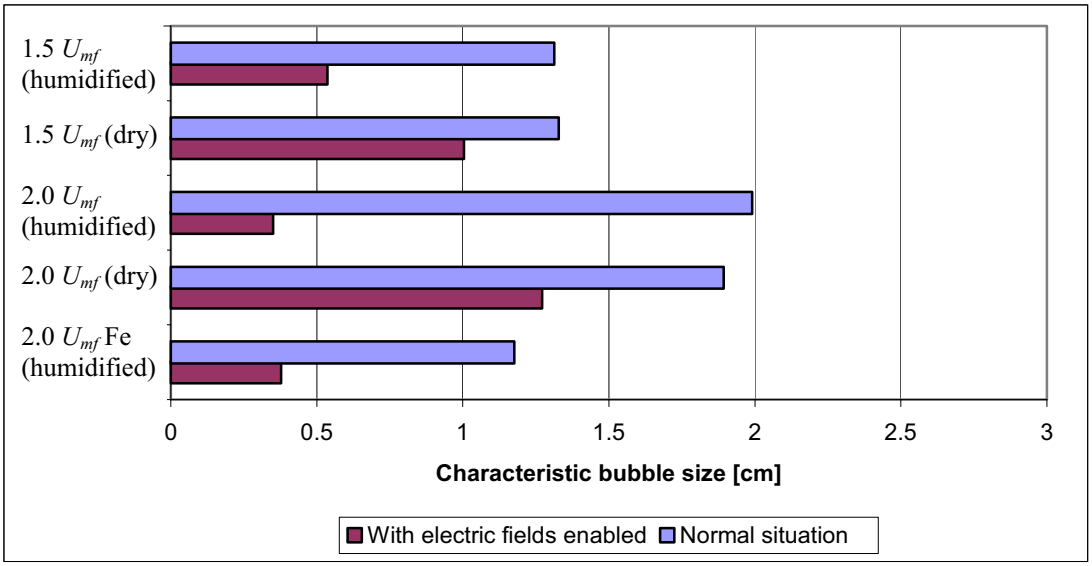

Figure 7-7. Effect of electric field (7.2 kV/cm, 15 Hz) on characteristic bubble size at 8 cm above the gas distributor.

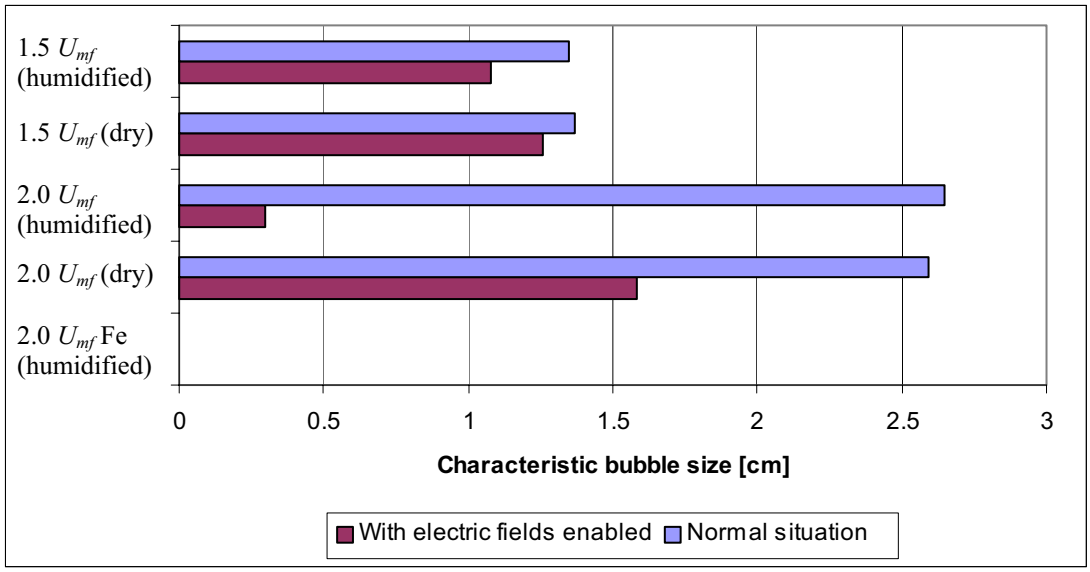

Figure 7-8. Effect of electric fields on characteristic bubble size at 18 cm above the gas distributor.

Figure 7-9 demonstrates the effect of the bubble size reduction on the O_3 decomposition efficiency. For all the experiments done, a decrease in the bubble size leads to a higher conversion. Note that as the experiments were conducted over extended lengths of time, the net conversion should not be compared between the various cases due to catalyst deactivation over extended periods of time. This deactivation was not significant within the duration of the experiments which were conducted in 18 minute cycles of applying the field and measuring the reference situation. The optimal conditions are those in which the electric field efficiency is maximized (i.e. with a raised humidity). While at the higher flow rate the total increase in O_3 decomposition due to the electric field is larger on a mass basis, the increase in conversion is lower, and therefore more difficult to measure accurately.

A greater gain can be achieved when the conversion rate is increased by impregnating the catalyst particles with 0.5 % wt/wt iron. The absolute conversion is increased (from 11% to 25%), while the conversion gain by the electric field increases from 6% to 13%. This is consistent with the modeling results (Figure 7-4) which show that a low reaction rate limits the positive effects of smaller bubbles.

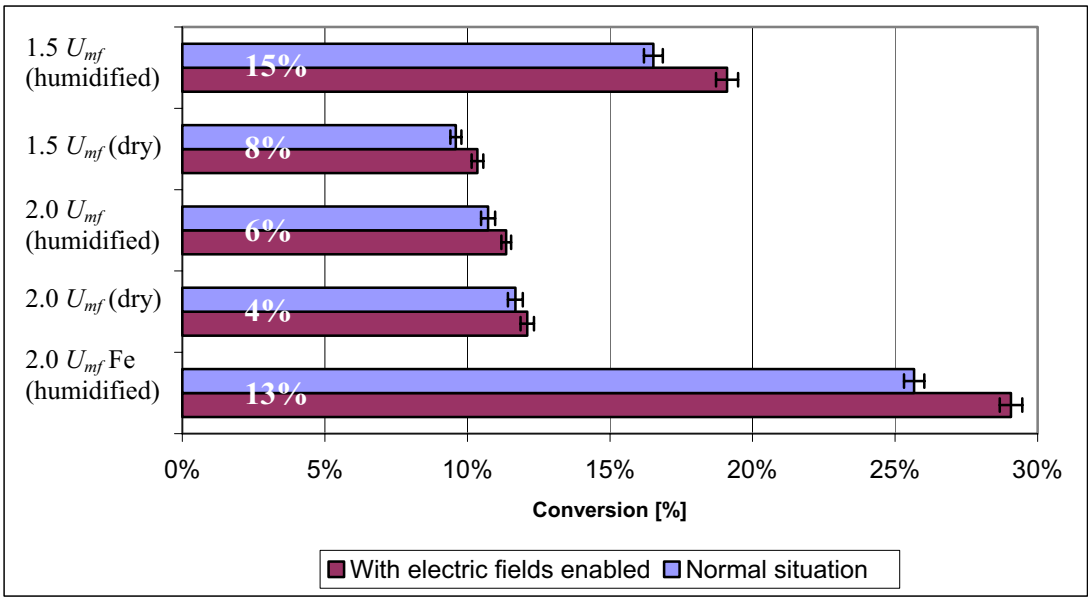

Figure 7-9. Change in O_3 conversion due to bubble size reduction. The top bar for each experiment shows the conversion in the normal situation, the bottom bar the higher conversion with the application of the electric field. The inset percentages show the increase in conversion due to the electric field.

7.6 Conclusions

The aim of this work was to demonstrate the higher conversions that can be reached in a fluidized bed by the application of an electric field to reduce bubble size. The adapted Kunii and Levenspiel model shows that decreasing the bubble size leads to a higher conversion, depending on the flow rates and reaction rate. It was shown experimentally how electric fields lead to a bubble size reduction up to 80%, especially when a small amount of moisture is present. Raising the reaction rate by impregnating the particles with 0.5% wt/wt iron makes the results much clearer, showing that more active catalyst particles benefit more from the bubble size reduction than less active catalysts. The results are consistent with the qualitative predictions of the Kunii and Levenspiel model.

7.7 Notation

A	cross-sectional area of bed, m^2
C_A	concentration of reactant A, mol m^{-3}

D	diffusion constant, $m^2\ s^{-1}$
d_b	bubble diameter, m
E	electric field efficiency factor, -
f_i	volume of solids in phase i / volume of bed, -
g	gravititational constant, $m^2\ s^{-1}$
h	height, m
k	reaction rate constant, s^{-1}
K_{i-j}	diffusion rate constant from phase i to j, $m^3_{bed}\ m^{-3}_{bub}\ s^{-1}$
r	rate of reaction, mol $m^{-3}_{solids}\ s^{-1}$
u_0	superficial gas velocity, $m^3_{gas}\ m^{-2}_{bed}\ s^{-1}$
u_{br}	rise velocity of single bubble, $m\ s^{-1}$
u_b	rise velocity of bubbles in bubbling bed, $m\ s^{-1}$
u_{mf}	minimum fluidization velocity, $m\ s^{-1}$
X	overall conversion, %
α	volume of wake/volume of bubble, -
δ	bed fraction in bubbles, m^3 bubbles/m^3 bed
ε_i	porosity of phase i, -
ε_{mf}	porosity at minimum fluidization, -
ρ	density, $kg\ m^{-3}$
Φ	volumetric flow, $m^3\ s^{-1}$

subscripts

bub	bubble phase
cl	cloud phase
em	emulsion phase
mf	minimum fluidization
f	bubbling fluidized bed conditions

7.8 References

Chavarie, C., and Grace, J.R., 'Performance Analysis of a Fluidized Bed Reactor. II. Observed Reactor Behavior Compared with Simple Two-Phase Models', *Ind. Eng. Chem. Fundam.*, **14** (1975), 79-86.

Cheng, Y., van den Bleek, C.M., and Coppens, M.-O., 'Hydrodynamics of gas-solid fluidized beds using a fractal injector', in: Proc. 10th Int. Conf. on Fluidisation, United Engineering Foundation, NY (2001), 373-380.

Coppens, M.-O. and van Ommen, J.R., 'Structuring chaotic fluidized beds', *Chem. Eng. J.*, **96** (2003), 117-124.

Darton, R.C., LaNauze, R.D., Davidson, J.F., and Harrison, D., 'Bubble growth due to coalescence in fluidised beds', *Trans. I. ChemE.*, **55** (1977). Pp 274-280.

Dutta, S., and Suciu, G.D., 'An experimental study of the effectiveness of baffles and internals in breaking bubbles in fluid beds', *J. Chem. Eng. Jpn.*, **25** (1992), 345-348.

Kunii, D., and Levenspiel, O., 'Bubbling Bed Model. Model for Flow of Gas through a Fluidized Bed', *Ind. Eng. Chem. Fundam.*, **7** (1968). Pp.446-452.

Kunii, D., and Levenspiel, O., 'Fluidized reactor models. 1. For bubbling beds of fine, intermediate, and large particles. 2. For the lean phase: freeboard and fast fluidization', *Ind. Eng. Chem. Res.*, **29** (1990), 1226-1234.

Kunii, D., and Levenspiel, O., 'Fluidization Engineering' (2nd ed.), Butterworth-Heinemann, Boston (1991).

Kleijn van Willigen, F., van Ommen, J.R., van Turnhout, J., and van den Bleek, C.M., 'Bubble size reduction in a fluidized bed by electric fields', *Int. J. Chem. Reactor Eng.*, **1**: A21 (2003). http://www.bepress.com/ijcre/vol1/A21.

Kleijn van Willigen, F., van Ommen, J.R., van Turnhout, J., and van den Bleek, C.M., 'Bubble size reduction in electric-field-enhanced fluidized beds', *J. Electrostat.,* **63** (2005), 943-948.

Kwauk, M., 'Fluidization: Idealized and Bubbleless, with Applications', Science Press, Beijing (1992).

Levenspiel, O. 'Chemical Reaction Engineering' (3rd ed.), Wiley, New York (1999).

Rosensweig, R.E., 'Process concepts using field-stabilized two-phase flow', *J. Electrost.*, **34** (1995), 163-187.

Rowe, P.N., and Partridge, B.A., 'An X-ray study of bubbles in fluidised beds', *Trans. Inst. Chem. Eng.*, **43** (1965), 157-175.

Van den Bleek, C.M., Coppens, M.-O., and Schouten, J.C., 'Application of chaos analysis to multiphase reactors', *Chem. Eng. Sc.*, **57** (2002), 4763-4778.

Van der Schaaf, J., Schouten, J.C., Johnsson, F., and van den Bleek, C.M., 'Non-intrusive determination of bubble and slug length scales in fluidized beds by decomposition of the power spectral density of pressure time series', *Int. J. Multiphas. Flow*, **29** (2002), 865-880.

Svensson, A., Johnsson, F., and Leckner, B., 'Fluidization regimes in non-slugging fluidized beds: the influence of pressure drop across the air distributor', *Powder Technol.*, **86** (1996), 299-312.

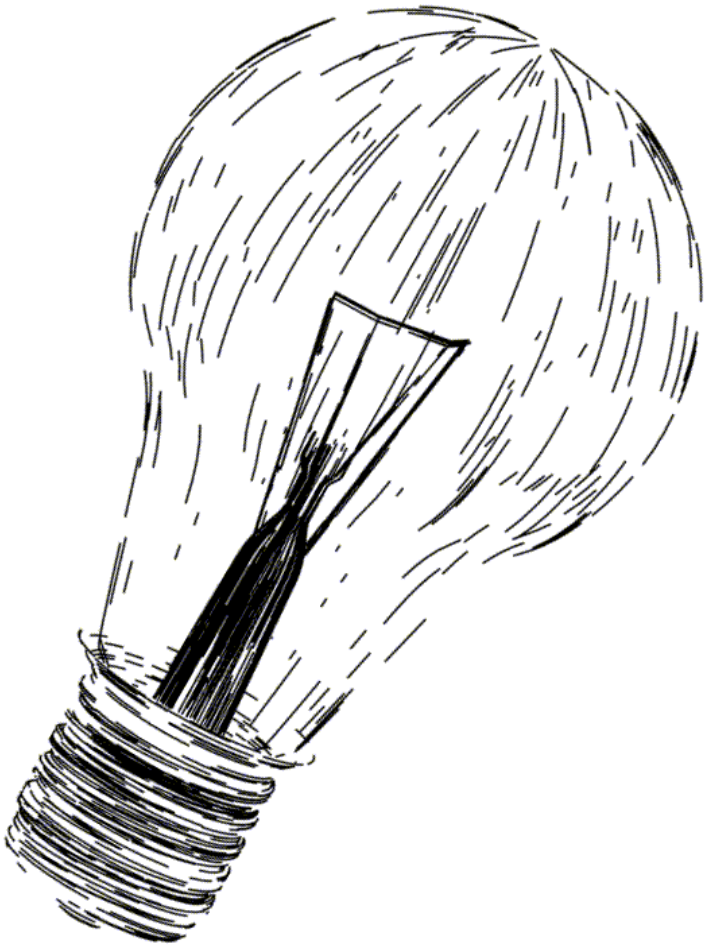

The energy requirement of electric field enhanced fluidized beds is approximately 40 Watt per cubic meter of reactor – the same amount of energy as consumed by a single incandescent light bulb!

8. Conclusions and Outlook

8.1 Conclusions

This thesis describes the effect of applied electric fields on the bubble size and conversion in gas-solid fluidized. The goal was to use low-energy electric fields to manipulate the interparticle forces in such a way that a more homogeneous fluidization regime is achieved, and to demonstrate that this is beneficial to the effectiveness of a fluidized bed reactor in catalytically converting reactants to products.

It was found that low-energy alternating electric fields, using thin wire strung through the bed as electrodes, can reduce the diameter of bubbles by up to 80%, and this was demonstrated to increase conversion by 15%. An understanding was developed and discussed on the mechanisms and parameters leading to such significant improvement, as well as the advantages and disadvantages. These insights will be summarized below. Although the research was fundamental in nature, both experimentally and in modeling, the future viability of industrial application was always a guiding element.

Besides the *application* of electric fields in electric field enhanced fluidized bed systems, the work was extended to *measuring* electric fields to gain an understanding of how triboelectrically charged particles are distributed around bubbles in fluidized beds. It was found that there is a decrease in charge density when moving inwards from the negatively charged emulsion phase towards the bubble interface, with essentially zero charge density inside the bubble. However, the charge distribution was shown to be non-trivial in that the wake of a bubble typically contains particles with a much stronger charge, of the same sign, than the particles in the emulsion phase.

The phenomena, results and insights on electric field enhanced fluidized beds were considered on three scales:

- The microscopic or particle scale
- The mesoscopic or bubble scale
- The macroscopic or reactor scale

Microscopic scale

When a particle in a fluidized bed is subjected to an electric field, it electrically polarizes with a dipole moment in the direction of this field. While the total charge on the particle remains zero, a charge separation occurs to the poles of the particle. The mechanism of this polarization is described by the Maxwell-Wagner theory of surface polarization. As described by this theory, charge migrates to the poles of the particle; hence, there is a strong dependence of the degree of polarization on the bulk and surface conductivity. In addition, an optimal frequency in the range of 1-100 Hz, and a slight dependence of the degree of polarization on the particle size due to charge diffusion have been predicted. In the work described in this thesis, the system remains relatively highly resistive despite the slightly raised relative humidity.

The influence of the relative humidity on both the dielectric response and the mesoscopic bubble scale were demonstrated experimentally and show a qualitatively similar trend as expected from the theory. As the relative humidity is raised from bone-dry to ~40% RH, the dielectric response was both calculated and measured to increase by as much as four orders of magnitude. Similarly, the bubble size in an experimental electric field enhanced fluidized bed was found to be significantly smaller in a humidified system.

Mesoscopic scale

On the mesoscopic scale we studied how the interparticle forces resulting from the polarization of the particles leads to changes in the hydrodynamics and bubbles in a fluidized bed. To increase the amount of mass transfer between gas in the bubble phase and the emulsion phase, it is desirable to decrease the bubble size as much as possible.

The design and operation of the experimental electric field enhanced fluidized beds, both of two-dimensional and circular cross section columns, was such that the average field density was as high as possible, the design scalable, the ‘fluidity’ of the system, i.e. the free movement of particles, preserved, and the reduction in bubble size as large as possible. This was achieved experimentally by stringing thin wire electrodes through the bed, which, when unenergized, showed no measurable influence on the hydrodynamics of the system.

The applied electric field can reduce the size of bubbles by as much as 85% at lower flow rates and 30% at 3.5 times the minimum fluidization velocity. The

number of bubbles was found to increase, and the bubble hold-up decreases. The combination of a smaller mean bubble size with a lower bubble hold-up suggests an increase in emulsion phase flow.

While the experiments clearly demonstrated that bubbles were smaller when an electric field was applied, it was difficult to deduce exactly *how* and *why* smaller bubbles are observed. To answer these questions, computer simulations were carried out. A discrete particle model (DPM), which models the behavior of each individual particle in the gas flow, was extended with an electric field induced interparticle force. Although the electric fields in the simulations were homogeneous (i.e. only vertical or horizontal), as compared to the multipole fields in the experiments, and the simulated column was several orders of magnitude smaller than the experimental columns, the results clearly suggest two effects of electric fields. First, the gas injected into the column is distributed over more bubbles spread over the width of the column. Secondly, in the higher regions of the column, the rate of bubble coalescence is decreased.

Macroscopic scale

The results at the microscopic and mesoscopic scale (i.e. the electric field induced interparticle force leading to a smaller bubble size) do not directly show an enhancement of fluidized bed reactors: in the end, the level of conversion attainable in the system, and the cost at which this can be done, are the most important results.

That electric field enhanced fluidization can reduce the size of bubbles in a fluidized bed significantly was shown convincingly. To demonstrate that this is also chemically beneficial, and not only hydrodynamically, we demonstrated both by modeling and by experiments that the conversion is increased with smaller bubble size. Experimentally, this proof of principle was demonstrated using the ozone decomposition reaction, an essentially first order reaction which already runs easily at room temperature. It was found that the conversion of ozone in a circular cross-section electric field enhanced fluidized bed can be raised by 15%. The model, an extension of the Kunii and Levenspiel model (Kunii and Levenspiel, 1990), shows that the gains can be significantly greater or less, depending on such parameters as the reaction rate and the flow rate.

Clearly, the chemical conversion benefits can be significant, depending on the application. It is even more interesting when the energy cost of the application of

electric fields is considered. Although it varies slightly with the relative humidity of the system (which, as described above, directly influences the conductivity of the bed), the typical power consumption of an electric field enhanced fluidized bed is approximately 40 Watt per cubic meter of reactor – about as much as a single incandescent light bulb.

8.2 Outlook

In the work presented in this thesis, the electric field enhanced fluidized bed reactor has been shown to offer a significant advantage over conventional bubbling fluidized beds. There is much potential for applying the current work and insights both to new applications and existing chemical reactors.

Technology development

A number of aspects of the electric field enhanced fluidized bed system are suggested as the focus of future reasearch. A most promising extension of the work is the use of corona discharges to control the amount of free charge in the fluidized bed. This concept can be applied to both the electric field enhanced fluidized bed, where it may reduce the raised humidity requirement by supplying an alternate charge carrier, as well as to the control of triboelectric charging in fluidized beds. The use of corona discharge has been reported before (Taillet, 2001), but here a corona stream of positive and negative ions was sprayed on top of the bed. The use of selectively positive or negative corona discharge in the feed (or a makeup stream) to the fluidized bed may yield significantly better results. An initial attempt has been made (Van Burgh, 2004), but difficulties in both measuring the corona stream and measuring the buildup of charge in the bed means that further work is required.

The application of electric fields in a fluidized bed is not limited to gas-solid systems; the application of electric fields in gas-liquid-solid systems may also give a better control of the distribution of the solid particles in three-phase reactors. Possible methods include electrophoresis of particles in a non-uniform field, flotation of particles, control of the injection of gas bubbles, and introduction of more viscous regions to divide the system into a number of zones (Moerman, 2005). Many parallels exist between electric field enhanced slurry columns and electrorheological systems.

Application driven

An obvious route for continuing the development of the electric field enhanced fluidized bed is to work towards an (industrial) application. A wide range of systems can be envisioned: catalytic chemical reactors with organic and/or inorganic reactants, pharmaceutical processes requiring very well-defined product properties, physical processes such as (spray) drying, nano-fluidized beds, fluidized bed nuclear reactors, etc. For a useful and safe application of electric fields, the electrical properties of the system must fulfill a number of requirements. First and foremost, the system should not be conductive if (a) the freedom of movement of particles is to be preserved, and (b), the electric power is to remain as low as reported in this thesis. Common catalytic (carrier) materials such as silica and alumina have been shown in this thesis to be applicable. Also, the particles in the system must be susceptible to polarization, a property which can be influenced by controlling the relative humidity and/or the conductivity. In addition, the chemical composition in the system should not be susceptible to electrical breakdown. Although air was used as fluidizing gas in the work reported in this thesis, the dielectric breakdown strength of many pure organic is high enough for these gases to be used in electric field enhanced fluidized beds. Many diatomic gases, however, do have significantly lower break-down strenghts, and therefore may require dilution before they can be safely used in electric field enhanced reactors. The influence of temperature on both polarization behavior, conductivity, and electrical stability of the materials has not been addressed in this thesis, but is certain to be a relevant parameter when developing applications.

The range of gas flow rates at which the experimental work in this thesis was done is the first point that must be addressed when considering the design of a reactor. Many existing applications of bubbling fluidized bed reactors operate at significantly higher flow rates. Either the electric field enhanced fluidized bed must be operated under such higher flow rates, possibly requiring a strong field effect in order to gain a benefit, or, more preferably, the flow rates in current reactors can be decreased due to the more homogeneous and efficient fluidization.

The second point that must be addressed when designing a potential application of electric field enhanced fluidized beds is the electrode design. The use of thin wire electrodes has so far been interesting and convenient because the electrodes themselves do not influence the fluidized bed behavior. In addition, the

design itself is scalable – it is theoretically possible to generate the same electric field in a larger column, which is not doable if parallel plate electrodes situated outside the column had been used. Possible future designs could use sturdier electrodes, perhaps grids, which themselves may influence bubble behavior. However, because the efficiency of electric field enhanced fluidized beds is higher than normal systems, it may be possible to reduce flow rates, in turn leading to less attrition and a longer life-time of the electrodes in the bed. The use of existing heat exchanger tubes as electrodes is also a possibility. The risk of sparks occurring after breakage of an electrode will undoubtedly exclude any reactor containing potentially explosive mixtures.

8.3 References

Kunii, D., and Levenspiel, O., 'Fluidized reactor models. 1. For bubbling beds of fine, intermediate, and large particles. 2. For the lean phase: freeboard and fast fluidization', *Ind. Eng. Chem. Res.*, **29** (1990), 1226-1234.

Moerman, M.J., 'Slurry Bubble Columns: Improving Performance by Electric Fields', internal report, Delft University of Technology (2005).

Taillet, J., 'Using supersonic injection for eliminating electrostatic charges in large mass flows of polyethylene pellets: an emerging chemical engineering technology', *J. Electrost.*, **51-52** (2001), 50-56.

Van Burgh, M., 'Elimination of Electrostatic Charges in Fluidized Beds', B.Sc. thesis, Technische Hogeschool Rijswijk (2004).

List of Publications

Kleijn van Willigen, F., van Ommen, J.R., van Turnhout, J., and van den Bleek, C.M., 'Bubble Size Reduction in a Fluidized Bed by Electric Fields', *Int. J. Chem. Reactor Eng.*, **1**: A21 (2003). http://www.bepress.com/ijcre/vol1/A21.

Kleijn van Willigen, F., van Ommen, J.R., van Turnhout, J., and van den Bleek, C.M., 'The influence of AC electric fields on bubbles in gas-solid fluidized beds', in: Proceedings of the 11th International Conference on Fluidization, Arena, U., Chirone, R., Miccio, M., and Salatino, P. (eds) (2004), 643-649.

Kleijn van Willigen, F., van Ommen, J.R., van Turnhout, J., and van den Bleek, C.M., 'Bubble control in fluidized beds by applied electric fields', paper presented at AIChE Annual Meeting and Fall Showcase 2004, Austin, U.S.A. (2004). Paper 274b.

Kleijn van Willigen, F., van Ommen, J.R., van Turnhout, J., and van den Bleek, C.M., 'Bubble Control in Fluidized Beds by Applied Electric Fields', proceedings of the 7th World Congress of Chemical Engineering, Glasgow, Scotland (2005).

Kleijn van Willigen, F., Christensen, D., van Ommen, J.R., and Coppens, M.-O., 'Imposing Dynamic Structures on Fluidised Beds', *Catal. Today*, **105** (2005), 560-568.

Kleijn van Willigen, F., van Ommen, J.R.,van Turnhout, J., and van den Bleek, C.M., 'Bubble Size Reduction in Electric-Field-Enhanced Fluidized Beds', *J. Electrostat.* **63** (2005), 943-948.

Chen, A., Bi, H.T., Grace, J.R., Kleijn van Willigen, F., and van Ommen, J.R., 'Measurement of charge distribution around a rising bubble in a 2-D fluidized bed', *AIChE J.*, **52** (2006), 174-184.

Acknowledgement

Een promotieonderzoek gaat gepaard met vele *ups* en (eentje minder) *downs*. De steun, kritiek, gezelligheid, discussies, en vooral aanwezigheid van alle collega's, begeleiders, familie, en vrienden hebben ervoor gezorgd dat ik dit pad met plezier en opgewektheid heb bewandeld: dank jullie wel voor alles!

Een aantal mensen heeft wel bijzonder veel bijgedragen aan dit proefschrift, en wil ik graag hiervoor bedanken. *First and foremost*, mijn begeleiders ('bazen'): Ruud, Prof. van Turnhout, en Cock. Ik heb veel van jullie geleerd, en hoewel ik wel eens met de handen in het haar zat voor een werkbespreking over wat ik nu weer ver/geprutst had, is jullie sturing altijd erg doelgericht geweest. De combinatie tussen vrijheid om mijn eigen richting te gaan, zowel in onderzoek als fysiek in het buitenland, en de constante focus op het einddoel, heb ik als bijzonder plezierig ervaren. Het was een eer met jullie samen te werken!

Veel, zoniet al dit werk, was nooit gelukt zonder de constante hulp van de technici van de proeffabriek, evenals de verschillende werkplaatsen waar ik zo vaak ben geweest. Ton, Thomas, Ruud, en Piet, niet alleen zijn jullie kennis van apparatuur, de verscheidene opslagplekken voor van alles en nog wat, en jullie gouden handen absoluut onmisbaar geweest, de regelmatige praatjes zijn voor mij altijd een zeer welkome afleiding van de dagelijkse beslommeringen geweest!

Albert en Anton, jullie hebben mij in korte tijd wegwijs gemaakt in veel aspecten van het promoveren en TU leven. Albert, je programmeerkunsten en vooral ook de snelheid waarmee je programma's kan maken bewonder ik nog steeds! Dank jullie wel.

Een aparte rol in de proeffabriek wordt nog steeds gespeeld door John. Behalve het vele inhoudelijke waar je mij mee hebt geholpen, ben je op zowel lastige als mooie momenten een welkom klankbord geweest, en ik weet zeker dat dat in de toekomst ook nog zo zal zijn!

Een aantal afstudeerders hebben inhoudelijk een grote bijdrage geleverd aan dit proefschrift, maar vooral ook voor afleiding gezorgd op momenten dat mijn ogen te vierkant werden van het staren naar dat eeuwige Matlab: Guido, Jurrian, Martin, Birol en Marloes. Ik hoop dat ik niet teveel van jullie vragen heb afgedaan met 'Ja zeg, het is jouw project!'…

Stefan, Irina, VJ, Kourosh, Malte, Dana, Prasant, Gerard, Vinit, Kalyani, Eivind, Els and Elly, and all the other more or less permanent R&CE'ers, PCMT'ers, researchers, students, and others in and out of the proeffabriek, I thank you for the many things you have taught me and the great bbq's we have had! Krish, thank you for helping me out with the 'dirty' chemistry that I tried to avoid for so long.

A very large thank-you is due to my hosts in Vancouver during my six month stay at the University of British Columbia. Aihua, Xiaotao, and John, the openness with which you received me and the very extensive and stimulating discussions were a sincere pleasure. Doing a part of my research with you has certainly contributed to quality of my work. Poupak, Monica, and Gorkem, it was great working with you!

Zonder jou, Gwen, zou ik mij niet eens voor kunnen stellen waar ik nu zou zijn. Niet alleen ben je de onontbeerlijke mentale steun en afleiding geweest, maar ook heb je altijd geprobeerd mij inhoudelijk te helpen op momenten dat ik metaforisch niet meer wist of ik iets nou links- of rechtsom vast moest draaien. Wat je voor mij betekent is niet in woorden te vangen!

Oh, and don't forget, a Calvin a day keeps the doctor away!

About the Author

Flip Kleijn van Willigen was born July 3, 1976, in Marum, The Netherlands. After an international school career, he completed his secondary education in 1994 at the Bahrain School with both an American High School and an International Baccalaureate diploma. Returning to the Netherlands, he chose to study chemical engineering at the Delft University of Technology, and completed this education with a M.Sc. degree in 2001. His graduate work was done in what was then the CRE group, under the supervision of Ruud van Ommen, Jan van Turnhout (PME), and Cor van den Bleek. Interested in trying to bring together the fields of reactor engineering and electrical engineering, he continued his graduate work as a Ph.D. student in the newly formed R&CE group, still under the guidance of Ruud van Ommen, Jan van Turnhout, and Cor van den Bleek. In 2003, six months were spent doing research at the University of British Columbia in the group of Dr. Aihua Chen, Dr. Xiaotao Bi, and Dr. John Grace. In 2005 he was honored to receive a 'Young Scientist' award from the working party "Static Electricity in Industry" of the European Federation of Chemical Engineering. He joined IPCOS Technology in Boxtel in December 2005 as a consultant advanced process control.